# 9. SITE 1006[1]

Shipboard Scientific Party[2]

## HOLE 1006A

**Position:** 24°23.989′N, 79°27.541′W

**Start hole:** 1100 hr, 15 March 1996

**End hole:** 0945 hr, 19 March 1996

**Time on hole:** 3 days, 22 hr, 48 min

**Seafloor (drill pipe measurement from rig floor, mbrf):** 669.4

**Total depth (drill pipe measurement from rig floor, mbrf):** 1386.7

**Distance between rig floor and sea level (m):** 11.5

**Water depth (drill pipe measurement from sea level, m):** 657.9

**Penetration (mbsf):** 717.3

**Coring totals:**
Type: APC; No: 29; Cored: 273.1 m; Recovered: 102.7%
Type: XCB; No: 48; Cored: 444.2 m; Recovered: 82.5%

**Formation:**
Unit I: 0–125.95 mbsf, Pleistocene to late Pliocene
White, light gray, and pale yellow nannofossil ooze with intermittent clay layers
Unit II: 125.95–360 mbsf, late Pliocene to early Pliocene
White, light gray, and pale yellow nannofossil ooze and chalk
Unit III: 360–528.7 mbsf, early Pliocene to late Miocene
Alternating light gray to light greenish gray nannofossil chalk
Unit IV: 528.7–594.25 mbsf, late Miocene to middle Miocene
Alternating light gray and greenish gray nannofossil chalk
Unit V: 594.25–717.3 mbsf, middle Miocene
Alternating light greenish gray to olive and light gray nannofossil chalk with foraminifers

## HOLE 1006B

**Position:** 24°23.9907′N, 79°27.5526′W

**Start hole:** 0945 hr, 19 March 1996

**End hole:** 2000 hr, 19 March 1996

**Time on hole:** 10 hr, 15 minutes

**Seafloor (drill pipe measurement from rig floor, mbrf):** 669.0

**Total depth (drill pipe measurement from rig floor, mbrf):** 854.5

**Distance between rig floor and sea level (m):** 11.5

**Water depth (drill pipe measurement from sea level, m):** 657.5

**Penetration (mbsf):** 176.5

**Coring totals:**
Type: APC; No: 19; Cored: 176.5 m; Recovered: 103.3%

**Formation:**
Unit I: 0–127.9 mbsf, Pleistocene to late Pliocene
White, light gray, and pale yellow nannofossil ooze with intermittent clay layers
Unit II: 127.9–176.5 mbsf, late Pliocene to early Pliocene
White, light gray, and pale yellow nannofossil ooze and chalk

## HOLE 1006C

**Position:** 24°23.9911′N, 79°27.5591′W

**Start hole:** 2000 hr, 19 March 1996

**End hole:** 2115 hr, 19 March 1996

**Time on hole:** 1 hr, 15 min

**Seafloor (drill pipe measurement from rig floor, mbrf):** 669.9

**Total depth (drill pipe measurement from rig floor, mbrf):** 676.5

**Distance between rig floor and sea level (m):** 11.5

**Water depth (drill pipe measurement from sea level, m):** 658.4

**Penetration (mbsf):** 6.6

**Coring totals:**
Type: APC; No: 1; Cored: 6.6 m; Recovered: 99.2%

**Formation:**
Unit I: 0–6.6 mbsf, Pleistocene
Nannofossil ooze

## HOLE 1006D

**Position:** 24°23.9911′N, 79° 27.5591′W

**Start hole:** 2115 hr, 19 March 1996

**End hole:** 0115 hr, 20 March 1996

**Time on hole:** 4 hr

**Seafloor (drill pipe measurement from rig floor, mbrf):** 668.9

**Total depth (drill pipe measurement from rig floor, mbrf):** 676.5

**Distance between rig floor and sea level (m):** 11.5

**Water depth (drill pipe measurement from sea level, m):** 657.4

**Penetration (mbsf):** 7.6

**Coring totals:**
Type: APC; No: 1; Cored: 7.6 m; Recovered: 100%

**Formation:**
Unit I: 0–7.6 mbsf, Pleistocene
Nannofossil ooze

**Principal results:** Site 1006 is located in 658 m of water approximately 30 km from the western platform edge of the Great Bahama Bank (GBB). It is the most distal site of the Bahamas Transect positioned at the crossing of seismic Lines 105 and 106. Drilling at Site 1006 was designed to core and log a thick sequence of drift deposits thought to extend through the

[1]Eberli, G.P., Swart, P.K., Malone, M.J., et al., 1997. *Proc. ODP, Init. Repts.*, 166: College Station, TX (Ocean Drilling Program).
[2]Shipboard Scientific Party is given in the list preceding the Table of Contents.



Previous Chapter Table of Contents Next Chapter

Neogene with relatively few hiatuses. There were two principal objectives at this site. First, as the sediments at Site 1006 were believed to have a greater pelagic component than the more proximal sites (1003, 1004, 1005, and 1007) of the transect, they were thought to be well suited for dating and establishing an oxygen isotope stratigraphy for the Neogene, thereby providing an independent indicator of sea level. The biostratigraphic datums could be traced on the seismic reflections to the distal lobes of the prograding margins in the proximal sites using the sequence stratigraphic framework. This approach will aid in the dating of the proximal sites where the chronostratigraphy is occasionally unclear as a result of missing sequences, poor recovery, diagenesis, and/or dilution by neritic sediments. Second, changes in the composition of the sediments were postulated to vary in conjunction with variations in the strength of the Florida Current. These variations would be able to be correlated with changes in sea level as recorded by the prograding and regressive sequences at platform sites and the oxygen isotopic signature of the foraminifers.

A final objective was to examine pore-water chemistry in a more basinward site where pore water and geothermal gradients, in contrast to the slope sites, were believed to be predominantly diffusive in nature and not influenced by fluid flow.

A 717.3-m-thick Pleistocene to middle Miocene section was recovered at Site 1006. The sedimentary section consists of mixed pelagic and bank-derived carbonates with varying amounts of clay material believed to have been derived from Cuba and Hispaniola. The biostratigraphic control throughout Site 1006 is very good and almost all planktonic foraminiferal and nannofossil zones from the Pleistocene to upper middle Miocene are found. The abundant pelagic biogenic components are less diluted by platform-derived material, and microfossil preservation is less affected by diagenesis than in the upper slope sites (Sites 1003, 1004, and 1007). Benthic foraminifers indicate an upper middle bathyal paleodepth of deposition. An excellent record of magnetic susceptibility variations exists showing fluctuations between negative and positive values reflecting the input of clay material. A magnetic reversal was found between 4.5 and 6.0 mbsf that has been tentatively correlated with the Blake Event (0.13 Ma). A good agreement was found between the integrated sonic and VSP logs and the calculated depth of the sequence boundaries. Chemical profiles reveal a shallow flushed zone extending to 30 mbsf. Below this depth, profiles are mainly diffusionally controlled with the exception of certain elements that are locally influenced by diagenetic reactions. Sediments were divided into five lithostratigraphic units on the basis of compositional and textural changes.

Unit I (0–125.95 mbsf, Hole 1006A; 0–127.9 mbsf, Hole 1006B) is Pleistocene to late Pliocene in age. It consists of largely unlithified, bioturbated nannofossil ooze (sand- to silt-sized foraminifers) with a small component of aragonite needles in Subunit IA. Particle abundance and grain size increase downhole to the base of the subunit. In Subunit IB this ooze is interbedded with gray and olive clays that reflect erosion of siliciclastics from Cuba and/or Hispaniola.

Unit II (125.95–360 mbsf, Hole 1006A; 127.9–176.5 mbsf, Hole 1006B) is late Pliocene to early Pliocene in age and consists of nannofossil ooze and chalk in which some grains have been infilled as a result of pyritization. In Subunit IIA there is an alternation between nannofossil ooze and a more aragonite-rich ooze containing some peloids. Subunit IIB is defined by the occurrence of chalk, but is generally very uniform with high rates of sedimentation. Minor to moderate bioturbation is pervasive.

Unit III (360–528.7 mbsf) is early Pliocene to late Miocene in age and is composed primarily of light gray and light greenish gray chalk. The unit consists of a series of fining upward intervals. Firmgrounds characterized by sharp burrowed contacts are frequent in the upper part.

Unit IV (528.7–594.25 mbsf) is late Miocene to latest middle Miocene in age and is composed of light gray and greenish gray nannofossil chalk. The uppermost part contains a series of thick intervals with sharp basal contacts. Within each interval, nannofossil chalk with bioclasts grade upward into nannofossil chalk and clay. The lower part of the sequence is punctuated by a series of firmgrounds.

Unit V (594.25–717.3 mbsf) is middle Miocene in age and is composed of alternating intervals of olive nannofossil chalk and light gray nannofossil chalk with foraminifers. Throughout the entire unit, no primary sedimentary structures are visible. The degree of lithification increases downhole with the result that the lower portion consists of alternating intervals of chalk and limestone. The greenish gray to olive intervals are characterized by well-defined, compacted burrows that occur in association with Chondrites-type burrows. The light gray intervals contain larger noncompacted and well-defined burrows.

The facies succession at Site 1006 is interpreted as being governed by an interplay of current activity and sea-level fluctuations. It is suggested that the bottoms of cycles, which contain clay intervals, reflect periods of erosion of siliciclastics. The clay intervals and increased weathering are covered by nannofossil ooze with platform-derived bioclasts corresponding to neritic production. The top of the cycle consists of nannofossil ooze and planktonic foraminifers. These changes are reflected in the bulk mineralogy, with high aragonite recording high sea level. Aragonite content also appears to be highly correlated with the color reflectance at 700 nm.

All nannofossil and planktonic foraminiferal zones were present throughout the Pleistocene to middle Miocene section. The lower Pliocene sequence is expanded and is ideal for paleoceanographic studies. The foraminifers show little evidence of diagenetic alteration. An excellent record of magnetic susceptibility is present throughout the entire record. The magnetic susceptibility signal is suspected to be tied to changes in the clay content of the sediments. A magnetic reversal was found between 4.5 and 6.0 mbsf, which has been correlated with the Blake Event (0.13 Ma).

Sedimentation rate varies considerably at Site 1006. The rates can be divided into four distinct periods. The rate for the Pliocene–Pleistocene section is 5 cm/k.y., considerably lower than the sedimentation rates at Sites 1003–1005 over the same interval. The rate for the lower Pliocene and uppermost Miocene is 12 cm/k.y., similar to the proximal sites, which suggests that similar depositional processes were influencing the sites during this period. The upper Miocene has a low sedimentation rate (3 cm/k.y.) that is within the range of normal pelagic sedimentation. The middle Miocene has slightly higher rates, which are perhaps accounted for by contourite deposition and the deposition of fine-grained platform-derived material.

The depths of the sequence boundaries were calculated by using velocities from the integrated sonic log and the vertical seismic profile. Velocities measured aboard ship, however, predicted significantly lower interval velocities, a phenomenon resulting from the soft nature of the rocks and the fact that shipboard velocities are not measured under in situ pressure. The boundaries fell in the expected stratigraphic positions based on sequence stratigraphic interpretation and the correlations determined at Site 1003.

A full suite of logs, with the exception of the GLT, was run from 103 to 716.8 mbsf. Throughout the entire sequence, the logs are characterized by small-scale cyclicity observed as alternations between thin, resistive, low natural gamma-ray layers and conductive layers with higher gamma-ray counts. The cyclicity is also well defined by porosity, density, and velocity. Firmgrounds are recognized by increased gamma ray, resistivity, and sonic velocity. A pattern of larger scale cyclicity reflects changes in the abundance and spatial frequency of the cycles. These patterns may be related to depositional changes associated with current intensity and can be tentatively correlated with sequence boundaries. As a result of the high percentage core recovery, these logs offer an excellent opportunity for core-log correlation.

The mineralogy is dominated by low-Mg calcite. Aragonite is abundant in the Pleistocene sediments and decreases to less than 5% in the upper Pliocene sequence. The concentration of aragonite increases to 40% in upper Miocene sediments. High-Mg calcite is present in the uppermost 20–30 mbsf, but quickly disappears coincident with the presence of dolomite. Dolomite is a minor, but ubiquitous component throughout. With the exception of the upper 30 mbsf, the sediment profiles are dominated by diffusion from an underlying brine with local reactions involving $Ca^{2+}$, $Mg^{2+}$, $Sr^{2+}$, $K^{+}$, $Li^{+}$, $F^{-}$, and $H_4SiO_4$, providing deviations from the ideal diffusive profiles. In the upper 30 mbsf, there are no gradients in the major

elements and only very small increases in alkalinity and $Sr^{2+}$. Below this depth, $Cl^-$ increases steadily to the base of the Hole 1006A, reaching a concentration of 717 mM. The $Sr^{2+}$ concentration rises steadily over this interval as a result of the dissolution of aragonite and the precipitation of calcite and dolomite. At 452.95 mbsf, the $Sr^{2+}$ concentration reaches 7 mM, the highest values recorded in ODP or DSDP history. The $Sr^{2+}$ can attain this high concentration primarily because sulfate has been completely utilized in the oxidation of organic material. Concentrations of $H_2S$ are low at this site as a result of the abundance of iron, which allows the formation of pyrite.

In summary, Site 1006 has met and exceeded all of its initial expectations. Based on shipboard biostratigraphy, the sequence boundaries have been dated and traced to the proximal sites where the ages agree well with those determined at Sites 1003 and 1005. The position of the boundaries has been verified using a combination of VSP and integrated sonic logs. The excellent continuous sedimentary sequence contains abundant well-preserved foraminifers that can be dated using O- and Sr-isotope stratigraphy and tied to the shallow sites for dating sea-level changes, thereby providing its own independent record of these changes. With this correlation, another primary goal of Leg 166 will be achieved as the isotopic and sedimentary records can be compared. The expanded Pliocene and upper Miocene sequence, combined with the excellent preservation of the foraminifers, will allow this site to become a classic site for late Cenozoic paleoceanography in the low-latitude Atlantic.

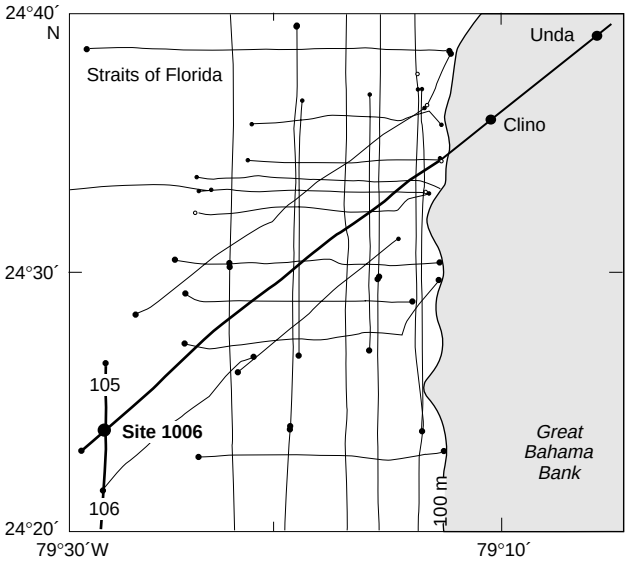


Figure 1. Location map of Site 1006. The site is located on the same seismic line as the two drill sites, Unda and Clino, as well as Sites 1003, 1004, 1005, and 1007.

## BACKGROUND AND OBJECTIVES

Site 1006 is located in 658 m of water in the northern portion of the Santaren Channel approximately 30 km from the western platform edge of the Great Bahama Bank (GBB). It is the most distal member of the five transect sites located at the crossing of seismic Lines 105 and 106 (Fig. 1). Site 1006 is positioned on a thick continuous sequence of Neogene-aged drift sediments (Fig. 2). These deposits onlap and interfinger with prograding bank deposits where Sites 1007, 1003, 1004, and 1005 are situated.

There are two principal objectives at Site 1006. First, as the sediments at this site have a greater pelagic component than at the more proximal sites of the transect (Sites 1003, 1004, 1005, and 1007), they are well suited for dating and establishing an oxygen and strontium isotope stratigraphy for the Neogene. Thus, they are able to provide additional indicators of sea-level changes in this time period. The datums can then be traced along the seismic reflections to the clinoforms of the prograding margin and the proximal sites. This approach will aid in the dating of the proximal sites where the chronostratigraphy is occasionally unclear as a result of missing sequences, poor recovery, diagenesis, and/or dilution by neritic sediments. Second, changes in the composition of the sediments at Site 1006 are postulated to vary in conjunction with changes in (1) the strength of the Florida Current, and (2) variations in the input of platform-derived sediment and sediment derived from terrestrial sources, such as Hispaniola and Cuba (see "Background and Objectives" section, "Site 1003" chapter, this volume). Although low input of carbonate to the basinal areas occurs generally when platforms backstep, or are exposed (Kendall and Schlager, 1981; Handford and Loucks, 1993), these sea-level lowstands are also periods of the increased erosion of minerals such as quartz, feldspars, and clay minerals from siliciclastic areas. Contributions from these areas, therefore, should be expected to increase. In the case of the location of Site 1006 between Cay Sal Bank and the western margin of GBB, the most plausible sources for such materials are Hispaniola and Cuba. Changes in sea level should therefore be reflected as transitions between: (1) carbonate-rich pelagic and neritic sediments derived from the platform; (2) normal pelagic sedimentation; and (3) siliciclastic-rich intervals mixed with pelagic-derived materials with perhaps a small remnant amount of platform sediments. Variations in the sedimentation patterns, X-ray mineralogy, and carbonate content, supplemented by the acquisition of a log suite focusing on the changes in the gamma-ray character, physical properties (sonic and resistivity), and the Formation MicroScanner (FMS), can be used to quantify these changes. Changes in the gamma-ray signal in particular can be expected to correlate with changes in U, K, and Th, and can be associated with clay materials and organic material and more cemented layers. These variations can be correlated with changes in sea level as recorded by the prograding and regressive sequences at platform sites and the oxygen isotopic compositions of the foraminifers.

A critical component of the study of sea level using sequence stratigraphy is the correlation between the seismic lines and the core using VSP. This allows the velocities of the sediments to be measured in situ, rather than on cored material, and the depths of seismic sequence boundaries to be accurately predicted.

A final objective of Site 1006 is to examine pore-water chemistry in a more basinward site where pore-water geochemical and geothermal gradients, in contrast to the slope sites, are believed to be predominantly diffusive in nature and not influenced by fluid flow to the same extent as the proximal sites.

The original target depth of Site 1006 was 820 mbsf, using a combination of APC, XCB, and RCB coring. However, as a result of the relatively unconsolidated nature of the sediments, it was possible to extend the XCB to a depth of 717.3 mbsf, and it was not considered time effective to change to the RCB to retrieve the remaining 102.7 m. Therefore, coring was terminated at this depth and logging carried out through the XCB bit.

In summary, the objectives at Site 1006 were to:

1. Date precisely the sedimentary section in order to carry the ages to sequences in the platform margin sites;
2. Retrieve material for performing shore-based stable strontium and oxygen isotopic studies in order to establish a more accurate chronostratigraphy for the Neogene in this site;
3. Examine the interplay between sea-level changes, input of sediment from GBB, continental sources, and changes in the Florida current; and
4. Assess geothermal and geochemical gradients in a basinal setting for comparison with Sites 1003, 1004, 1005, and 1007.

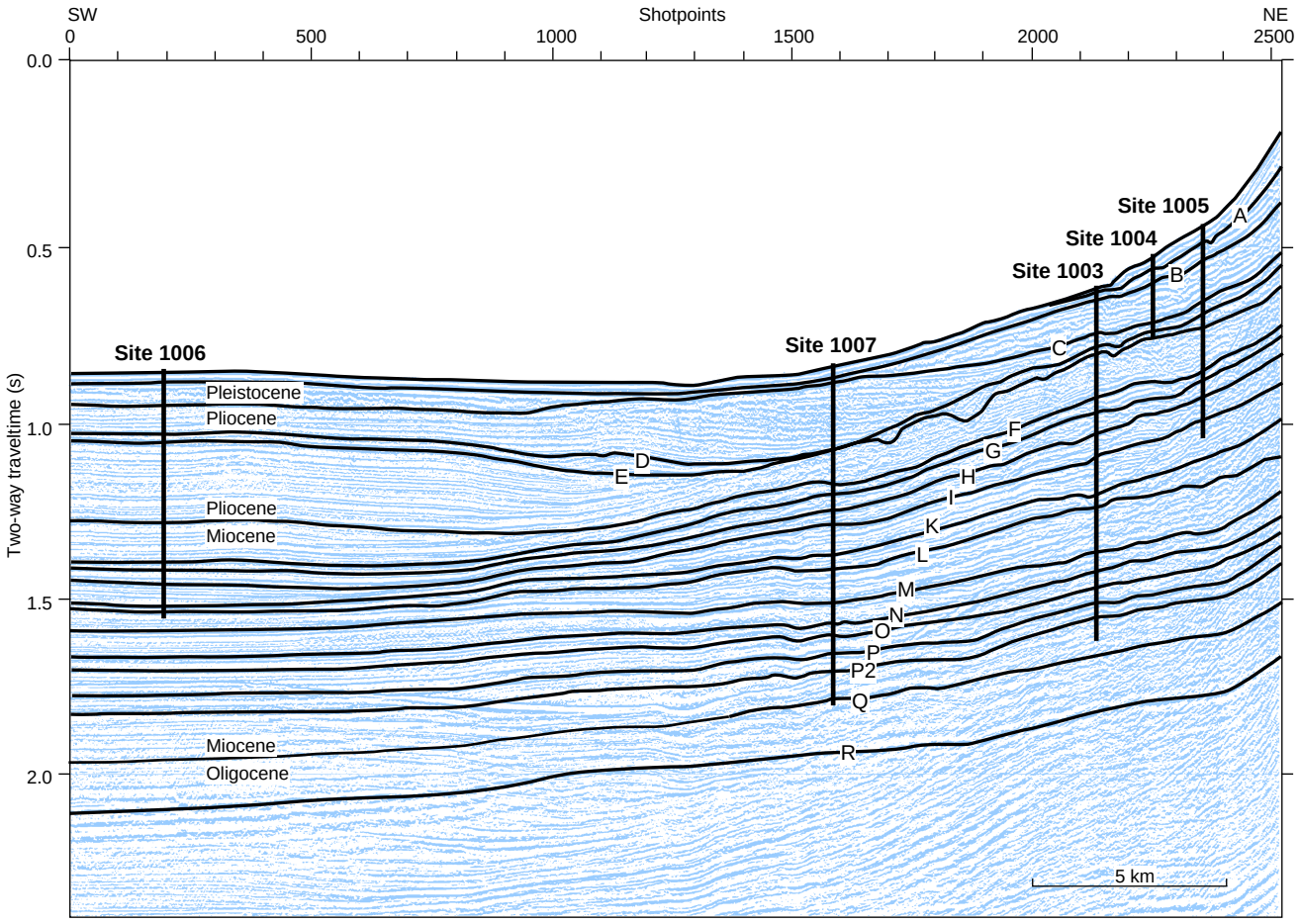


Figure 2. Portion of the high-resolution multichannel seismic Line 106 that retraced the cross-bank Western Geophysical seismic line with the positions of Sites 1003, 1004, 1005, and 1007. Site 1006 was positioned on a thick, continuous sequence of Neogene-aged drift deposits. These deposits onlap and interfinger with prograding bank deposits.

## OPERATIONS

### Transit, Site 1005 to Site 1006

The transit from Site 1005 to Site 1006 covered approximately 15.6 nmi in just over 1.5 hr. We proceeded directly to GPS coordinates 24°23.989′N, 79°27.541′W and deployed a retrievable beacon at 1054 hr, 15 March.

#### *Hole 1006A*

We assembled a bottom-hole assembly (BHA) similar to that used at previous sites and ran the bit to the seafloor. Hole 1006A was initiated at 1355 hr on 15 March. The water depth was 657.9 mbsl based on recovery of the mudline core. Continuous APC cores were cut to 273.1 mbsf with 97.4% recovery (Table 1). Cores 1006A-3H through 29H were oriented with the Tensor tool. Adara heat flow measurements were performed from Cores 3H through 11H, and every third APC core thereafter. Core 29H required 80,000 lb overpull; therefore, APC coring was terminated. XCB Cores 30X through 77X were cut from 273.1 to 717.3 mbsf with 82.5% recovery. The WSTP was deployed after Cores 32X, 35X, 38X, and 43X. Core jamming in the core catcher or in the core liner was observed in 14 of the last 19 cores. Coring operations were terminated at 717.3 mbsf after achieving the objectives for this hole. A wiper trip was performed to condition the hole, and the drill string was positioned at 104 mbsf for logging. The following logging runs were performed to total depth (717 mbsf) without incident: DIT/sonic, IPLT/GR, FMS, and a VSP experiment with the WST tool. The bit cleared the seafloor at 0940 hr on 19 March.

#### *Hole 1006B*

The ship was moved 20 m to the west, and Hole 1006B was spudded at 1045 hr on 19 March. The water depth was 657.5 mbsl based on recovery of the mudline core. APC Cores 1006B-1H through 19H were cut from 0 to 176.5 mbsf with 103.2% recovery. Cores 3H through 19H were oriented with the Tensor tool. The bit cleared the seafloor at 1955 hr on 19 March.

#### *Hole 1006C*

The ship was moved another 20 m to the west, and Hole 1006C was initiated at 2045 hr on 19 March. Hole 1006C was spudded to acquire a single, oriented mudline core in an attempt to obtain sediments recording the Blake paleomagnetic event that appeared to be present in the top few meters of the first core of Holes 1006A and 1006B. The water depth was 658.4 mbsl based on the core recovery. Core 1H was cut from 0 to 6.6 mbsf with 99% recovery. The core liner was badly splintered, probably due to the coral debris found jammed in the coring shoe.

**Table 1. Site 1006 coring summary.**

| Core | Date (March 1996) | Time (UTC) | Depth (mbsf) | Length cored (m) | Length recovered (m) | Recovery (%) |
|---|---|---|---|---|---|---|
| 166-1006A- | | | | | | |
| 1H | 15 | 1905 | 0.0–7.1 | 7.1 | 7.1 | 100.0 |
| 2H | 15 | 1940 | 7.1–16.6 | 9.5 | 9.69 | 102.0 |
| 3H | 15 | 2025 | 16.6–26.1 | 9.5 | 9.85 | 103.0 |
| 4H | 15 | 2105 | 26.1–35.6 | 9.5 | 9.90 | 104.0 |
| 5H | 15 | 2145 | 35.6–45.1 | 9.5 | 9.04 | 95.1 |
| 6H | 15 | 2230 | 45.1–54.6 | 9.5 | 9.60 | 101.0 |
| 7H | 15 | 2320 | 54.6–64.1 | 9.5 | 10.02 | 105.5 |
| 8H | 16 | 0000 | 64.1–73.6 | 9.5 | 9.98 | 105.0 |
| 9H | 16 | 0045 | 73.6–83.1 | 9.5 | 9.81 | 103.0 |
| 10H | 16 | 0130 | 83.1–92.6 | 9.5 | 9.88 | 104.0 |
| 11H | 16 | 0210 | 92.6–102.1 | 9.5 | 9.80 | 103.0 |
| 12H | 16 | 0235 | 102.1–111.6 | 9.5 | 9.86 | 104.0 |
| 13H | 16 | 0300 | 111.6–121.1 | 9.5 | 10.04 | 105.7 |
| 14H | 16 | 0345 | 121.1–130.6 | 9.5 | 9.09 | 95.7 |
| 15H | 16 | 0410 | 130.6–140.1 | 9.5 | 9.92 | 104.0 |
| 16H | 16 | 0435 | 140.1–149.6 | 9.5 | 9.82 | 103.0 |
| 17H | 16 | 0530 | 149.6–159.1 | 9.5 | 10.03 | 105.6 |
| 18H | 16 | 0600 | 159.1–168.6 | 9.5 | 9.82 | 103.0 |
| 19H | 16 | 0625 | 168.6–178.1 | 9.5 | 9.73 | 102.0 |
| 20H | 16 | 0710 | 178.1–187.6 | 9.5 | 9.92 | 104.0 |
| 21H | 16 | 0735 | 187.6–197.1 | 9.5 | 9.89 | 104.0 |
| 22H | 16 | 0800 | 197.1–206.6 | 9.5 | 9.56 | 100.0 |
| 23H | 16 | 0840 | 206.6–216.1 | 9.5 | 9.90 | 104.0 |
| 24H | 16 | 0910 | 216.1–225.6 | 9.5 | 9.87 | 104.0 |
| 25H | 16 | 0940 | 225.6–235.1 | 9.5 | 10.03 | 105.6 |
| 26H | 16 | 1020 | 235.1–244.6 | 9.5 | 9.82 | 103.0 |
| 27H | 16 | 1055 | 244.6–254.1 | 9.5 | 9.07 | 95.5 |
| 28H | 16 | 1120 | 254.1–263.6 | 9.5 | 9.88 | 104.0 |
| 29H | 16 | 1250 | 263.6–273.1 | 9.5 | 9.58 | 101.0 |
| 30X | 16 | 1345 | 273.1–278.9 | 5.8 | 6.84 | 118.0 |
| 31X | 16 | 1410 | 278.9–284.7 | 5.8 | 7.44 | 128.0 |
| 32X | 16 | 1430 | 284.7–293.9 | 9.2 | 9.81 | 106.0 |
| 33X | 16 | 1555 | 293.9–303.1 | 9.2 | 9.16 | 99.5 |
| 34X | 16 | 1625 | 303.1–312.4 | 9.3 | 9.92 | 106.0 |
| 35X | 16 | 1650 | 312.4–321.5 | 9.1 | 9.32 | 102.0 |
| 36X | 16 | 1805 | 321.5–330.6 | 9.1 | 8.86 | 97.3 |
| 37X | 16 | 1830 | 330.6–339.8 | 9.2 | 9.93 | 108.0 |
| 38X | 16 | 1855 | 339.8–348.9 | 9.1 | 8.37 | 92.0 |
| 39X | 16 | 2035 | 348.9–358.1 | 9.2 | 8.29 | 90.1 |
| 40X | 16 | 2100 | 358.1–367.3 | 9.2 | 9.32 | 101.0 |
| 41X | 16 | 2120 | 367.3–376.4 | 9.1 | 9.28 | 102.0 |
| 42X | 16 | 2145 | 376.4–385.6 | 9.2 | 3.89 | 42.3 |
| 43X | 16 | 2215 | 385.6–394.7 | 9.1 | 0.98 | 10.7 |
| 44X | 16 | 2340 | 394.7–404.0 | 9.3 | 9.85 | 106.0 |
| 45X | 17 | 0010 | 404.0–413.4 | 9.4 | 9.68 | 103.0 |
| 46X | 17 | 0045 | 413.4–422.8 | 9.4 | 8.34 | 88.0 |
| 47X | 17 | 0115 | 422.8–432.0 | 9.2 | 9.27 | 101.0 |
| 48X | 17 | 0145 | 432.0–441.0 | 9 | 8.01 | 89.0 |
| 49X | 17 | 0205 | 441.0–450.1 | 9.1 | 9.02 | 99.1 |
| 50X | 17 | 0230 | 450.1–459.3 | 9.2 | 9.79 | 106.0 |
| 51X | 17 | 0255 | 459.3–468.7 | 9.4 | 9.83 | 104.0 |
| 52X | 17 | 0330 | 468.7–478.1 | 9.4 | 9.89 | 105.0 |
| 53X | 17 | 0355 | 478.1–487.2 | 9.1 | 9.45 | 104.0 |
| 54X | 17 | 0420 | 487.2–496.3 | 9.1 | 9.34 | 102.0 |
| 55X | 17 | 0450 | 496.3–505.4 | 9.1 | 9.82 | 108.0 |
| 56X | 17 | 0525 | 505.4–515.0 | 9.6 | 9.69 | 101.0 |
| 57X | 17 | 0600 | 515.0–524.7 | 9.7 | 7.36 | 75.9 |
| 58X | 17 | 0640 | 524.7–534.3 | 9.6 | 8.86 | 92.3 |
| 59X | 17 | 0750 | 534.3–543.9 | 9.6 | 4.34 | 45.2 |
| 60X | 17 | 0850 | 543.9–553.5 | 9.6 | 7.96 | 82.9 |
| 61X | 17 | 0945 | 553.5–563.2 | 9.7 | 9.37 | 96.6 |
| 62X | 17 | 1040 | 563.2–572.8 | 9.6 | 8.86 | 92.3 |
| 63X | 17 | 1145 | 572.8–582.4 | 9.6 | 9.45 | 98.4 |
| 64X | 17 | 1330 | 582.4–592.1 | 9.7 | 7.60 | 78.3 |
| 65X | 17 | 1500 | 592.1–601.7 | 9.6 | 8.67 | 90.3 |
| 66X | 17 | 1705 | 601.7–611.4 | 9.7 | 2.59 | 26.7 |
| 67X | 17 | 1810 | 611.4–621.0 | 9.6 | 9.84 | 102.0 |
| 68X | 17 | 1950 | 621.0–630.6 | 9.6 | 7.91 | 82.4 |
| 69X | 17 | 2125 | 630.6–640.2 | 9.6 | 1.00 | 10.4 |
| 70X | 17 | 2320 | 640.2–649.9 | 9.7 | 0.37 | 3.8 |
| 71X | 18 | 0050 | 649.9–659.5 | 9.6 | 0.11 | 1.1 |
| 72X | 18 | 0230 | 659.5–669.2 | 9.7 | 9.69 | 99.9 |
| 73X | 18 | 0405 | 669.2–678.8 | 9.6 | 6.38 | 66.4 |
| 74X | 18 | 0545 | 678.8–688.4 | 9.6 | 9.65 | 100.0 |
| 75X | 18 | 0740 | 688.4–698.1 | 9.7 | 4.62 | 47.6 |
| 76X | 18 | 0925 | 698.1–707.7 | 9.6 | 1.46 | 15.2 |
| 77X | 18 | 1110 | 707.7–717.3 | 9.6 | 6.92 | 72.1 |
| Coring totals | | | | 717.3 | 646.93 | 90.2 |
| 166-1006B- | | | | | | |
| 1H | 19 | 1550 | 0.0–5.5 | 5.5 | 5.58 | 101.0 |
| 2H | 19 | 1610 | 5.5–15.0 | 9.5 | 9.96 | 105.0 |
| 3H | 19 | 1635 | 15.0–24.5 | 9.5 | 10.03 | 105.6 |
| 4H | 19 | 1705 | 24.5–34.0 | 9.5 | 10.01 | 105.3 |
| 5H | 19 | 1735 | 34.0–43.5 | 9.5 | 9.97 | 105.0 |
| 6H | 19 | 1755 | 43.5–53.0 | 9.5 | 9.38 | 98.7 |
| 7H | 19 | 1825 | 53.0–62.5 | 9.5 | 9.78 | 103.0 |
| 8H | 19 | 1845 | 62.5–72.0 | 9.5 | 9.51 | 100.0 |
| 9H | 19 | 1910 | 72.0–81.5 | 9.5 | 10.12 | 106.5 |
| 10H | 19 | 1935 | 81.5–91.0 | 9.5 | 9.52 | 100.0 |
| 11H | 19 | 2005 | 91.0–100.5 | 9.5 | 9.93 | 104.0 |
| 12H | 19 | 2030 | 100.5–110.0 | 9.5 | 9.92 | 104.0 |
| 13H | 19 | 1555 | 110.0–119.5 | 9.5 | 9.91 | 104.0 |
| 14H | 19 | 2120 | 119.5–129.0 | 9.5 | 9.80 | 103.0 |
| 15H | 19 | 2145 | 129.0–138.5 | 9.5 | 9.86 | 104.0 |
| 16H | 19 | 2215 | 138.5–148.0 | 9.5 | 10.01 | 105.3 |
| 17H | 19 | 2245 | 148.0–157.5 | 9.5 | 9.66 | 101.0 |
| 18H | 19 | 2310 | 157.5–167.0 | 9.5 | 9.81 | 103.0 |
| 19H | 19 | 2340 | 167.0–176.5 | 9.5 | 9.96 | 105.0 |
| Coring totals | | | | 176.5 | 182.70 | 103.5 |
| 166-1006C- | | | | | | |
| 1H | 20 | 0155 | 0.0–6.6 | 6.6 | 6.55 | 99.2 |
| Coring totals | | | | 6.6 | 6.55 | 99.2 |
| 166-1006D- | | | | | | |
| 1H | 20 | 0300 | 0.0–7.6 | 7.6 | 7.60 | 100 |
| Coring totals | | | | 7.6 | 7.60 | 100 |

Note: An expanded version of this coring summary table that includes lengths and depths of sections, location of whole-round samples, and comments on sampling disturbance is included on CD-ROM in the back pocket of this volume.

### *Hole 1006D*

While the ship remained at the location of Hole 1006C, another oriented mudline core was attempted. Hole 1006D was spudded at 2200 hr on 19 March. The water depth was 668.9 mbsl based on core recovery. Core 1H was cut from 0 to 7.6 mbsf with 100% recovery. The drill pipe was pulled and secured at 0113 hr on 20 March.

## LITHOSTRATIGRAPHY

### Introduction

A nearly continuous section of Pleistocene to middle Miocene sediments was recovered at Site 1006, drilled in the Straits of Florida at the distal end of the Bahamas Transect. Hole 1006A, the deepest of four holes drilled at Site 1006, recovered 717.3 m of nannofossil ooze, planktonic foraminifer nannofossil ooze, planktonic foraminifer nannofossil chalk, and nannofossil limestone, with variable amounts of admixed silt and clay. Hole 1006B recovered 176.5 m of Pleistocene- to early Pliocene-aged nannofossil ooze, planktonic foraminifer nannofossil ooze, and thin layers of silt and clay. Carbonate contents are generally greater than 80 wt% in sediments recovered at Site 1006, but are as low as 50 wt% within clay layers in the upper 130 m (see “Organic Geochemistry” section, this chapter). Holes 1006C and 1006D were designated magnetostratigraphic holes consisting of one core each that were not described.

Sediments at Site 1006 are divided into five lithostratigraphic units on the basis of compositional and textural changes (Fig. 3). Primary data used to describe the lithostratigraphic changes include visual core descriptions, determination of sand-sized allochems in wash samples, and smear-slide analyses. Most unit boundaries correspond to inferred periods of reduced deposition. In limestones, these boundaries are expressed as firmgrounds. In the unlithified portions, boundaries consist of more lithified layers. The boundary between Units I and II is the only exception. This boundary marks the lowermost occurrence of a series of interbedded, centimeter-scale clay layers observed in both Holes 1006A and 1006B. The degree of lithification increases steadily downhole. Unit I and most of Unit II are un-

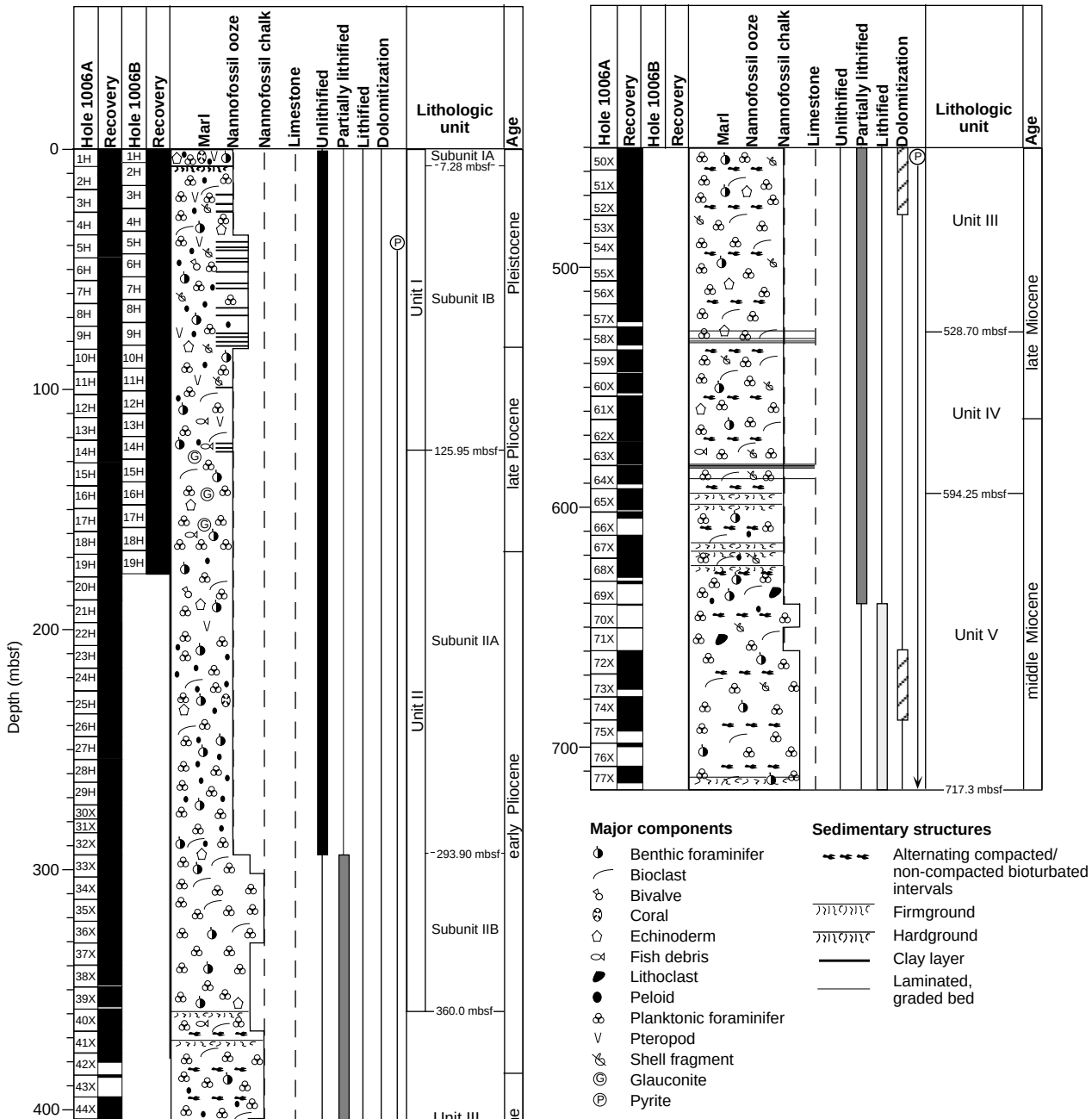


Figure 3. Synthesis of the lithostratigraphy at Site 1006.

lithified, Unit III and most of Unit IV are partially lithified (chalks), and most of Unit V is lithified (limestone). Parts of Units III and V are partially dolomitized.

## Description of Units

### *Lithologic Unit I*

Intervals: 166-1006A-1H through 14H-4, 35 cm; 166-1006B-1H through 14H-6, 100 cm

Age: Pleistocene to late Pliocene
Depth: 0–125.95 mbsf, Hole 1006A; 0–128 mbsf, Hole 1006B

Unit I consists of light gray, white, and pale yellow nannofossil ooze interbedded with gray and olive gray clays and silt. The most abundant allochems are planktonic foraminifers. Other allochems in Unit I are silt- to sand-sized benthic foraminifers, echinoderm spines, pteropods, and peloids. Planktonic and benthic foraminifers become increasingly dominant downhole. Matrix constituents, which make

up the majority of Unit I sediments, consist primarily of calcareous nannofossils with relatively minor amounts of micrite and aragonite needles. In general, the proportion of micrite increases downhole. Moderate to heavy bioturbation is visible as (1) indistinct (pale yellowish to brownish) color mottling, (2) distinct 0.5- to 1-cm diameter burrows filled with fine-grained sediment, or as (3) concentrations of pyritized and/or sediment-filled grains (in Subunit IB only).

The nannofossil ooze sequence in Unit I is interrupted by a possible hardground in Section 166-1006A-2H, 35 cm; a chalky layer in Section 166A-2H-6, 130 cm; and a series of clay and silty clay layers in Cores 166-1006A-3H through 14H and Cores 166-1006B-3H through 14H. These features allow division of Unit I into Subunits IA and IB. The contact between Subunits IA and IB is defined at the top of the lithified layer in Section 166-1006A-2H-1, 18 cm, and at the top of a chalky layer observed in Section 166-1006B-2H-2, 45 cm. The lower limit of Subunit IB is defined at the base of the lowermost, clay-rich layer, which occurs in Sections 166-1006A-14H-4, 35 cm (125.95 mbsf), and 14H-6, 99 cm (127.99 cm).

*Lithologic Subunit IA*

Intervals: 166-1006A-1H through 2H-1, 18 cm; 166-1006B-1H through 2H-2, 45 cm
Age: Pleistocene
Depth: 0–7.28 mbsf

Subunit IA is a thin interval of light gray and white to pale yellow nannofossil ooze (Fig. 3). The base of Subunit IA is defined at the top of a possible hardground within a partially lithified layer that occurs at Section 166-1006A-2H-1, 18 cm. A chalky layer was identified at a similar depth in Hole 1006B (Section 166-1006B-2H-2, 45 cm). The dominant allochems in Subunit IA are silt- to sand-sized planktonic foraminifers. Other allochems include benthic foraminifers, echinoderm spines, peloids, pteropods, shell fragments, and rare fish debris (otoliths). The matrix constituents are composed primarily of calcareous nannofossils (up to 70%) and minor amounts of micrite (20%) and aragonite needles (10%), as determined in smear slides. Below 0.8 mbsf, minor to moderate bioturbation is pervasive. Bioturbation is visible as either a slight color mottling or sediment-filled burrows with diameters of 1 cm. In general, burrow fill is slightly darker than the surrounding sediment and has a more grain-supported fabric.

Particle abundance and grain size increase downhole to the base of Subunit IA. Blackened grains occur in several centimeter-thick horizons with well-defined bases in Section 166-1006A-1H-2. Below these horizons, blackened grains increase in abundance and occur scattered throughout the sediment. An interval containing reworked material, including deep-water solitary corals, blackened lithoclasts, and crab shell fragments, occurs in interval 166-1006A-1H-4, 109–143 cm. Below this interval, particle abundance, grain size, and the occurrence of blackened grains increase dramatically, and the sediment becomes slightly chalky.

*Lithologic Subunit IB*

Intervals: 166-1006A-2H-1, 18 cm, through 14H-4, 35 cm; 166-1006B-2H-2, 45 cm, through 14H-6, 102 cm
Age: Pleistocene to late Pliocene
Depth: 7.28–125.95 mbsf, Hole 1006A; 7.45–128 mbsf, Hole 1006B

Subunit IB is composed primarily of a cyclic variation of white, light gray, and pale yellow nannofossil ooze with interbedded clays and silty clays. Planktonic foraminifers are the dominant silt- to sand-sized grains within the nannofossil ooze. Other allochems include benthic foraminifers, pteropods, echinoderm spines, peloids, and rare fish debris (otoliths). Some grains appear gray either because of pyritization or, in the case of foraminifers, sediment infill. Subunit IB matrix constituents, identified in smear slides, consist primarily of calcareous nannofossils, with minor amounts of micrite and clay. The micrite percentage increases downhole. Moderate to strong bioturbation gives the sediments a mottled appearance. Pyritized and sediment-filled grains are commonly concentrated within small burrows of 1 to 2 mm in diameter, and less frequently within larger burrows of 1 cm in diameter. Bioturbation is also visible as a mottling in color and/or as burrows of 1 cm thickness, filled with fine-grained sediment.

Cycles in Subunit IB are marked by sharp lower contacts overlain by 2- to 35-cm-thick intervals composed primarily of dark gray clays, silt, bioclasts, and/or massive clays (Figs. 4, 5). *Chondrites*-type burrows often occur within clay-rich intervals. Silts and clays grade upward into intervals of pale yellow nannofossil ooze. Allochems occur in low abundance within the pale yellow portion of the cycles but display a high variability. They include silt- to fine sand-sized planktonic and benthic foraminifers, pteropods, echinoderm spines, peloids, ostracodes, and rare fish debris (otoliths). Many of these grains are micritized and show evidence of reworking. Within each cycle, pale yellow nannofossil oozes grade upward into white to light gray foraminifer-nannofossil oozes. Allochems are relatively abundant in the white-gray oozes, but consist almost exclusively of silt- to fine sand-sized planktonic foraminifers. Within these intervals, particle abundance increases upward, such that sediment texture becomes increasingly grain-supported toward the tops of each cycle. In some cases, an interval of grain-rich foraminifer nannofossil ooze is sharply overlain by an interval of grain-poor, pale yellow nannofossil ooze. Such transitions are interpreted as cycles in which the typical basal silt/clay interval is absent.

***Lithologic Unit II***

Intervals: 166-1006A-14H-4, 35 cm, through 40X-2, 40 cm; 166-1006B-14H-6, 102 cm, through 166-1006A-19H
Age: late to early Pliocene
Depth: 125.95–360 mbsf, Hole 1006A; 128–176.5 mbsf, Hole 1006B

Unit II consists of nannofossil ooze and chalk. Primary allochems include silt to fine sand-sized planktonic and benthic foraminifers, bioclasts, peloids, and fish remains. Throughout Unit II, some grains appear gray as a result of sediment infill and/or pyritization. Dark grains are commonly concentrated within small 1- to 2-mm-diameter burrows, and less frequently within larger (1 cm in diameter) burrows. The top of Unit II is defined at the base of the clay interval in the lowermost clay cycle at Site 1006 (Core 166-1006A-14H). The base of Unit II is defined at the top of a firmground that occurs in Section 166-1006A-40X-2, 40 cm. Unit II was divided into Subunits IIA and IIB on the basis of a downhole change from nannofossil ooze to nannofossil chalk between Cores 166-1006A-32X and 33X.

*Lithologic Subunit IIA*

Intervals: Cores 166-1006A-15H through 32X; Section 166-1006B-14H-6, 102 cm, through Core 166-1006B-19H
Age: late to early Pliocene
Depth: 125.95–293.9 mbsf

Subunit IIA is composed of white, light gray, and pale yellow nannofossil ooze with silt to fine sand-sized planktonic and benthic foraminifers, bioclasts, some peloids, and rare fish remains. In the upper part of Subunit IIA, glauconized planktonic foraminifers occur in addition to pyritized and sediment-filled specimens (Cores 166-1006A-14H through 17H). Two main lithologies were differentiated on the basis of grain type, particle abundance, and color: (1) pale yellow nannofossil ooze containing planktonic and benthic foraminifers, bioclasts, and rare fish remains; and (2) light gray to white foraminifer nannofossil ooze containing abundant planktonic foraminifers, some benthic foraminifers, and peloids. Particle abundance is higher in the second sediment type than in the first.

These sediment types alternate cyclically throughout the extent of Subunit IIA. Cycles are marked by sharp basal contacts that are overlain by pale yellow nannofossil ooze, which grades upward into light

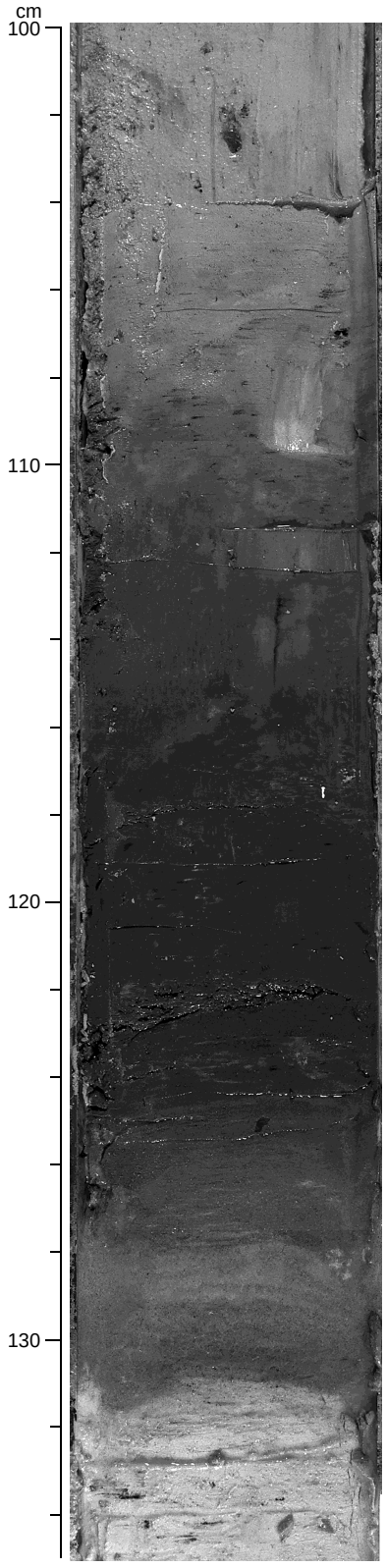


Figure 4. Close-up of a clay interval in Subunit IB (Section 166-1006B-3H-4, 100–135 cm). The gray clay overlies an unconsolidated bioclastic silt (128–131 cm). Sediment below the sharp base at 131 cm consists of greenish gray nannofossil oozes with planktonic foraminifers. Between 116 and 106 cm, the clay grades into yellowish to whitish nannofossil oozes. Black dots in the upper part of this succession are burrows infilled with pyritized foraminifers. Note the *Chondrites* burrows between 113 and 117 cm.

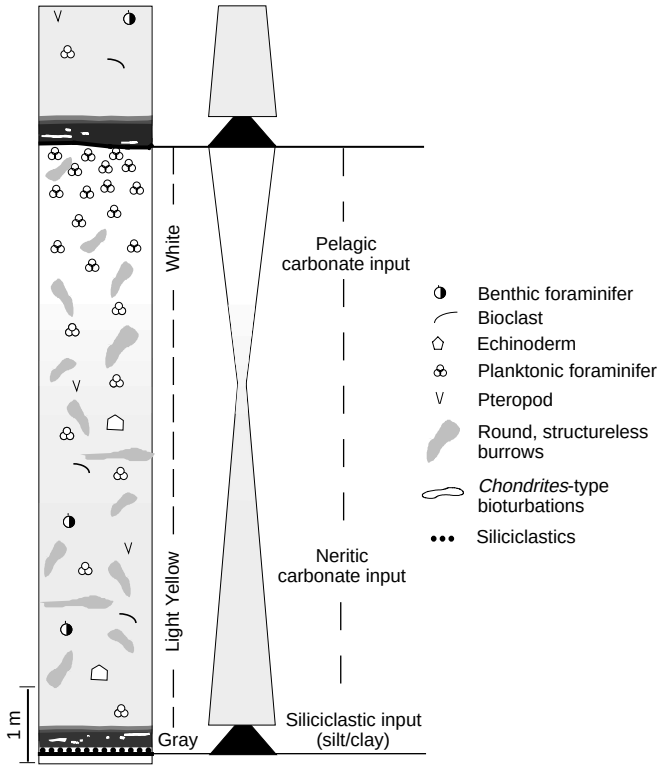


Figure 5. Schematic summary of a typical cycle in Subunit IB. The cycle consists of a sharp base overlain by silty bioclastic sediments, which is followed by gray clays. The clays gradually change into light yellowish to gray to white nannofossil oozes with abundant bioclasts and rare clay. The uppermost part of the cycle consists of light gray nannofossil oozes with planktonic foraminifers.

gray to white foraminifer nannofossil ooze. Cycle thicknesses range from 110 cm in the upper part of Subunit IIA to 300 cm in the lower part. Minor to moderate bioturbation is pervasive, and visible as (1) faint color mottling, (2) thin (less than 1 mm in diameter), pyritized, cylindrical vertical to subvertical burrows, and (3) large (up to 2 cm in diameter) cylindrical burrows filled with pyritized foraminifers.

This succession is interrupted by thin, centimeter-scale, grain-supported layers that contain concentrations of pyritized planktonic foraminifers (intervals 166-1006A-30X-2, 36–37 cm; 32X-3, 110–112 cm; and 32X-5, 38–40 cm). These layers have sharp upper and lower contacts, and in some cases are heavily bioturbated (e.g., interval 166-1006A-28H-4, 74–80 cm).

### *Lithologic Subunit IIB*

Interval: 166-1006A-33X through 40X-2, 40 cm
Age: early Pliocene
Depth: 293.9–360.0 mbsf

The top of Subunit IIB is defined at the first occurrence of nannofossil chalk in Core 166-1006A-33X. This subunit consists of a uniform interval of light gray and light greenish gray nannofossil chalk. Allochems include silt- to fine sand-sized planktonic foraminifers, bioclasts, minor benthic foraminifers, and rare echinoderm debris. Minor to moderate bioturbation is pervasive, and visible as (1) well-defined burrows in intervals of light gray chalk; (2) color mottling in gray to greenish gray intervals; and (3) concentrations of pyritized planktonic foraminifers. Some of the planktonic foraminifers were stained. Three colors were noted: (1) reddish, from disseminated organic matter; (2) blackish, from pyrite; and (3) green, from glauconite (Cores 166-1006A-14H through 17H). Pyrite accumulations are

present throughout the entire interval. Other than bioturbation, distinct sedimentary structures are present in this interval. The uniform character probably results from the high sedimentation rate in this interval (see "Biostratigraphy" section, this chapter). The general sedimentological character of this unit has great similarity with Unit II of both Sites 1003 and 1005.

### *Lithologic Unit III*

Interval: 166-1006A-40X-2, 40 cm, through 58X-3, 100 cm
Age: early Pliocene to late Miocene
Depth: 360.0–528.7 mbsf

Unit III is composed primarily of light gray and light greenish gray nannofossil chalk. Major allochems are silt- to fine sand-sized planktonic and benthic foraminifers, bioclasts, echinoderm debris, and rare peloids. Planktonic foraminifers are generally more abundant in light gray intervals than in light greenish gray intervals. Minor to moderate bioturbation is pervasive. In light gray intervals, burrows are generally darker in color (olive gray) than the surrounding sediment. In the greenish gray zones, burrows are better defined: large (up to 1 cm in diameter), slightly compacted, and representing well-defined *Chondrites*-type of bioturbation.

Firmgrounds are frequent in the upper part of Unit III (Cores 166-1006A-40X through 47X). Firmgrounds are characterized by sharp, burrowed contacts, which separate light greenish gray chalk above the contact from light gray chalk below (Fig. 6). In the lower part of Unit III (Cores 166-1006A-48X to Section 166-1006A-58X-3, 100 cm), the color change from light gray upward into light greenish gray intervals occurs at sharp contacts, whereas changes from light greenish gray upward into light gray intervals are more gradual (e.g., Core 166-1006A-56X). The base of Unit III is defined at the top of a series of sharp-based, fining-upward layers (Section 166-1006A-58X-3, 100 cm) with thicknesses of 3 to 12 cm.

### *Lithologic Unit IV*

Interval: 166-1006A-58X-5 through 65X-2, 65 cm
Age: late to middle Miocene
Depth: 528.70–594.25 mbsf

Unit IV is composed primarily of light gray and greenish gray nannofossil chalk. Dominant components are silt- to fine sand-sized planktonic foraminifers, bioclasts, and benthic foraminifers. Minor to moderate bioturbation is pervasive and visible as (1) round (up to 1 cm in diameter), structureless burrows filled with fine-grained sediment, (2) distinct burrows with backfill structures (e.g., interval 166-1006A-60X-2, 105–107 cm), and (3) as dark concentrations of pyritized foraminifers.

The uppermost part of Unit IV (Core 166-1006A-58X) contains a series of 10-cm-thick intervals with sharp basal contacts. Within each interval, nannofossil chalk with bioclasts grades upward into nannofossil chalk, with clay content increasing upward. Planar to very low-angle wavy lamination occurs at the base of each interval, with *Chondrites*-type burrows near the top. Laminated layers disappear below Core 166-1006A-58X, although some heavily bioturbated, clay-rich intervals (e.g., interval 166-1006A-59X-1, 128–129 cm) may represent the remnants of laminated intervals similar to those in Core 166-1006A-58X.

Sediments in the remainder of Unit IV consist entirely of alternating intervals of light gray and light greenish gray nannofossil chalk with foraminifers. Although color changes from light gray into light greenish gray intervals are predominantly gradual, some changes occur across sharp boundaries (e.g., Section 166-1006A-61X-4, 27 cm). The lower part of this sequence is punctuated by a series of firmgrounds in Core 166-1006A-65X. The lower boundary of Unit IV is defined at the top of the lowermost of these firmgrounds (Section 166-1006A-65X-2, 65 cm).

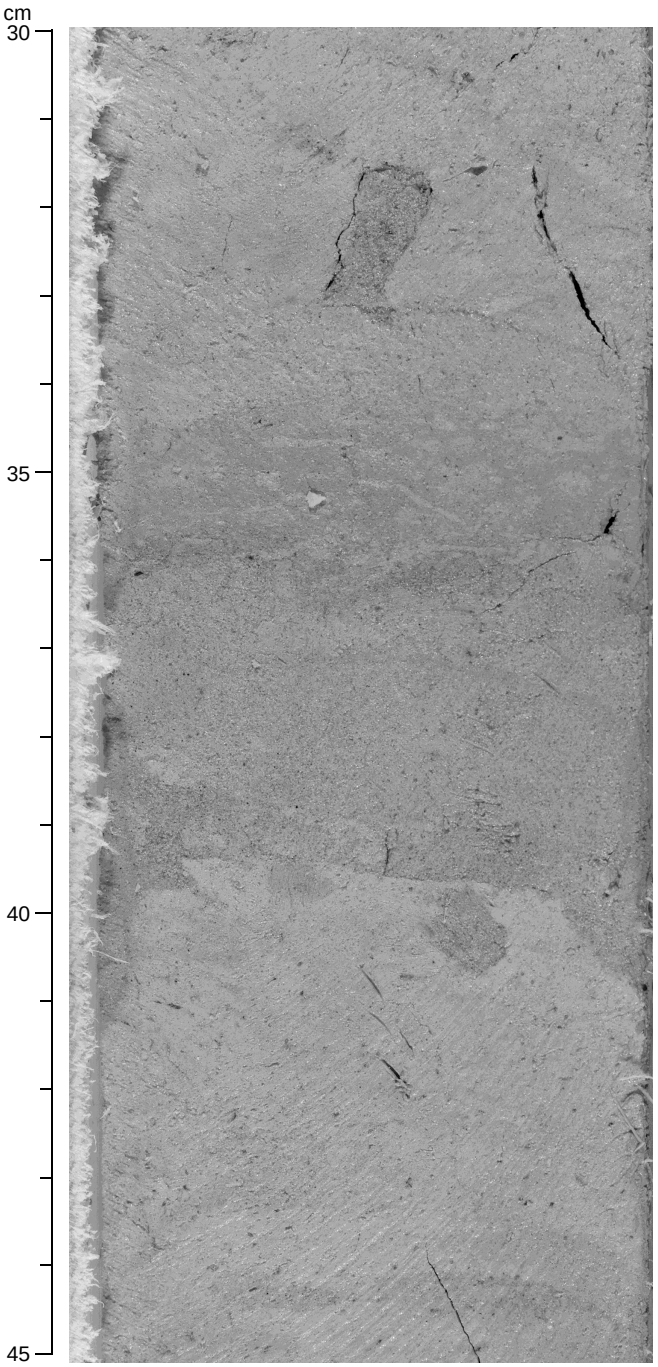


Figure 6. Close-up of a firmground at interval 166-1006A-40X-2, 30–45 cm. Note that the sharp boundary at 39–40 cm has been bored. Above the firmground, a burrowed zone is present (36–40 cm) followed by an interval with *Chondrites* burrows (34.5–36 cm). This firmground marks the top of Unit III.

### *Lithologic Unit V*

Interval: 166-1006A-65X-2, 65 cm, through 77X
Age: middle Miocene
Depth: 594.25–717.3 mbsf

Unit V is composed of alternating intervals of light greenish gray to olive nannofossil chalk and light gray nannofossil chalk with foraminifers. Throughout the entire unit, besides bioturbation, no primary sedimentary structures are visible. Smear-slide analyses suggest that greenish gray to olive intervals have higher clay contents than do

the light gray intervals. The degree of lithification increases downhole. As a result, the upper part of the unit consists of chalks, whereas the lower part consists of alternating intervals of chalk and limestone. Major allochems are silt- to fine sand-sized planktonic foraminifers, bioclasts, shell fragments, intraclasts, and benthic foraminifers. Some grains are pyritized and appear dark gray in color. Although the size of allochems is generally constant throughout Unit V, particle abundance varies. In general, light gray intervals are richer in allochems than are greenish gray to olive intervals.

Throughout the extent of Unit V, greenish gray to olive gray intervals show evidence of compaction and often contain *Chondrites*-type burrows. Light gray intervals contain well-defined burrows only, which are generally larger than those in the greenish gray to olive intervals (up to 1.5 cm in diameter). In some cases, contacts between the greenish gray and light gray intervals are sharp. In Cores 166-1006A-65X through 68X and in Section 166-1006A-77X-3, 39 cm, these contacts are burrowed and interpreted as firmgrounds (Fig. 3).

## Color Reflectance

Percent color reflectance was determined at 10-cm intervals throughout Hole 1006A. Although measurements are recorded over the visible spectrum from $\lambda$ = 400 to 700 nm, we report here only the results for $\lambda$ = 700 nm, as this part of the spectrum was shown to correspond to mineralogic variations at Site 1004.

A distinct relationship is observed between percent color reflectance and mineralogy in Hole 1006A. Intervals with high percent color reflectance generally correspond to intervals with high weight percent aragonite (as measured by XRD; see "Inorganic Geochemistry" section, this chapter) (Fig. 7). Intervals with low percent color reflectance correspond to intervals with low weight percent aragonite. No statistical correlation was made between these two data sets because of the differences between the sample resolution, but a high correlation is indicated by the close match of the curves.

Variations in color and aragonite content are also related to the lithologic units defined in Hole 1006A. Unit I is an interval of high percent color reflectance (generally >35%) and high weight percent aragonite (generally >30 wt%), with thin intervals of low color reflectance and low aragonite content but high clay content. Subunit IIA corresponds to an interval of decreasing color reflectance and decreasing weight percent aragonite. Subunit IIB is marked by relatively low percent color reflectance and low weight percent aragonite. Percent color reflectance and weight percent aragonite are low at the top of Unit III and increase downward to the middle of Unit III (approximately 460 mbsf). Below this level, in the lower part of Unit III and in Units IV and V, covariance between percent color reflectance and aragonite content is not as good as in the shallower portions of Hole 1006A. However, color data in this lower interval are less reliable than above as a result of coring disturbances, contamination by drilling mud, and data gaps.

In addition to the overall correlation between percent color reflectance and aragonite, a near peak-to-peak correlation is observed between color reflectance and dark gray to olive gray clay layers in Subunit IB (Fig. 8). Percent color reflectance drops to values near 20% at most of these levels. In addition, most clay layers are associated with higher values of magnetic susceptibility (see "Paleomagnetism" section, this chapter). Clay layers without corresponding low color reflectance may have higher carbonate contents than other clay layers.

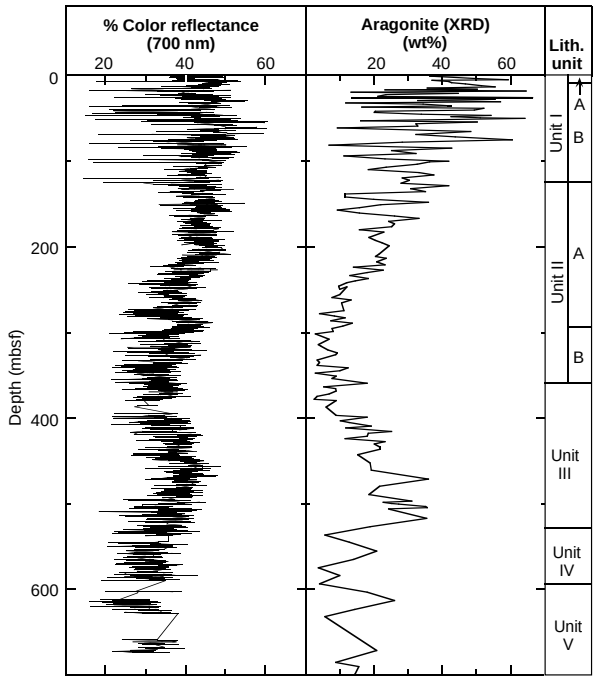


Figure 7. Percent color reflectance and weight percent aragonite measured by XRD at Hole 1006A (see text for discussion).

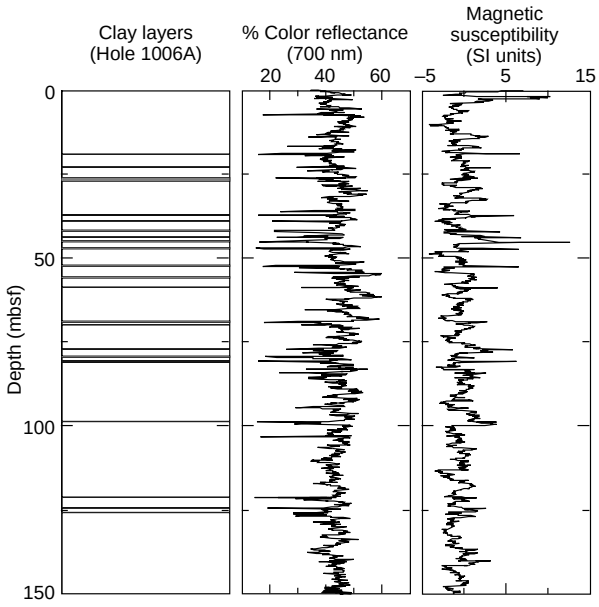


Figure 8. Clay layers, percent color reflectance, and magnetic susceptibility data for Hole 1006A (see text for discussion).

## Interpretation

The sediments cored at Site 1006 can be divided into three main facies associations: (1) light gray pelagic carbonates consisting of nannofossil ooze with planktonic foraminifers; (2) gray clays; and (3) light yellowish gray or greenish gray nannofossil ooze with low clay content, bioclasts, and planktonic foraminifers. The entire succession at Site 1006 consists of a cyclic alternation of these sediment types. Three end-member cycles occur.

1. Cycles of Unit I, with basal clays changing into nannofossil ooze with minor clay and nannofossil ooze with foraminifers in the uppermost part of the cycle (Fig. 5);
2. Cycles consisting of light yellowish gray or greenish gray nannofossil ooze in the lower part that grades into light gray nan-

nofossil ooze with planktonic foraminifers in the upper part (Units II through V); and
3. Cycles consisting of the same alternation, but displaying a sharp contact or a firmground on top of the light gray nannofossil ooze with planktonic foraminifers (Units III through V).

We interpret this cyclic alternation as a result of sea-level fluctuations and variations in bottom current velocities and position within the basinal trough. The facies succession within each cycle is interpreted to be governed by sea-level fluctuations in the following ways.

1. The bottom of the cycles, the clay intervals, or intervals containing clay, reflect redeposition of eroded of siliciclastics in elevated areas during sea-level lowstands and the incipient rises of relative sea level (transgressive stages).
2. Nannofossil ooze with platform-derived bioclasts in the middle of the cycle corresponds to phases of increased neritic input after the flooding of the platforms.
3. The topmost part of the cycles, the nannofossil oozes with planktonic foraminifers, reflect the pelagic background sedimentation. This facies was probably deposited during the incipient fall of relative sea level, when the neritic carbonate factory on the platform was switched off.

Changes in bulk carbonate mineralogy are also interpreted to reflect sea-level fluctuations (Fig. 7). High aragonite contents record sea-level highstands, during which neritic carbonate production was high, whereas low aragonite contents represent phases of low neritic input. Aragonite content is high in the Pliocene-Pleistocene section, low in the Messinian, and high in the Tortonian. Superimposed on these large-scale trends, higher order cyclicities occur.

Currents may also have played a significant role in the deposition of sediments at Site 1006. Both variations in current position and strength are important in packaging the sediments. The increase of winnowing in the topmost part of the cycles and the silt layers at the base give evidence for increased current strength during relative sea-level lowstands. Fluctuating bottom-current velocities mainly controlled the transition from one facies to the other. In the basinal setting of Site 1006, high current velocities probably are responsible for the generation of hardgrounds and firmgrounds as reduced sedimentation rates allowed for lithification on the seafloor.

## BIOSTRATIGRAPHY

Sediments recovered from Site 1006 yield common to abundant, upper Pleistocene through middle Miocene calcareous microfossils. Biostratigraphic control at Site 1006 is very good and almost all planktonic foraminiferal and nannofossil zones from the Pleistocene to upper middle Miocene are found. The abundant pelagic biogenic components are less diluted by platform-derived material, and microfossil preservation is less affected by diagenesis than at the upper slope sites. Site 1006 has an expanded lower Pliocene section that is ideal for paleoceanographic studies. Preservation of microfossils is generally good throughout, which allows a reliable, high-resolution biostratigraphy for Site 1006.

Nannofossils and planktonic foraminifers indicate that the Pleistocene to middle Miocene section recovered at Site 1006 is complete. The Pliocene/Pleistocene boundary is placed at 92 mbsf between Samples 166-1006B-10H-CC and 166-1006A-10H-CC. The lower/upper Pliocene contact is found between Samples 166-1006A-18H-CC and 19H-CC at a level of 172 mbsf. The last occurrence of the nannofossil *Discoaster quinqueramus* indicates that the Miocene/Pliocene contact occurs at 383 mbsf, between Samples 166-1006A-42X-CC and 43X-CC.

All nannofossil and planktonic foraminiferal zones in the upper and middle Miocene are recognized and in general agreement, although some minor discrepancies are noted. The middle/upper Miocene boundary is placed at a level of 567 mbsf between Samples 166-1006A-61X-CC and 62X-CC. The lowest Sample 166-1006A-77X-CC (714.60 mbsf) from the hole yields typical middle Miocene Zone N11 planktonic foraminifers and Zone NN6 nannofossils.

Benthic foraminifers indicate an upper middle bathyal paleodepth (600–800 m) at Hole 1006A. Shallow-water contaminants are rare to absent in core-catcher samples, except for Sample 166-1006A-1H-CC, which contains benthic foraminifers that are predominantly in situ and very shallow-water taxa that constitute <10% of the assemblage.

### Calcareous Nannofossils

Calcareous nannofossils at Site 1006 are moderately to well preserved in the upper Miocene through Pleistocene section, but have varying degrees of preservation in the Miocene interval. Eighty-six samples from Holes 1006A (65 samples), 1006B (19 samples), 1006C (one sample), and 1006D (one sample) were examined for nannofossil stratigraphy.

The Pleistocene is subdivided into three nannofossil zones, NN21–19. The uppermost zone, NN21 (0.25 Ma), is marked by the first appearance of *Emiliania huxleyi*, which occurs between Samples 166-1006B-1H-1, 0–1 cm, and 166-1006A-1H-CC (4.24 mbsf). The last appearance of *Pseudoemiliania lacunosa* defines the base of Zone NN20 (0.41 Ma) and is situated between Samples 166-1006A-2H-CC and 3H-CC (20.53 mbsf). The lowermost Pleistocene zone and longest in duration (0.41–2.0 Ma) is Zone NN19, which is bounded by the last appearance of *P. lacunosa* above and the last appearance of *Discoaster triradiatus* below. The base of NN19 is recognized between Samples 166-1006B-10H-CC and 166-1006A-10H-CC (92 mbsf). Within Zone NN19, several other significant nannofossil events are recognized. The top of *Reticulofenestra asanoi* (0.85 Ma) is placed between Samples 166-1006A-4H-CC and 166-1006B-5H-CC (39.5 mbsf). The total range of large-form (>6 µm) *Gephyrocapsa* spp. (1.20–1.44 Ma) is bounded by Samples 166-1006A-5H-CC and 166-1006B-6H-CC above and Samples 166-1006A-7H-CC and 166-1006B-8H-CC below (48.5–68 mbsf). The Pliocene/Pleistocene boundary is marked by the first appearance of *Gephyrocapsa caribbeanica* (1.72 Ma), which is placed between Samples 166-1006B-10H-CC and 166-1006A-10H-CC (92 mbsf). This datum and the last appearance of *D. triradiatus* indicate that both the Pliocene/Pleistocene (1.72 Ma) and NN18/19 (2.0 Ma) boundaries coincide at Site 1006. At present, we cannot resolve whether this reflects the presence of a minor unconformity or a condensed interval.

Three nannofossil zones subdivide the upper Pliocene. The uppermost zone in the Pliocene is Zone NN18, which is constrained by the last appearances of *D. triradiatus* (2.0 Ma) and *Discoaster pentaradiatus* (2.4 Ma). At Site 1006, this interval occurs between 92 and 120 mbsf and is bounded above by Samples 166-1006B-10H-CC and 166-1006A-10H-CC and below by Samples 166-1006B-13H-CC and 166-1006A-13H-CC. Zone NN17 is short in duration (2.4–2.56 Ma), extending down to Samples 166-1006A-14H-CC and 166-1006B-15H-CC (134 mbsf), and is marked by the last appearance of *Discoaster surculus.* Zone NN16 is the lowermost zone in the upper Pliocene, extending down to the last appearance of *Sphenolithus abies* (3.66 Ma). This datum also defines the upper/lower Pliocene boundary and occurs between Samples 166-1006A-18H-CC and 166-1006B-19H-CC (172.5 mbsf). Within Zone NN16, the last appearance of *Discoaster tamalis* (2.75 Ma) is placed between Samples 166-1006A-16H-CC and 166-1006B-16H-CC.

The lower Pliocene is subdivided into three zones, Zones NN15, NN14–13, and NN12. The interval between the last appearances of *S. abies* and *Amaurolithus* spp. defines NN15 (3.66–4.5 Ma). At Site 1006, this interval occurs from the upper/lower Pliocene boundary at 172 mbsf to 259 mbsf, between Samples 166-1006A-27H-CC and 28H-CC. Zones NN14 and NN13 are combined and are bounded by

last occurrence of *Amaurolithus* spp. above and the first appearance of *Ceratolithus rugosus* (4.7 Ma). At Site 1006, the base of Zone NN14–13 was found between Samples 166-1006A-35X-CC and 36X-CC (326 mbsf). Within the short duration of NN14–13 (0.2 Ma), more than 60 m of sediment accumulated. The base of Zone NN12 at the Miocene/Pliocene boundary is defined by the last appearance of *Discoaster quinqueramus* (5.6 Ma) and occurs between Samples 166-1006A-42X-CC and 43X-CC (383 mbsf).

At Site 1006, well-preserved specimens of *D. quinqueramus* and *Discoaster berggrenii*, marker species for upper Miocene Zone NN11, were found in contrast to the slope Sites 1003 and 1005. The total range of both species (5.6–8.6 Ma) defines Zone NN11, which extends from the Miocene/Pliocene boundary (383 mbsf) to 501 mbsf, between Samples 166-1006A-54X-CC to 55X-CC. Rare specimens of *D. quinqueramus* are present in Samples 166-1006A-38X-CC, 40X-CC, and 42X-CC. However, these samples also contain the middle Miocene species *Discoaster neorectus* and *Discoaster calcaris*, indicating that these assemblages are reworked. Therefore, Sample 166-1006A-43X-CC is identified as the highest unequivocal level of *D. quinqueramus*, and hence the top of the Miocene. Within upper Miocene Zone NN11, the top of the small *Reticulofenestra* spp. interval (6.5 Ma) provides another useful datum. This level occurs between Samples 166-1006A-45X-CC and 46X-CC (418 mbsf). The base of this interval is coeval with the base of *D. quinqueramus* in time as well as in depth at Site 1006. In addition, the base of *Amaurolithus primus*, which indicates upper part of Zone NN11, was found in Sample 166-1006A-45X-CC. Zone NN10 ranges from the base of *D. quinqueramus* (8.6 Ma) to the last appearance of *Discoaster hamatus* (9.4 Ma). The base of NN10 is placed between Samples 166-1006A-57X-CC and 59X-CC (530.5 mbsf). The total range of *D. hamatus* defines Zone NN9 (9.4–10.7 Ma). The base of this zone defines the middle/upper Miocene boundary and is found between Samples 166-1006A-61X-CC and 62X-CC.

Middle Miocene Zones NN6 through NN8 are recognized at Site 1006. The first appearance of *Catinaster coalitus* and the last appearance of *Coccolithus miopelagicus* both occur at the NN7/8 boundary (11.3 Ma). This level is identified between Samples 166-1006A-65X-CC and 66X-CC (602.5 mbsf). The base of Zone NN7 (13.2) is marked by the last appearance of *Cyclicargolithus floridanus*. This level is placed between Samples 166-1006A-75X-CC and 76X-CC. Sample 166-1006A-77X-CC, the lowest sample, occurs within Zone NN6.

## Planktonic Foraminifers

Core-catcher samples from Hole 1006A were investigated for planktonic foraminifers. The upper Pliocene to Pleistocene section contains very abundant, well-preserved planktonic foraminifers (Samples 166-1006A-1H-CC through 18H-CC). The lower Pliocene to uppermost Miocene section is expanded and characterized by abundant specimens of planktonic foraminifers with moderately to well-preserved tests. In general, the middle to upper Miocene interval yields common to abundant planktonic foraminifers with preservation that varies from moderate to good. Only in Samples 166-1006A-69X-CC and 70X-CC are the foraminifers rare and poorly preserved.

The youngest identifiable biohorizons are the last occurrences of *Globigerinoides obliquus* (1.3 Ma) and *Globigerinoides extremus* (1.77 Ma), which were found in Samples 166-1006A-8H-CC and 9H-CC, respectively. The lowest level of *Globorotalia truncatulinoides*, marking the base of Zone N22 (2.0 Ma), occurs in Sample 166-1006A-10H-CC. Below this level, we found the last occurrences of the upper Pliocene planktonic foraminifers *Globorotalia exilis* (2.2 Ma; Sample 166-1006A-12H-CC), *Globorotalia miocenica* (2.3 Ma; Sample 166-1006A-13H-CC), *Globorotalia limbata* (2.4 Ma; Sample 166-1006A-15H-CC), and *Dendoglobigerina altispira* (3.0 Ma; Sample 166-1006A-16H-CC). The N20/21 boundary (3.2 Ma) is marked by the first appearance of *Globorotalia tosaensis* and occurs between Samples 166-1006A-16H-CC and 17H-CC (155 mbsf). The lower limit of Zone N20 is placed between Samples 166-1006A-18H-CC and 19H-CC (173 mbsf) on the basis of the first appearance of *Globorotalia miocenica* (3.55 Ma). Coeval with this level is the last appearance of *Globorotalia margaritae* (3.58 Ma).

Lower Pliocene Zones N18 and N19 extend from Samples 166-1006A-19H-CC through 42H-CC; the boundary between Zones N18/19 is tentatively placed between Samples 166-1006A-42X-CC and 43X-CC on the basis of the first occurrence of *Sphaeroidinella dehiscens* (5.2 Ma) in Sample 166-1006A-42X-CC. This species is rare in this region. However, this level coincides with the Miocene/Pliocene boundary and corroborates the placement of the boundary as indicated by the nannofossils (last occurrence of *D. quinqueramus* at 5.6 Ma; see "Calcareous Nannofossils," this section). Within Zone N19, the last appearance of *Globigerina nepenthes* (4.2 Ma) is recorded between Samples 166-1006A-25H-CC and 26H-CC (240 mbsf). The last appearance of *Globorotalia cibaoensis* (4.6 Ma) was found between Samples 166-1006A-38X-CC and 39X-CC (353 mbsf).

The upper Miocene planktonic foraminiferal events of the first occurrences of *Globigerinoides conglobatus* (6.2 Ma) and *G. margaritae* (6.4 Ma) were found between Samples 166-1006A-47X-CC and 48X-CC (436 mbsf) and Samples 166-1006A-49X-CC and 50X-CC (455 mbsf), respectively. However, the last appearance of small *Reticulofenestra* spp. (6.5 Ma) occurs much higher, at a level of 419 mbsf (see "Calcareous Nannofossils," this section). Either the first appearances of *G. conglobatus* and *G. margaritae* are older in this area or the age for the top of the last appearance of small *Reticulofenestra* spp. is too young.

The base of *G. extremus* (8.3 Ma) is a useful datum in the upper Miocene because the first appearance of this species is coeval with *Globorotalia plesiotumida*, the marker for the base of Zone N17 (Berggren et al., 1995). At Site 1006, *G. extremus* first appears between Samples 166-1006A-53X-CC and 54X-CC (492 mbsf). The base of Zone N16 is marked by the first appearance of *Neogloboquadrina acostaensis* (10.9 Ma). This event occurs between Samples 166-1006A-64X-CC and 65X-CC (595 mbsf). The last appearance of *Globorotalia mayeri* (11.4 Ma) occurs between Samples 166-1006A-64X-CC and 65X-CC (595 mbsf) as well and defines the N14/15 zonal boundary. The juxtaposition of *N. acostaensis* and *G. mayeri* indicates that Zone N15 is not present at Site 1006 and thus is either missing or condensed. Within Core 166-1006A-65X, there is a series of firmgrounds that is indicative of a break in continuous sedimentation (see "Lithostratigraphy" section, this chapter). The short middle Miocene Zone N13, characterized by the absences of *G. nepenthes* and the *Fohsella* species, was found in Sample 166-1006A-68X-CC. This zone could possibly extend farther downhole, but the preservation of the planktonic foraminifers in the next two lower core-catcher Samples 166-1006A-69X-CC and 70X-CC is not good enough to make a zonal assignment. The interval including Samples 166-1006A-71X-CC through 77X-CC, the lowest part of Hole 1006A, corresponds to Zones N11 and N12, as indicated by the presence of *Fohsella fohsi fohsi*, *Fohsella fohsi robusta*, and *Fohsella lobata* (Zone N12) and *Fohsella praefohsi* (Zone N11).

## Benthic Foraminifers

Shallow-water contaminants are rare to absent in core-catcher samples examined from Hole 1006A, with the exception of Sample 166-1006A-1H-CC. Benthic foraminifers are predominantly in situ in this sample, with very shallow-water taxa constituting <10% of the assemblage. Redeposited foraminifers originated from reefal (e.g., *Asterigerina carinata*), shallow neritic (e.g., *Cibicides lobatulus*, *Elphidium* spp.), and upper bathyal (e.g., *Planulina foveolata*) environments and were deposited with species generally found at middle bathyal and deeper depths (e.g., *Anomalinoides globulosus*, *Cibicidoides robertsonianus*, *Pyrgo murrhina*). The paleobathymetric estimate for the Pleistocene section is upper middle bathyal (600–800 m)

on the basis of the upper depth limit of these taxa (approximately 600 m) and the lower depth limit of *Planulina ariminensis* (approximately 800 m).

Below the Pliocene/Pleistocene boundary, the benthic foraminiferal assemblages have a more open-ocean nature with the presence of deeper water planulinids. These include *Planulina rugosa* and *Planulina wuellerstorfi*, which together with *Cibicidoides compressus*, *C. robertsonianus*, *Hanzawaia mantaensis*, *Melonis pompilioides*, *P. ariminensis*, rare *Planulina dohertyi*, *Plectofrondicularia vaughani*, *Pyrgo murrhina*, and *Siphonina tenuicarinata* indicate that the paleodepth was about 600–800 m, as it is for the overlying Pleistocene section. The shift from planulinids that are typical of open-ocean settings to the more restricted planulinids in the Pleistocene section at Hole 1006A most likely reflects a change in water-mass properties rather than a change in paleodepth.

## Sedimentation Rates

Site 1006 is the most distal site drilled on the Great Bahama Bank transect. Site 1006 is in a basinal position approximately between Cay Sal Bank and Great Bahama Bank. Because of its position farthest from Great Bahama Bank, the sedimentary record at Site 1006 should be less influenced by platform-derived material. Sediments recovered from Hole 1006A provide a record that is generally continuous from the upper Pleistocene through the middle Miocene. Lowermost Sample 166-1006A-77X-CC, 0–2 cm, (714.62 mbsf) contains calcareous fossils characteristic of planktonic foraminiferal Zone N11 and nannofossil Zone NN6 (13.2–13.6 Ma). The nannofossil and planktonic foraminiferal biostratigraphic events are listed in Tables 2 and 3.

The sedimentation rate varies considerably at Site 1006. On the basis of core-catcher samples, the section at Site 1006 can be divided into four distinct periods within the biochronological framework (Fig. 9). The sedimentation rate for the upper Pliocene-Pleistocene section (0–3.5 Ma) was 5 cm/k.y. Unlike at Sites 1003 and 1005 on the slope, where sedimentation rates increased substantially during the last 1 m.y., the sedimentation rate remained constant at Site 1006, which is one-third of the rate observed at Site 1005 and one-half of the rate observed at Site 1003. The increased sedimentation rates at the slope sites reflect the onset of major platform production and export to the more distal lower platform. Accordingly, platform-derived benthic foraminifers are most abundant at proximal Site 1005 and least abundant at distal Site 1006. The sections spanning 1–3.5 Ma at Sites 1003 and 1005 show a slow, essentially pelagic, sedimentation

**Table 2. Calcareous nannofossil bioevents.**

| Event | Age (Ma) | Interval (cm) | Depth* (mbsf) |
|---|---|---|---|
| B *E. huxleyi* (NN20/21) | 0.25 | 1006B-1H-1, 0–1, to 1006A-1H-CC | 4.24 |
| T *P. lacunosa* (NN19/20) | 0.41 | 1006A-2H-CC to 1006A-3H-CC | 20.53 |
| T *R. asanoi* | 0.85 | 1006A-4H-CC to 1006B-5H-CC | 39.53 |
| T *Gephyrocapsa* spp. (large) | 1.20 | 1006A-5H-CC to 1006B-6H-CC | 48.49 |
| B *Gephyrocapsa* spp. (large) | 1.44 | 1006A-7H-CC to 1006B-8H-CC | 68.03 |
| B *G. caribbeanica* (NN18/19) | 1.72 | 1006B-10H-CC to 1006A-10H-CC | 91.78 |
| T *D. pentaradiatus* | 2.4 | 1006B-13H-CC to 1006A-13H-CC | 120.28 |
| T *D. surculus* | 2.56 | 1006A-14H-CC to 1006B-15H-CC | 134.33 |
| T *D. tamalis* | 2.75 | 1006A-16H-CC to 1006B-16H-CC | 148.78 |
| T *R. pseudoumbilicus* (NN15/16) | 3.66 | 1006A-18H-CC to 1006B-19H-CC | 172.53 |
| T *Amaurolithus* spp. | 4.5 | 1006A-27H-CC to 1006A-28H-CC | 258.62 |
| B *C. rugosus* | 4.7 | 1006A-35X-CC to 1006A-36X-CC | 325.98 |
| T *D. quinqueramus* (NN11/12) | 5.6 | 1006A-42X-CC to 1006A-43X-CC | 383.42 |
| T small *Reticulofenestra* int. | 6.5 | 1006A-45X-CC to 1006A-46X-CC | 417.80 |
| B *D. quinqueramus* (NN10/11) | 8.6 | 1006A-54X-CC to 1006A-55X-CC | 500.95 |
| T *D. hamatus* (NN9/10) | 9.4 | 1006A-57X-CC to 1006A-59X-CC | 530.48 |
| B *D. hamatus* (NN8/9) | 10.7 | 1006A-61X-CC to 1006A-62X-CC | 567.45 |
| B *C. coalitus* (NN7/8) | 11.3 | 1006A-65X-CC to 1006A-66X-CC | 602.51 |
| T *C. floridanus* (NN6/7) | 13.2 | 1006A-75X-CC to 1006A-76X-CC | 696.27 |

Notes: B = base, T = top. * = average depth for the interval; for actual interval depth, see coring summary on CD-ROM. Average depth was used for constructing Figure 9.

**Table 3. Planktonic foraminiferal bioevents.**

| Event | Age (Ma) | Interval (cm) | Depth* (mbsf) |
|---|---|---|---|
| T *G. obliquus* | 1.3 | 1006A-7H-CC to 1006A-8H-CC | 69.35 |
| T *G. extremus* | 1.77 | 1006A-8H-CC to 1006A-9H-CC | 88.20 |
| B *G. truncatulinoides* (N21/22) | 2.0 | 1006A-10H-CC to 1006A-11H-CC | 97.69 |
| T *G. exilis* | 2.2 | 1006A-11H-CC to 1006A-12H-CC | 107.18 |
| T *G. miocenica* | 2.3 | 1006A-12H-CC to 1006A-13H-CC | 116.80 |
| T *G. limbata* | 2.4 | 1006A-14H-CC to 1006A-15H-CC | 135.36 |
| T *D. altispira* | 3.09 | 1006A-15H-CC to 1006A-16H-CC | 145.42 |
| B *G. tosaensis* (N20/21) | 3.2 | 1006A-16H-CC to 1006A-17H-CC | 154.78 |
| B *G. miocenica* (N19/20) | 3.55 | 1006A-18H-CC to 1006A-19H-CC | 173.25 |
| T *G. margaritae* | 3.58 | 1006A-18H-CC to 1006A-19H-CC | 173.25 |
| T *G. nepenthes* | 4.18 | 1006A-25H-CC to 1006A-26H-CC | 240.28 |
| T *G. cibaoensis* | 4.6 | 1006A-38X-CC to 1006A-39X-CC | 352.68 |
| B *S. dehiscens* (N17/18) | 5.2 | 1006A-42X-CC to 1006A-43X-CC | 383.42 |
| B *G. conglobatus* (N16/17) | 6.2 | 1006A-47X-CC to 1006A-48X-CC | 436.04 |
| B *G. margaritae* | 6.4 | 1006A-49X-CC to 1006A-50X-CC | 454.96 |
| B *G. cibaoensis* | 7.7 | 1006A-52X-CC to 1006A-53X-CC | 483.07 |
| B *G. extremus* | 8.1 | 1006A-53X-CC to 1006A-54X-CC | 492.05 |
| B *N. acostaensis* (N15/16) | 10.9 | 1006A-64X-CC to 1006A-65X-CC | 595.39 |
| T *G. mayeri* (N14/15) | 11.4 | 1006A-64X-CC to 1006A-65X-CC | 595.39 |
| B *G. nepenthes* (N13/14) | 11.8 | 1006A-67X-CC to 1006A-68X-CC | 625.08 |
| T *Fohsella* (N12/13) | 11.9 | 1006A-68X-CC to 1006A-71X-CC | 639.96 |
| B *Fohsella fohsi* (N11/12) | 12.7 | 1006A-73X-CC to 1006A-74X-CC | 682.02 |

Notes: B = base, T = top. * = average depth for the interval; for actual interval depth, see coring summary on CD-ROM. Average depth was used for constructing Figure 9.

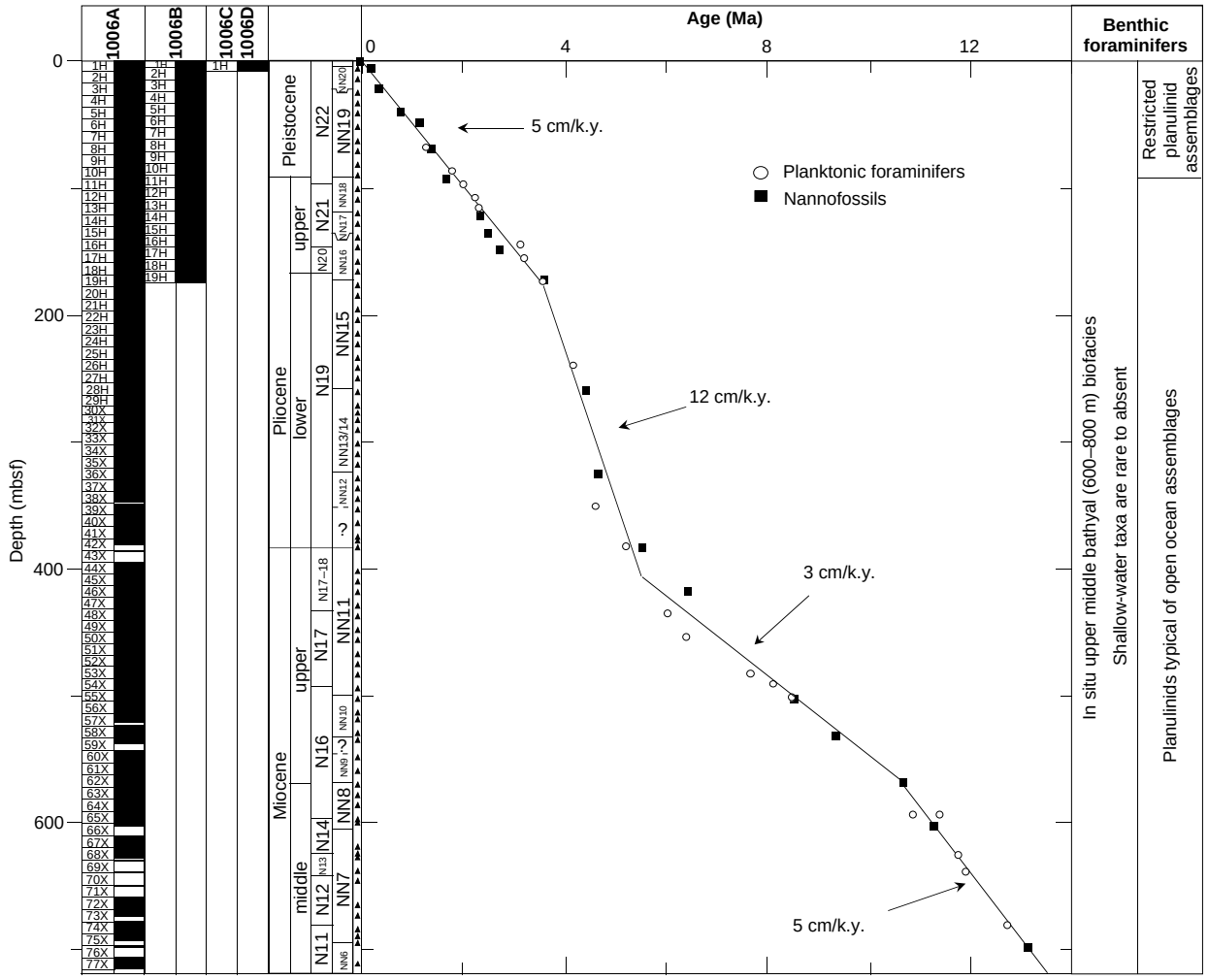


Figure 9. Calcareous nannofossil and planktonic foraminiferal zonation and benthic foraminiferal faunal changes for Site 1006. Recovery for each hole is adjacent to the cores. Solid triangles mark the position of samples examined for stratigraphy and benthic foraminiferal faunas. The age-depth plot is based on the biohorizons in Table 2.

rate (2–2.5 cm/k.y.). In contrast, the sedimentation rate at Site 1006 is twice as high as at coeval levels at the upper slope sites, indicating a different depositional mechanism at Site 1006. The higher sedimentation rate in the basin cannot be the result of platform production and export; therefore, sediment must have been laterally transported to this site by ocean currents (drift deposits).

The sedimentation rate for the lower Pliocene and uppermost Miocene (planktonic foraminiferal Zone N18) is 12 cm/k.y. at Site 1006. Similar sedimentation rates were found during the same period at Sites 1003 and 1005, indicating that the same depositional processes influenced all transect sites. The high sedimentation rate coincides with platform production and shedding to the upper slope (Sites 1003 and 1005). The change from lower Pliocene uniform sedimentation rates at all transect sites to strongly diverging sedimentation rates (highest near the platform site and lowest in the basin) in the middle–late Pleistocene reflects the change from a ramp-type platform to a flat-topped platform (Reijmer et al., 1992).

The upper Miocene has a low sedimentation rate (3 cm/k.y.) that is within the range of normal pelagic deposition. The large hiatus at Sites 1003 and 1005 is not present at Site 1006. Slightly higher sedimentation rates (5 cm/k.y.) in the middle Miocene could be accounted for by higher pelagic productivity, contourite deposition, and/or deposition of fine-grained platform-derived material. Coeval sedimentation rates were much higher closer to the platform at Sites 1003 and 1005, indicating that material was shed from the platform at this time. In addition, contourite deposition may have migrated up- or downslope at different times, resulting in the sedimentation rate changes observed at Site 1006.

## PALEOMAGNETISM

Shipboard paleomagnetic measurements were conducted at Hole 1006A, 1006B (Core 1H) and Hole 1006D (Core 1H) on the archive-half of cores at 10- or 20-cm intervals. Measurements, using a whole-core cryogenic magnetometer with in-line AF demagnetizer, were made of the natural remanent magnetization (NRM), and the response of the sediment to a combination of demagnetization steps was recorded. The NRM values ranged from 87.51 to 0.14 mA/m, with an average intensity of 1.38 mA/m (Fig. 10). However, only 40% of the NRM intensities were above the lower limit of the magnetometer's sensitivity range (>1.0 mA/m).

Demagnetization steps of 5 and 15 mT were applied to Cores 166-1006A-1H through 19H. By 15 mT, the NRM was typically reduced by 40%, with intensities varying from 50.69 to 0.074 mA/m (with an average value of 0.40 mA/m). The NRM of Cores 166-1006B-1H and

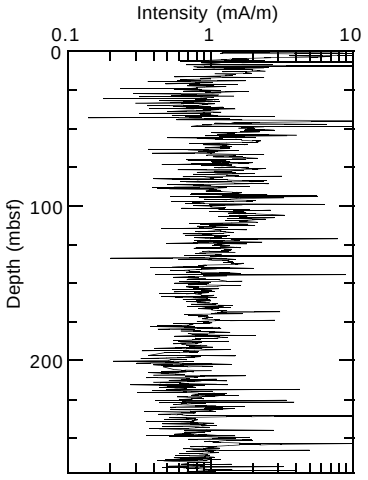


Figure 10. Archive-half NRM intensity for the interval from 0 to 272.55 mbsf in Hole 1006A.

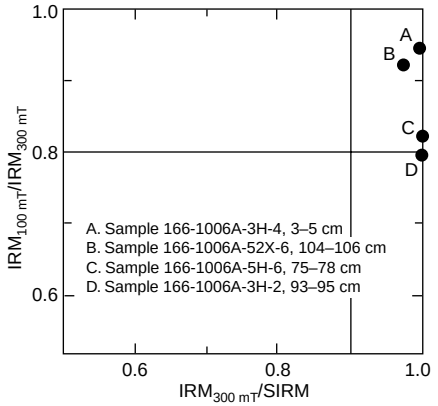


Figure 11. Plot of $IRM_{300\ mT}$/SIRM vs. $IRM_{100\ mT}/IRM_{300\ mT}$ for samples taken from the working half of Cores 166-1006A-3H, 5H, and 52X. All the data are closely grouped and plot within the single-domain magnetite region of the plot, suggesting little variation in grain size or composition. However, it is possible to divide the data into subgroups of carbonate-dominated sediment (A and B) and clay-dominated sediment (C and D).

166-1006D-1H were measured, and intensity values were found to range from 30.63 to 0.93 mA/m (with a mean value of 10.88 mA/m). These cores were then subjected to demagnetization fields of 2, 4, 6, 8, 10, 15, 20, and 25 mT, with the NRM intensity decreasing to between 9.07 and 0.11 mA/m (with an average value of 1.833 mA/m) by 25 mT.

Saturation isothermal remanent magnetization (SIRM) acquisition tests were conducted on individual samples from the working-half of Cores 166-1006A-3H, 5H, and 52X (clay Sample 166-1006A-3H-2, 93–95 cm; nannofossil ooze Sample 166-1006A-3H-4, 3–5 cm; clay Sample 166-1006A-5H-6, 75–78 cm; and nannofossil chalk Sample 166-1006A-52X-6, 104–106 cm), indicating that, throughout Hole 1006A, the remanence is carried by single-domain magnetite (Fig. 11) with little variation in grain size or composition, irrespective of lithology.

The magnetic susceptibility records for Hole 1006A, 1006B, 1006C, and 1006D were measured on the whole-core MST at 10-cm intervals, which revealed a signal that fluctuated in a cyclic manner between a minimum negative value of −4.2 and a maximum positive value of 39.7 (Fig. 12, corrected for spikes at core boundaries).

Because the susceptibility of a natural material is mainly a consequence of magnetite content, susceptibility can be used as a surrogate measure of magnetite concentration. The uniform nature of ferrimagnetic grains at Site 1006 suggests that the susceptibility record is a product of changing levels of preservation or dilution of ferrimagnetic material, or that the susceptibility record reflects periods of increasing/decreasing clastic input (clay) of similar source. Furthermore, the poor correlation between magnetic susceptibility and NRM intensity suggests that a paramagnetic component, as well as a ferrimagnetic component, have contributed to the magnetic susceptibility record. This implies that variations in clastic input are responsible for the susceptibility fluctuations observed at Site 1006.

Variations in magnetic inclination during the demagnetization of Core 166-1006A-1H have enabled the tentative definition of a polarity event at Site 1006 (Fig. 13). Inclination values from Core 166-1006A-1H, before being demagnetized, ranged from 85° to −17°, with an average value of 55°. Less than 0.5% of the NRM values possessed negative inclinations, indicating a dominantly normal polarity NRM component. Demagnetization at 5 and 15 mT caused a reduction in inclination of approximately 50°, with an increase of negatively inclined measurement intervals (38%). Between 0.25 and 2.15 mbsf, an average inclination of 38° was observed, suggesting an interval of normal polarity. Eighty-five percent of the negatively inclined measurement intervals were located between 2.35 and 4.95

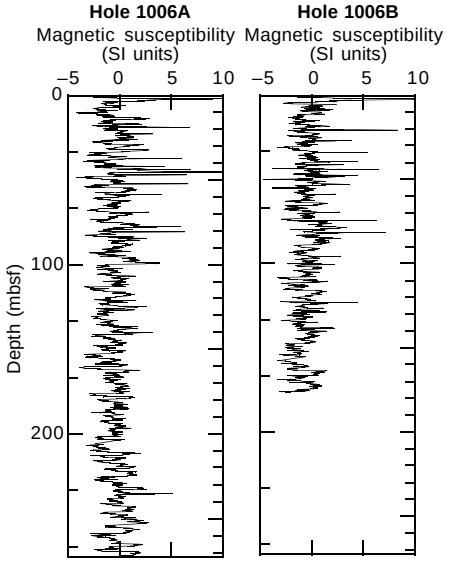


Figure 12. Plots of magnetic susceptibility for APC cores at Holes 1006A and 1006B. Good correlation exists between the separate records, with high positive values coinciding with clay layers between 0 and 150 mbsf.

mbsf, defining a 2.6-m-thick interval of reversed polarity. However, application of an intensity-based reliability threshold for directional data (>1.0 mA/m) reduced the thickness of this reversal by approximately 50% to 1.1 m. Furthermore, a combination of axial bias within the magnetometer and the inability to orient the core made determination of declination impossible. Below this zone, magnetic inclination became positive, implying an interval of normal polarity (Brunhes). Further polarity determination was not attempted in Hole 1006A because magnetic intensity became too low. Attempts to define this reversed polarity event in Cores 166-1006B-1H and 166-1006D-1H failed because a maximum demagnetization field of 25 mT was unable to resolve the primary magnetization component.

The proposed reversal/excursion has been correlated with the Blake Event (0.13 Ma), based upon the first occurrence of the nannofossil *Emiliania huxleyi*, which appears between 4.5 and 6.0 mbsf (0.25 Ma) in Sample 166-1004A-1H-CC, 0–1 cm.

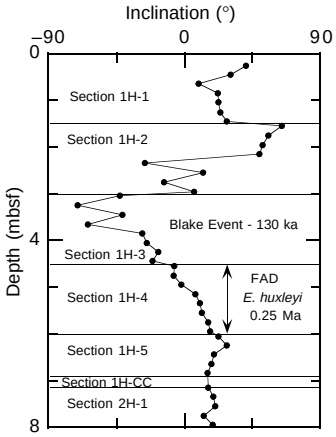


Figure 13. Magnetic inclination vs. depth (mbsf) in Sections 166-1006A-1H-1 through 1H-5 and in Section 166-1006A-2H-1. A reversed polarity event can be defined on the basis of variations in inclination. No declination control exists. Application of an intensity-based reliability threshold for directional data of 1.0 mA/m reduces the thickness of this event by 50%. This polarity event has been correlated with the Blake Event, based on the first occurrence of nannofossil *Emiliania huxleyi.*

## COMPOSITE SECTION

The continuity of the sedimentary section at Site 1006 was evaluated by correlating high-resolution multisensor track (MST) data collected on whole cores and percent color reflectance data collected on split cores from Holes 1006A and 1006B (Fig. 14). The MST measures magnetic susceptibility, GRAPE, natural gamma ray, and *P*-wave velocities. Records from Holes 1006C and 1006D were also examined, although each hole consists of only a single core. Downcore color reflectance data maintain a strong coherence between the holes, but a significant data gap (20 m) in the reflectance record (Cores 166-1006B-7H and 8H were not measured) renders correlations below this depth uncertain. In addition, the sampling interval increased from the standard 10-cm interval to a 25-cm interval in several cores in Hole 1006B (Cores 166-1006B-4H, 5H, 6H, 9H, 10H), resulting in the lower resolution of correlatable data in these cores. Hole to hole correlation below 54 mbsf therefore was based primarily on the magnetic susceptibility data. Natural gamma ray (NGR) and GRAPE data were used to improve correlations.

Overlap of the sedimentary events in the cored intervals at each hole is necessary to correlate the cores. Offset of the second hole, relative to the first, is achieved by coring a short first core in the second hole to create a drilling offset. Working from the top down, cores are aligned, based on unequivocal sedimentary events identified in both holes. As drilling can result in either gaps between cores or the re-coring of the base of the previous core, positive or negative constants are added to the core depth to align the mbsf depths for each hole to calculate the composite depth. The aligned records are then spliced together to create a composite section (Table 4), so that features that may not have been cored in one hole are patched into the spliced record from the other core. This results in a stratigraphically complete composite of the events in both cores that is used as a guide for sampling to ensure complete coverage of all stratigraphic events, and for comparison to the log data.

The meters composite depth (mcd) scale grows relative to the mbsf depth scale, because core expansion results in core depths that are greater than the 9.5 m recorded by ODP depth convention, and also because offset between cores is compensated for by adding a constant. The growth of the mcd is approximately 5% (Fig. 15; Table 5) at Site 1006. This low growth rate may be a result of the greater incidence of re-coring (negative offsets) or other factors such as the

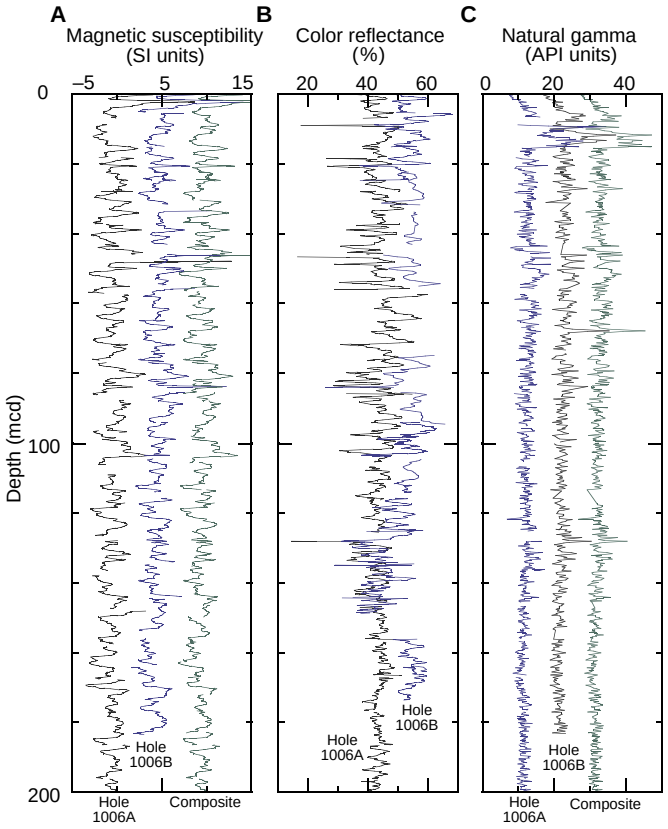


Figure 14. **A.** The magnetic susceptibility for Holes 1006A and 1006B, and the spliced composite record, plotted on the composite depth scale (mcd). The Hole 1006B and composite section records are offset for clarity by 5 units and 10 units, respectively. **B.** The percent color reflectance data for Holes 1006A and 1006B are plotted on the composite depth scale (mcd). The Hole 1006B records are offset for clarity by 10 units. **C.** The natural gamma-ray data from the MST for Holes 1006A and 1006B, and the spliced composite record, plotted on the composite depth scale (mcd). The Hole 1006B and composite section records are offset for clarity by 10 units and 20 units, respectively.

effect of sea state on drilling (see Hagelberg et al., 1992, for a complete discussion of potential effects of drilling methods on recovery).

Visual inspection of the magnetic susceptibility and percent color reflectance data indicates a similar number of cycles in both holes (Fig. 14). The variation in both signals is driven by sedimentation changes (see "Lithostratigraphy" section, this chapter) that are consistent downhole, despite differences in signal strength. No significant gaps in the core are apparent in the correlation between the two holes.

There is some misalignment of events within cores because each core is moved as a whole up and down, relative to cores in the other hole. Positive offsets account for gaps between the cores and add length to the mcd, whereas negative offsets (e.g., between 55 and 60 mcd; Fig. 15) indicate re-coring. Not all of the peaks and troughs can be perfectly aligned by adding a constant to the core because compression and expansion occur differentially along the core length. As a third hole that could verify coring gaps and overlap at the first two holes was not drilled, it is possible that the intervals of lower correlation may be caused by a poor correlation of the records to the composite depth scale.

Sedimentary features present in both cores can be used to improve intervals in which the correlation is ambiguous. For example, the stratigraphic position of Core 166-1006B-4H in Hole 1006B (Fig.

**Table 4. Composite section for Site 1006.**

| Hole | Core | Depth (mbsf) | Depth (mcd) | | Hole | Core | Depth (mbsf) | Depth (mcd) |
|---|---|---|---|---|---|---|---|---|
| A | 1H | 6.15 | 6.15 | tie to | B | 2H | 6.15 | 6.15 |
| B | 2H | 14.45 | 14.45 | tie to | A | 2H | 12.75 | 14.45 |
| A | 2H | 15.45 | 17.15 | tie to | B | 3H | 17.15 | 17.15 |
| B | 3H | 23.25 | 23.25 | tie to | A | 3H | 21.55 | 23.25 |
| A | 3H | 22.95 | 24.65 | tie to | B | 3H | 24.65 | 24.65* |
| B | 3H | 32.85 | 30.45 | tie to | A | 4H | 28.85 | 30.45 |
| A | 4H | 35.25 | 36.86 | tie to | B | 5H | 37.25 | 36.86 |
| B | 5H | 42.39 | 42.00 | tie to | A | 5H | 40.4 | 42.00 |
| A | 5H | 44.35 | 45.96 | tie to | B | 6H | 43.55 | 45.96 |
| B | 6H | 47.26 | 49.67 | tie to | A | 6H | 46.86 | 49.67 |
| A | 6H | 53.85 | 56.66 | tie to | B | 6H | 53.85 | 56.66 |
| B | 6H | 57.55 | 60.36 | tie to | A | 6H | 57.55 | 60.36 |
| A | 7H | 63.45 | 66.26 | tie to | B | 8H | 63.85 | 66.26 |
| B | 8H | 67.45 | 69.86 | tie to | A | 8H | 67.05 | 69.86 |
| A | 8H | 72.15 | 74.96 | tie to | B | 9H | 72.55 | 74.96 |
| B | 9H | 80.75 | 83.16 | tie to | A | 9H | 79.95 | 83.16 |
| A | 9H | 82.67 | 85.88 | tie to | B | 10H | 82.05 | 85.88 |
| B | 10H | 84.25 | 88.08 | tie to | A | 10H | 83.55 | 88.08 |
| A | 10H | 91.95 | 96.48 | tie to | B | 11H | 93.35 | 96.48 |
| B | 11H | 94.95 | 98.08 | tie to | A | 11H | 94.05 | 98.08 |
| A | 11H | 101.53 | 105.56 | tie to | B | 12H | 101.75 | 105.56 |
| B | 12H | 109.55 | 113.36 | tie to | A | 12H | 106.55 | 113.36 |
| A | 13H | 119.75 | 125.22 | tie to | B | 14H | 120.14 | 125.22 |
| B | 14H | 127.05 | 132.13 | tie to | A | 14H | 125.55 | 132.13 |
| A | 14H | 128.65 | 135.23 | tie to | B | 15H | 129.65 | 135.23 |
| B | 15H | 137.65 | 143.23 | tie to | A | 15H | 135.95 | 143.23 |
| A | 15H | 139.25 | 146.53 | tie to | B | 16H | 140.75 | 146.53 |
| B | 16H | 143.95 | 149.73 | tie to | A | 16H | 141.75 | 149.73 |
| A | 16H | 149.05 | 157.03 | tie to | B | 17H | 148.95 | 157.03 |
| B | 17H | 154.65 | 162.73 | tie to | A | 17H | 154.26 | 162.73 |
| A | 17H | 158.83 | 167.3 | tie to | B | 18H | 160.73 | 167.3 |
| B | 18H | 165.54 | 172.13 | tie to | A | 18H | 163.65 | 172.13 |
| A | 18H | 168.35 | 176.83 | tie to | B | 19H | 169.85 | 176.83 |
| B | 19H | 176.05 | 183.03 | tie to | A | 19H | 174.55 | 183.03 |

Note: Negative offset (re-coring) creates an overlap between successive cores in the same hole and is marked with an asterisk. To ensure complete stratigraphic coverage for the site, sampling should occur within the intervals shown.

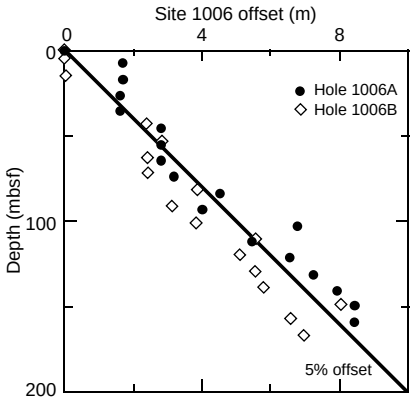


Figure 15. Offset from the mbsf depth scale, or amount added to the conventional depth scale (mbsf) for correlation on the mcd. Note the low (approximately 5%) growth.

16) is not clear from the magnetic susceptibility data alone, but upon integration of the clay layers, the correlation is improved. Cyclic sedimentation patterns are recorded in both the magnetic susceptibility and the color reflectance records at Site 1006. The base of each cycle is marked by a layer with high clay content (see "Lithostratigraphy" section, this chapter). Low color reflectance (see "Lithostratigraphy" section, this chapter) and high magnetic susceptibility values are measured at these levels. Clay layers (2–35 cm thick) were identified in core photographs, and the cores were compared. Thick clay layers remain consistent between the two holes, whereas some thin layers (<1 cm) seem not to be present in both holes. The thick clay layers were thus plotted on the composite depth scale and used to verify the correlation of Holes 1006A to 1006B (Fig. 16). The correlation of the

**Table 5. The offset of Hole 1006B relative to Hole 1006A.**

| | 1006A | | 1006B | |
|---|---|---|---|---|
| Core | Depth (mbsf) | Offset | Depth (mbsf) | Offset |
| 1 | 0.00 | 0.00 | 0.00 | 0.00 |
| 2 | 7.10 | 1.70 | 5.50 | 0.00 |
| 3 | 16.60 | 1.70 | 15.00 | 0.00 |
| 4 | 26.10 | 1.61 | 24.50 | –2.40 |
| 5 | 35.60 | 1.61 | 34.00 | –0.39 |
| 6 | 45.10 | 2.81 | 43.50 | 2.41 |
| 7 | 54.60 | 2.81 | 53.00 | 2.81 |
| 8 | 64.10 | 2.81 | 62.50 | 2.41 |
| 9 | 73.60 | 3.21 | 72.00 | 2.41 |
| 10 | 83.10 | 4.53 | 81.50 | 3.83 |
| 11 | 92.60 | 4.03 | 91.00 | 3.13 |
| 12 | 102.10 | 6.81 | 100.50 | 3.81 |
| 13 | 111.60 | 5.47 | 110.00 | 5.57 |
| 14 | 121.10 | 6.58 | 119.50 | 5.08 |
| 15 | 130.60 | 7.28 | 129.00 | 5.58 |
| 16 | 140.10 | 7.98 | 138.50 | 5.78 |
| 17 | 148.60 | 8.47 | 148.00 | 8.08 |
| 18 | 159.10 | 8.48 | 157.50 | 6.57 |
| 19 | | | 167.00 | 6.98 |

Note: Add the offset to the depth (mbsf) to determine the meters composite depth (mcd).

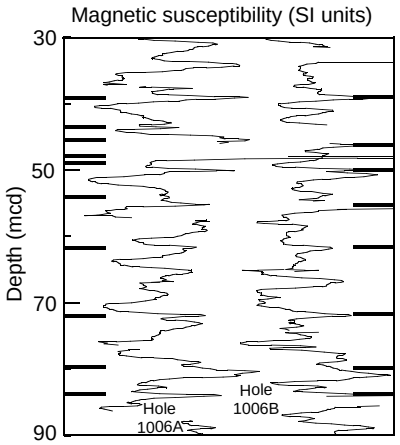


Figure 16. Calibration of the Site 1006 correlation using clay layers. The magnetic susceptibility records for Holes 1006A and 1006B are compared to clay layers (black bars) identified from the core.

clay layers between holes, especially below 50 mcd, is remarkable. Eight clay layers are found in both Holes 1006A and 1006B at equivalent depths and in association with peaks in magnetic susceptibility. Each magnetic susceptibility peak is not necessarily associated with a thick, dark clay layer, but those peaks that are correlated to clay layers are consistent between holes over approximately 30 m. The only exceptions are the clay horizons at 43 and 45 mcd at Hole 1006A. These peaks are defined by sets of clay layers rather than by individual events as at Hole 1006B (Fig. 16), and may represent a succession of thin layers. The lack of correlation of the thin clay layers suggests that either the finer layers represent sporadic depositional events that are unrelated to higher frequency cyclicity, or that the deviation in correlation is process driven. That is, the clay layers are produced by scour and subsequent deposition, which results in an undulatory surface (see "Lithostratigraphy" section, this chapter).

A final test of the continuity of recovery is the correlation of core data with the log data (Fig. 17). The natural gamma ray measurements from the core and the log are in good general agreement, but the low gamma ray values below approximately 15 mbsf, in combination with data gaps in the log data, prevent high-resolution comparisons. The gaps are present because the NGR log data in the upper 100 m were collected through the drill pipe, so the very low gamma

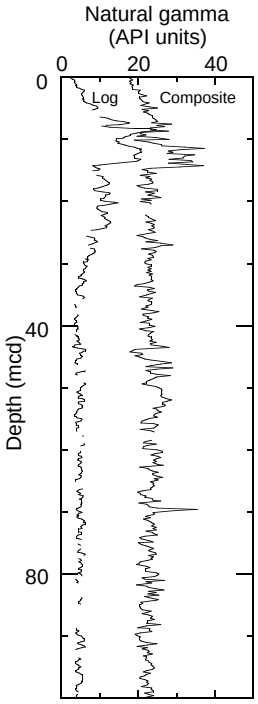


Figure 17. Comparison of the upper 100 m of the composite section and log measurements of natural gamma-ray data. Meaningful comparison between the log and the MST gamma-ray data requires that the mcd be converted to a mbsf depth scale. Compression of the composite depth scale was approximated with a simple linear transformation.

values that occur when the data are collected through the drill collar (approximately every 10 m) were removed from the data.

## ORGANIC GEOCHEMISTRY

At Site 1006, the shipboard organic geochemistry program included determinations of inorganic carbon, total carbon, total nitrogen, total sulfur, and Rock-Eval pyrolysis, in addition to safety monitoring for hydrocarbon gases. The analytical procedures are described in the "Explanatory Notes" chapter (this volume).

### Volatile Hydrocarbons

At Site 1006, methane ($C_1$) concentrations are low (2–11 ppm) between 0 and 143.1 mbsf. Below this depth, methane shows a steady increase from 26 to 25,295 ppm at 712.2 mbsf (Table 6 on CD-ROM; Fig. 18). Ethane ($C_2$) was detected at 171.5 mbsf (Table 6). The $C_1/C_2$ ratio increases from 355 at 171.5 mbsf to 1470 at 190.6 mbsf. Below 190.6 mbsf, $C_1/C_2$ gradually decreases to a low of 200 at the base of the hole (Fig. 18).

Propane ($C_3$) was first detected at 228.6 mbsf at Site 1006 (Fig. 18). Below 306.1 mbsf, trace levels (0.2–5 ppm) of isobutane, *n*-butane, isopentane, and *n*-pentane (Table 6) were also present in the samples. An increase in heavy-weight hydrocarbons (up to 18 ppm of isopentane) and propane below 630.6 mbsf was also observed (Fig. 18).

### Inorganic and Organic Carbon, Total Sulfur, and Total Nitrogen

Carbonate data for Site 1006 are presented in Figure 19 and in Table 7 on CD-ROM. The carbonate content ranges between 80 and 90

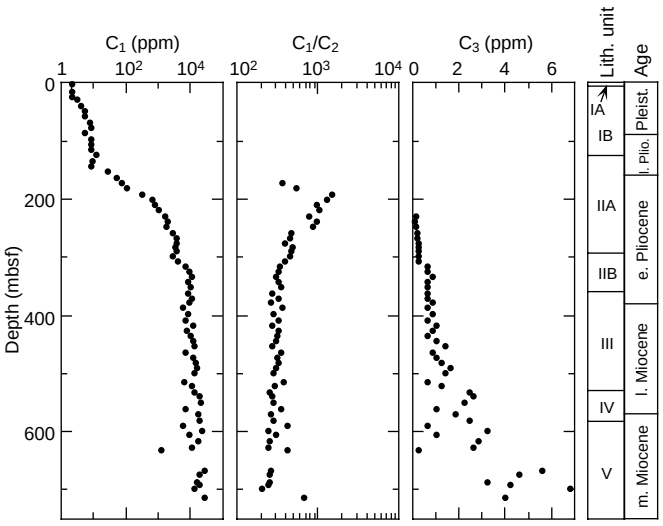


Figure 18. Concentration of methane ($C_1$), methane/ethane ($C_1/C_2$), and propane ($C_3$) of headspace gases from Hole 1006A.

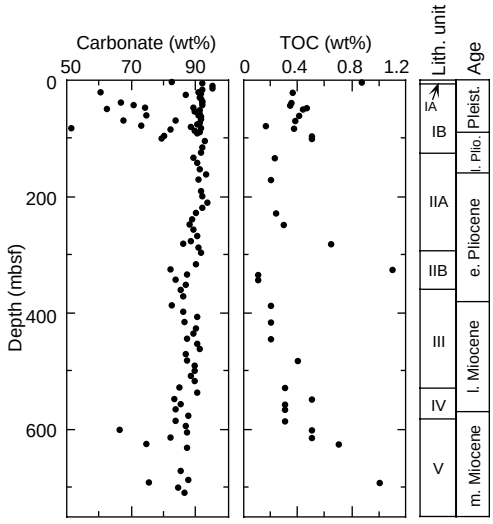


Figure 19. Concentration of carbonate and TOC from Hole 1006A.

wt% for much of the hole; however, lithologic Subunit IB displays a particularly high variation (51.2–94.8 wt%) (Fig. 19).

Thirty-three samples with low carbonate content were selected for analysis of total organic carbon (TOC), total sulfur (TS), and total nitrogen (TN). As a result of combustion problems, the measurements of total sulfur are suspect, and are not presented. Total organic carbon at Site 1006 varies from 0.1 to 1.1 wt% with the highest concentrations (>1.0 wt%) observed in lithologic Subunits IIB (323.4 mbsf) and IVC (690.3 mbsf) (Fig. 19B). Systematic increases in the TOC content with depth are observed within lithologic Units II and IV. Less well constrained TOC variations are observed within lithologic Units I and III. Total nitrogen concentrations are low (0.00–0.15 wt%) and generally below detection limits (<0.1 wt%; Table 7).

### Characterization and Maturity of Organic Matter

Seven samples with TOC values greater than 0.5 wt% from Site 1006 were characterized by Rock-Eval pyrolysis. The results are reported in Table 8 on CD-ROM. $T_{max}$ values range from 311° to

430°C. At Site 1006, the hydrogen index (HI) increases from 3 mg HC/g TOC at 1.9 mbsf to 305 mg HC/g TOC at 690.3 mbsf (Table 8 on CD-ROM).

## Discussion

The increase in methane concentrations in the upper part of Site 1006 corresponds to a decrease in sulfate concentrations in the pore water (see "Inorganic Geochemistry" section, this chapter). Ethane was detected at the base of the sulfate reduction zone (172 mbsf) and the high $C_1/C_2$ ratio above 190 mbsf indicates a high amount of biogenic methane production. The organic matter content within the sulfate reduction and methanogenesis zones (roughly coinciding with lithologic Subunits IA and IB) is low and the organic matter is characterized by low HI values (<70 mg HC/g TOC). The low HI values indicate that most of the organic matter has been largely oxidized and is therefore refractory in nature. The organic matter of lithologic Unit IV is characterized by increasing HI values (80–305 mg HC/gTOC from the top (545.8 mbsf) to the base of the unit (690.3 mbsf).

The increase in HI values through lithologic Unit IV may result from more efficient oxygenation of the organic matter leading to low HI values or from a differential origin of the organic matter between the top and base.

The low $T_{max}$ values at Site 1006 indicate that the organic matter is immature with regard to petroleum formation. The presence of trace levels of heavy-weight hydrocarbons and the low $C_1/C_2$ ratio below 190.6 mbsf indicates the migration of thermogenic hydrocarbon gases. The increase in heavy-weight hydrocarbons in the headspace at 660 mbsf coincides with a horizon (640–660 mbsf) characterized by high velocities (see "Downhole Logging" section, this chapter). This horizon is the same high sonic-velocity interval encountered at 735 mbsf at Site 1003 (see "Physical Properties" section, this chapter) where an enrichment in hydrocarbons was observed (see "Organic Geochemistry" section, "Site 1003" chapter, this volume). However, the concentrations of hydrocarbons at Site 1006 are significantly less than at Site 1003. In addition, the hydrocarbons at Site 1006 are dominated by the light hydrocarbons ($C_1$–$C_3$), whereas at Site 1003 the headspace hydrocarbons are dominated by heavier components ($C_3$–$C_5$). These differences might be related to differential migration of the light hydrocarbons relative to heavy hydrocarbon gases between the two sites.

# INORGANIC GEOCHEMISTRY

The inorganic geochemistry at Site 1006 followed procedures described in the "Inorganic Geochemistry" section of the "Explanatory Notes" chapter (this volume). Interstitial water samples were collected at a frequency of two per core in the first three cores, one per core down to Core 166-1006A-35X, and once every three cores for the remainder of the hole (a total of 52). Approximately 180 sediment samples were subjected to quantitative X-ray diffraction (XRD) analysis of their carbonate mineralogy.

Concentrations of interstitial water constituents are given in Table 9, and depth profiles are shown in Figure 20. In Figure 21, selected elemental profiles have been reported relative to $Cl^-$ (to account for large changes in salinity downcore) or $Ca^{2+}$ (to illustrate diagenetic trends). Mineralogical data were corrected to include the noncarbonate fraction as determined by carbonate analysis (see "Organic Geochemistry" section, this chapter). These are presented in Table 10 on CD-ROM and Figure 22.

## Interstitial Waters

### *Salinity, Chloride, Sodium, and Potassium*

The conservative parameters salinity, chloride ($Cl^-$), and sodium ($Na^+$) exhibit little change in the first 20 mbsf of Hole 1006A, and subsequently increase to approximately 1.5 times seawater values at 711 mbsf (Fig. 20). Although $Na^+$ displays a primarily diffusional profile downcore, its behavior deviates slightly from purely conservative behavior. This is shown by the $Na^+/Cl^-$, which initially increases above the seawater value of 0.85 to 0.89 at approximately 200 mbsf, then decreases downhole to 0.82 (Fig. 21). A previous observation of such behavior at Site 823 off northeast Australia was attributed to reactions involving clay minerals (Davies, McKenzie, Palmer-Julson, et al., 1991).

Dissolved potassium ($K^+$) is nonconservative at Site 1006, exhibiting a linear concentration gradient of approximately –0.01 mM/m downcore. Decreases in the $K^+/Cl^-$ downcore are greater in the first 300 mbsf than farther downcore (Fig. 21). At 711 mbsf, the $K^+$ concentration (~7 mM) represents a threefold depletion relative to a fluid with a seawater $K^+/Cl^-$. This $K^+$ depletion is also attributed to uptake of $K^+$ during reactions involving clay minerals.

### *Calcium, Magnesium, Strontium, and Lithium*

Little change in the concentrations of calcium ($Ca^{2+}$), magnesium ($Mg^{2+}$), and lithium ($Li^+$) occurs in the upper 20 mbsf of Site 1006 (Fig. 20). Dissolved strontium ($Sr^{2+}$), however, increases from a mudline value of 150 to 200 µM within the first 20 mbsf. Dissolved $Ca^{2+}$ concentrations immediately below the mudline (~9.4 mM) are already depleted relative to local seawater; they decrease further between 20 and 134 mbsf to 7.6 mM, but subsequently increase downcore to a maximum of 19.3 mM at 711 mbsf. The $Ca^{2+}$ profile below 134 mbsf is characterized by at least four zones delimited by boundaries at 250, 370, and 515 mbsf that correspond to lithologic transitions between the major units (see "Lithostratigraphy" section, this chapter). Another less pronounced zone may also exist below 630 mbsf within lithologic Unit V. The $Ca^{2+}/Cl^-$ indicates that $Ca^{2+}$ is depleted above 300 mbsf and slightly enriched below this depth at Site 1006 (Fig. 21).

The dissolved-$Mg^{2+}$ profile at Site 1006 is characterized by a sharp decrease from 54.5 mM at 20 mbsf to approximately 26 mM at 240 mbsf. Below this depth, concentrations increase gradually to 37 mM at 711 mbsf. The $Mg^{2+}/Cl^-$ indicates that $Mg^{2+}$ is depleted throughout the core (Fig. 21). Between 20 and 340 mbsf, the $Mg^{2+}/Ca^{2+}$ decreases by more than two-thirds, from 5.8 to 1.8, and then exhibits a very gradual rise to 2.3 near 530 mbsf before returning to 1.9 at the bottom of the hole (Fig. 21).

The $Sr^{2+}$ concentration profile (Fig. 20) increases noticeably below 20 mbsf, reaching a broad maximum of 6500–7000 µM centered at about 480 mbsf. The Li profile is relatively flat in the upper 20 mbsf, subsequently displaying a nearly linear increase of approximately 0.49 µM/m to a maximum of 311 µM at 600 mbsf. Dissolved $Sr^{2+}$ and $Li^+$ both decrease slightly below their respective maxima. The peak concentrations of these two constituents at Site 1006 are approximately 70% higher and 25% lower, respectively, than observed at Site 1003 (see "Inorganic Geochemistry" section, "Site 1003" chapter, this volume). This observation suggests that these two elements, although displaying trends that generally track each other at all sites occupied to date, may not be as intimately linked as previously thought (see "Inorganic Geochemistry" section, "Site 1003," "Site 1004," and "Site 1005" chapters).

### *Alkalinity, Sulfate, pmH, Ammonium, and Phosphate*

At Site 1006, a complete depletion of sulfate ($SO_4^{2-}$) occurs between 20 and 200 mbsf and is maintained throughout the remainder of the core, except for several samples that are thought to be contaminated with drill water. Because no $H_2S$ was detected at Site 1006 (see "Organic Geochemistry" section, this chapter) and disseminated pyrite was observed throughout much of the core (see "Lithostratigraphy" section, this chapter), it is likely that the $HS^-$ produced during $SO_4^{2-}$ reduction was consumed by the precipitation of $FeS_2$ or other metastable iron sulfides such as marcasite (Morse and Mackenzie, 1990).

**Table 9. Composition of interstitial waters from Site 1006.**

| Core, section, interval (cm) | Depth (mbsf) | pmH | pH | Alkalinity (mM) | Salinity | $Cl^-$ (mM) | $Na^+$ (mM) | $Mg^{2+}$ (mM) | $Ca^{2+}$ (mM) | $SO_4^{2-}$ (mM) | $HPO_4^{2-}$ (µM) | $NH_4^+$ (µM) | $H_4SiO_4$ (µM) | $K^+$ (mM) | $Li^+$ (µM) | $Sr^{2+}$ (µM) | $F^-$ (µM) | $Fe^{2+}$ (µM) |
|---|---|---|---|---|---|---|---|---|---|---|---|---|---|---|---|---|---|---|
| 166-1006A- | | | | | | | | | | | | | | | | | | |
| 1H-2, 143–150 | 3 | 7.78 | 7.66 | 3.78 | 35.0 | 563 | 481 | 53.7 | 9.4 | 27.1 | 0.0 | 130 | 168 | 10.7 | 30 | 154 | 133 | 12 |
| 1H-4, 128–135 | 6 | 7.71 | 7.57 | 3.06 | 35.0 | 564 | 482 | 53.9 | 9.6 | 27.9 | 0.0 | 120 | 100 | 10.9 | 32 | 138 | 130 | 2 |
| 2H-2, 143–150 | 10 | 7.85 | 7.62 | 2.94 | 35.0 | 560 | 481 | 54.5 | 9.7 | 28.4 | 0.0 | 80 | 60 | 10.2 | 31 | 174 | 138 | 1 |
| 2H-5, 143–150 | 15 | 7.74 | 7.64 | 2.76 | 35.0 | 563 | 482 | 54.3 | 9.3 | 27.5 | 0.0 | 90 | 92 | 10.9 | 31 | 180 | 156 | 1 |
| 3H-2, 143–150 | 20 | 7.66 | 7.61 | 2.89 | 35.5 | 564 | 482 | 54.5 | 9.5 | 28.0 | 0.0 | 130 | 117 | 11.1 | 31 | 208 | 170 | 2 |
| 3H-5, 143–150 | 24 | 7.64 | 7.64 | 3.18 | 35.0 | 566 | 485 | 54.4 | 9.4 | 29.0 | 0.0 | 20 | 119 | 11.5 | 33 | 222 | 195 | 4 |
| 4H-2, 140–150 | 29 | 7.61 | 7.60 | 3.94 | 35.5 | 569 | 489 | 54.1 | 9.5 | 27.4 | 0.0 | 220 | 134 | 11.0 | 38 | 455 | 221 | 14 |
| 5H-2, 140–150 | 39 | 7.37 | 7.77 | 5.47 | 36.0 | 577 | 499 | 51.0 | 9.2 | 23.9 | 0.0 | 550 | 172 | 10.1 | 46 | 674 | 263 | 5 |
| 6H-2, 140–150 | 48 | 7.32 | 7.46 | 6.14 | 36.0 | 589 | 518 | 48.1 | 8.7 | 20.9 | 0.0 | 940 | 189 | 10.8 | 48 | 840 | 287 | 7 |
| 7H-2, 140–150 | 58 | 7.32 | 7.39 | 7.27 | 36.0 | 595 | 525 | 45.0 | 8.5 | 17.7 | 0.3 | 1160 | 193 | 10.7 | 53 | 992 | 301 | 9 |
| 8H-2, 140–150 | 67 | 7.29 | 7.31 | 7.67 | 36.0 | 600 | 530 | 41.6 | 7.9 | 15.4 | 2.6 | 1810 | 193 | 10.1 | 59 | 1209 | 300 | 28 |
| 9H-2, 140–150 | 77 | 7.20 | 7.90 | 7.17 | 36.0 | 606 | 530 | 39.1 | 7.7 | 12.7 | 0.9 | 1630 | 197 | 10.4 | 62 | 1335 | 302 | 5 |
| 10H-2, 140–150 | 86 | 7.17 | 7.87 | 7.80 | 36.0 | 616 | 547 | 36.9 | 7.7 | 10.6 | 1.6 | 2060 | 214 | 10.3 | 70 | 1498 | 307 | 6 |
| 11H-2, 140–150 | 96 | 7.17 | 7.41 | 7.92 | 36.0 | 618 | 542 | 35.0 | 7.3 | 9.1 | 0.6 | 2350 | 231 | 10.3 | 73 | 1670 | 297 | 12 |
| 12H-2, 140–150 | 105 | 7.17 | 7.23 | 7.90 | 36.0 | 626 | 560 | 34.0 | 7.8 | 8.2 | 0.6 | 3070 | 254 | 9.8 | 75 | 1756 | 305 | 8 |
| 13H-2, 140–150 | 115 | 7.25 | 7.88 | 7.23 | 36.5 | 630 | 550 | 32.7 | 9.2 | 6.8 | 0.0 | 2650 | 278 | 10.4 | 79 | 1818 | 299 | 6 |
| 14H-2, 140–150 | 124 | 7.24 | 7.79 | 7.49 | 37.0 | 640 | 556 | 32.1 | 7.6 | 6.3 | 0.0 | 2290 | 273 | 9.8 | 85 | 1958 | 277 | 5 |
| 15H-2, 140–150 | 134 | 7.22 | 7.77 | 6.87 | 37.0 | 641 | 568 | 31.0 | 7.6 | 5.7 | 0.3 | 2760 | 275 | 10.2 | 90 | 2108 | 284 | 9 |
| 16H-2, 140–150 | 143 | 7.20 | 7.43 | 7.47 | 37.0 | 644 | 577 | 30.8 | 7.9 | 4.1 | 0.9 | 2850 | 256 | 9.9 | 97 | 2361 | 287 | 7 |
| 17H-2, 140–150 | 153 | 7.24 | 7.71 | 6.16 | 37.5 | 653 | 577 | 29.6 | 8.0 | 3.5 | 0.6 | 3190 | 231 | 9.7 | 103 | 2976 | 294 | 8 |
| 18H-2, 135–150 | 162 | 7.22 | 7.59 | 6.89 | 37.5 | 661 | 575 | 28.7 | 7.9 | 3.0 | 0.6 | 2920 | 218 | 9.9 | 108 | 3138 | 297 | 9 |
| 19H-2, 135–150 | 171 | 7.27 | 7.50 | 6.74 | 38.0 | 666 | 580 | 28.1 | 8.0 | 2.2 | 0.9 | 3350 | 208 | 9.5 | 114 | 3336 | 295 | 8 |
| 20H-2, 135–150 | 181 | 7.25 | 7.47 | 6.71 | 38.0 | 668 | 583 | 27.9 | 8.3 | 1.8 | 0.9 | 2960 | 218 | 9.5 | 119 | 3488 | 293 | 7 |
| 21H-2, 135–150 | 190 | 7.35 | 7.48 | 6.37 | 38.0 | 672 | 595 | 27.3 | 8.5 | 1.2 | 0.9 | 3480 | 231 | 9.7 | 124 | 3720 | 290 | 7 |
| 22H-2, 135–150 | 200 | 7.22 | 7.57 | 6.35 | 38.5 | 676 | 593 | 26.8 | 8.5 | 0.7 | 0.3 | 3410 | 248 | 9.0 | 132 | 3989.1 | 272 | 5 |
| 23H-2, 135–150 | 209 | 7.22 | 7.27 | 6.16 | 38.5 | 676 | 605 | 26.4 | 8.6 | 0.6 | 0.3 | 3570 | 256 | 8.9 | 125 | 3872.1 | 255 | 8 |
| 24H-2, 135–150 | 219 | 7.23 | 7.22 | 5.90 | 39.0 | 686 | 602 | 26.3 | 9.1 | 0.2 | 0.0 | 3530 | 291 | 9.3 | 129 | 4159 | 254 | 7 |
| 25H-2, 135–150 | 228 | 7.22 | 7.44 | 5.90 | 39.0 | 693 | 604 | 26.1 | 9.1 | 0.0 | 0.0 | 3770 | 318 | 9.1 | 133 | 4250 | 205 | 9 |
| 26H-2, 135–150 | 238 | 7.20 | 7.49 | 5.49 | 40.0 | 696 | 614 | 25.6 | 9.2 | 0.0 | 0.0 | 3880 | 374 | 9.2 | 134 | 4435 | 168 | 26 |
| 27H-2, 135–150 | 247 | 7.21 | 7.14 | 5.13 | 40.0 | 699 | 602 | 25.7 | 9.9 | 0.0 | 0.0 | 3570 | 469 | 8.4 | 139 | 4505 | 154 | 10 |
| 28H-2, 135–150 | 257 | 7.17 | 7.17 | 5.11 | 40.0 | 702 | 588 | 25.6 | 10.6 | 0.0 | 0.0 | 3980 | 503 | 8.6 | 147 | 4680 | 151 | 11 |
| 29H-2, 135–150 | 266 | 7.22 | 7.31 | 5.11 | 40.0 | 706 | 591 | 25.5 | 11.1 | 0.0 | 0.0 | 4060 | 408 | 9.1 | 153 | 4565 | 163 | 16 |
| 30X-2, 135–150 | 276 | 7.30 | 7.57 | 4.78 | 40.5 | 712 | 602 | 25.8 | 11.4 | 0.0 | 0.0 | 3410 | 389 | 9.0 | 159 | 4825 | 169 | 17 |
| 31X-2, 135–150 | 282 | | 7.58 | 4.75 | 40.5 | 715 | 598 | 28.3 | 11.7 | 1.8 | 1.3 | 4220 | 374 | 8.5 | 163 | 4935 | 171 | 12 |
| 32X-2, 135–150 | 288 | 7.25 | 7.62 | 4.71 | 40.5 | | | | | 1.9 | 0.0 | | 365 | | 162 | 4690 | 177 | 15 |
| 33X-2, 135–150 | 297 | 7.27 | 7.29 | 4.58 | 40.5 | 708 | 589 | 28.3 | 11.8 | 0.0 | 0.0 | 4060 | 363 | 8.0 | 158 | 4800 | 175 | 18 |
| 34X-2, 135–150 | 306 | 7.30 | 7.34 | 4.67 | 41.0 | 726 | 622 | 26.3 | 12.6 | 0.0 | 0.3 | 4290 | 498 | 8.1 | 179 | 5075 | 172 | |
| 35X-2, 135–150 | 315 | 7.29 | 7.51 | 4.90 | 42.0 | 731 | 636 | 26.5 | 12.9 | 0.0 | 0.0 | 4340 | 644 | 8.7 | 185 | 5355 | 178 | |
| 38X-2, 135–150 | 343 | 7.19 | 7.27 | 5.30 | 42.0 | 743 | 619 | 27.4 | 15.4 | 0.0 | 0.3 | 4470 | 522 | 8.3 | 198 | 5620 | 158 | |
| 41X-2, 135–150 | 370 | 7.12 | 7.23 | 5.78 | 43.0 | 759 | 627 | 27.5 | 14.2 | 0.0 | 0.0 | 4760 | 449 | 7.9 | 213 | 6103 | 147 | |
| 44X-2, 135–150 | 398 | 7.10 | 7.57 | 6.12 | 44.0 | 766 | 636 | 28.4 | 14.7 | 0.0 | 0.0 | 4940 | 689 | 7.7 | 226 | 6150 | 140 | |
| 47X-2, 135–150 | 426 | 7.05 | 7.47 | 6.51 | 44.5 | 783 | 644 | 29.5 | 14.6 | 0.0 | 0.0 | 4700 | 642 | 8.0 | 244 | 6353 | 177 | |
| 50X-2, 135–150 | 453 | 6.98 | 7.16 | 7.50 | 46.0 | 795 | 652 | 31.1 | 14.6 | 0.0 | 0.0 | 5460 | 425 | 7.6 | 261 | 7005 | 213 | |
| 53X-2, 135–150 | 481 | 6.98 | 7.06 | 7.53 | 46.0 | 803 | 703 | 34.2 | 15.4 | 0.0 | 0.0 | 5370 | 387 | 8.0 | 267 | 6550 | 229 | |
| 56X-5, 135–150 | 513 | 7.08 | 7.17 | 6.97 | 46.5 | 815 | 671 | 33.1 | 14.4 | 0.0 | 0.0 | 4920 | 373 | 7.6 | 277 | 6445 | 243 | |
| 59X-2, 135–150 | 537 | 7.07 | 7.24 | 6.48 | 47.0 | 820 | 697 | 33.8 | 14.9 | 0.0 | 0.3 | 5570 | 376 | 7.4 | 292 | 6600 | 248 | |
| 62X-2, 135–150 | 566 | 7.03 | 7.10 | 7.00 | 48.0 | 827 | 676 | 34.6 | 16.0 | 0.0 | 0.4 | 5100 | 434 | 6.9 | 297 | 6405 | 219 | |
| 65X-2, 135–150 | 595 | 7.07 | 7.16 | 6.27 | 48.0 | 843 | 694 | 35.3 | 16.5 | 0.0 | 0.5 | 5210 | 662 | 7.1 | 311 | 6305 | 195 | |
| 68X-4, 135–150 | 627 | 6.97 | 7.05 | 6.19 | 49.0 | 859 | 720 | 35.4 | 18.2 | 0.0 | 1.0 | 5640 | 807 | 7.0 | 311 | 6055 | 195 | |
| 72X-5, 135–150 | 667 | 7.02 | 7.09 | 6.67 | 50.0 | 865 | 710 | 36.5 | 19.1 | 0.0 | 0.5 | 4630 | 835 | 6.6 | 295 | 5380 | 202 | |
| 75X-2, 135–150 | 691 | 7.10 | 7.36 | 5.78 | 48.5 | 839 | 682 | 35.7 | 18.2 | 1.9 | 0.4 | 5350 | 853 | 6.9 | 266 | 4560 | | |
| 77X-2, 135–150 | 711 | 7.05 | 7.36 | 5.80 | 50.0 | 866 | 707 | 37.1 | 19.3 | 1.1 | 0.2 | 5590 | 699 | 6.6 | 290 | 5310 | | |

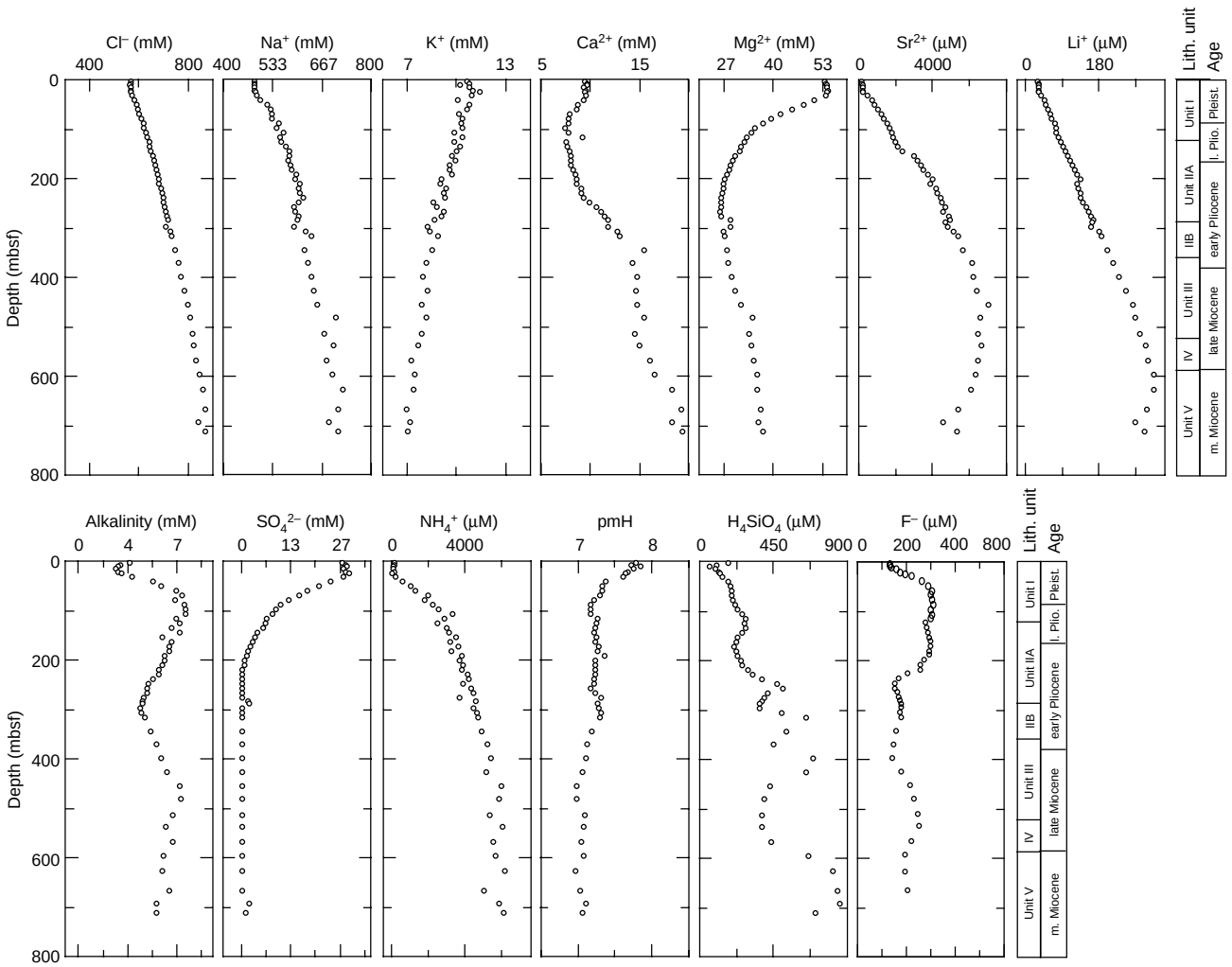


Figure 20. Depth profiles of interstitial water constituents at Site 1006.

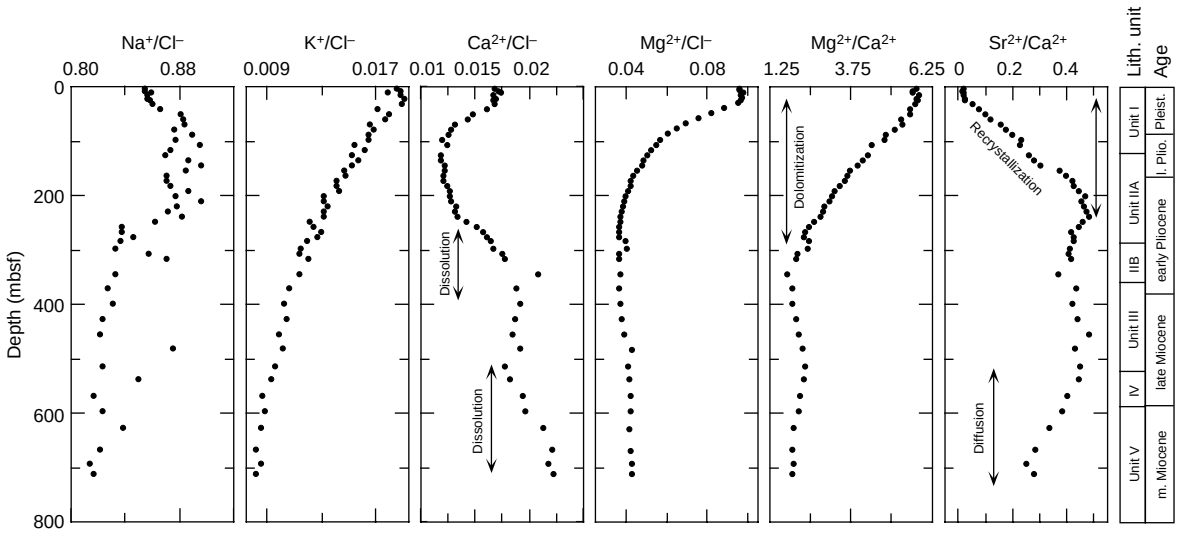


Figure 21. Depth profiles of ratios of selected interstitial water constituents at Site 1006 as elemental ratios and chloride normalized.

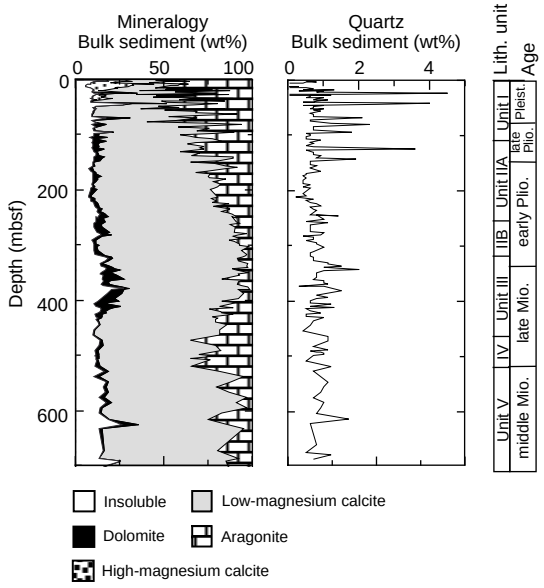


Figure 22. Quantitative X-ray mineralogy of sediments from Site 1006 showing relative abundances of carbonate minerals, acid-insoluble residues, and quartz.

The alkalinity profile initially decreases from 3.8 mM to 2.8 mM between 3 and 15 mbsf, before rising to a maximum near 7.9 mM at 100 mbsf. There is a subsequent gentle decrease in alkalinity to 4.6 mM at 300 mbsf, a depth coinciding with the boundary between lithologic Subunits IIA and IIB. This is followed by a gradual rise to 7.5 mM near 480 mbsf. The overall lower titration alkalinity values observed at Site 1006 are also consistent with precipitation of $FeS_2$, which would consume $HS^-$, thereby lowering titration alkalinity (e.g., Krauskopf, 1979; Davies, McKenzie, Palmer-Julson, et al., 1991).

The ammonium ($NH_4^+$) profile mirrors imperfectly the $SO_4^{2-}$ profile, exhibiting a steady but nonlinear increase from approximately 100 µM at 20 mbsf to approximately 5000 µM at 400 mbsf. Below this depth dissolved $NH_4^+$ remains between 4600 and 5600 µM.

The pmH, which is nearly constant within the upper 20 mbsf of Site 1006, exhibits a systematic decrease from 7.7 to 7.17 between 20 and 86 mbsf. It remains within a narrow range (7.2–7.35) down to 315 mbsf before decreasing to 7.0–7.1 farther downcore.

Dissolved phosphate ($HPO_4^{2-}$) concentrations at Site 1006 are very low, with most samples ranging from 0 to 2.6 µM (Table 9). Many of the samples displaying the higher concentrations, however, were collected within the zone of active $SO_4^{2-}$ reduction. It is most likely that $HPO_4^{2-}$ is actively removed from solution through adsorption onto clay minerals or carbonates.

### *Silica and Fluoride*

The silica ($H_4SiO_4$) and fluoride ($F^-$) profiles (Fig. 20) exhibit multiple localized maxima and minima throughout the sediments of Site 1006, reflecting the high reactivity of these constituents. Silica initially decreases in the uppermost 20 mbsf, probably as a result of its release during the early diagenesis of biogenic opal (e.g., Gieskes, 1983). A rise to 275 µM near 130 mbsf occurs in a zone of abundant clay layers, some of which are thick (see "Lithostratigraphy" section, this chapter). A small decrease below this depth is followed by a larger increase to 500 µM at 257 mbsf and two other concentration peaks of 640 and 680 µM at 315 and 398 mbsf, respectively. Concentrations of $SiO_2$ then return to a range of 375–425 µM down to 537 mbsf before rising to another maximum of 850 µM at 691 mbsf.

Dissolved $F^-$ exhibits smoother fluctuations than $H_4SiO_4$. Its concentration rises sharply from nearly 133 µM at the seafloor to a broad maximum of 305 µM between 60 and 190 mbsf. This is followed by a return to a range of 150–180 µM between 250 and 400 mbsf. A gradual increase then occurs to a peak concentration of 248 µM at 537 mbsf, below which $F^-$ concentrations decrease to approximately 200 µM. The major $F^-$ maxima coincide roughly with the alkalinity maxima (Fig. 20).

## Discussion and Summary of Results

Profiles of interstitial water constituents at Site 1006 are controlled by chemical reactions including the microbial degradation of organic matter, recrystallization of biogenic carbonates, silica diagenesis, ion-exchange reactions in clay minerals, and possibly interfacial-adsorptive phenomena. Unlike the pore-water profiles at Sites 1003, 1004, and 1005, which appear to be influenced by horizontal fluid flow delimited by lithologic boundaries, the profiles of major and minor dissolved constituents at Site 1006 are more characteristic of a relatively closed system in a pelagic sedimentary environment. The major control on the shape of the profiles at Site 1006 is diffusion from zones of high concentrations that result either from well-defined reaction zones within the sediments or from a high-salinity brine inferred to occur deep within the sediments (see "Inorganic Geochemistry" section, "Site 1003" and "Site 1005" chapters, this volume).

## Conservative Elements

The nearly linear increase of dissolved $Na^+$ and $Cl^-$ downhole suggest that horizontal fluid flow is minimal at Site 1006, except perhaps in the uppermost 20 mbsf. This zone may represent a layer that is relatively well-flushed owing to the action of energetic bottom currents, which enhance water penetration and irrigate the uppermost portion of the sediment column. Similar zones were described at Sites 1003 through 1005, although they were substantially thicker (about 40–50 mbsf) and underlain by well-defined lithologic boundaries. The mechanism for flushing of the uppermost layer of the sediments at Site 1006 remains unclear, but may be related to energetic eddies of a deep Western Boundary current (Gross, 1982; R. Lukas, pers. comm., 1996). Strong positive concentration gradients of $Na^+$ and $Cl^-$ downhole at Site 1006 also most likely reflect the influence of a high-salinity brine deep within the sediments, as was previously proposed (see "Inorganic Geochemistry" section, "Site 1003," "Site 1004," "Site 1005" chapters, this volume).

At Site 1006, the $K^+$ profile exhibits a strong negative concentration gradient probably as a result of its removal from solution by clay minerals and the formation of glauconite as observed at a number of DSDP and ODP sites (e.g., Gieskes, 1983; Davies, McKenzie, Palmer-Julson, et al., 1991; De Carlo, 1992). Clays are relatively abundant throughout Site 1006, as shown by the much larger "insoluble residue" fraction in the X-ray mineralogy (Table 10 on CD-ROM; Fig. 22). Furthermore, they occur in numerous intervals in the upper 100 mbsf (see "Lithostratigraphy" section, this chapter), where they contribute significantly to the removal of $K^+$ from solution. Glauconite was also observed in selected clay-rich intervals of Cores 166-1006A-14H and 15H. The role clay minerals play in affecting the pore-water composition at Site 1006 is also evident in the $Na^+/Cl^-$ (Fig. 21), where the curvature and deviation from a seawater ratio is indicative of clay mineral reactions (e.g., Davies, McKenzie, Palmer-Julson, et al., 1991). At Sites 1003–1005, clay minerals did not affect the $K^+/Cl^-$ and $Na^+/Cl^-$ significantly owing to their paucity throughout most of the sediments.

### Microbial Degradation of Organic Matter

The sharp decrease in $SO_4^{2-}$ between 20 and 200 mbsf marks a zone of active microbial degradation of organic matter at Site 1006. This steep profile can be maintained only by continued reaction within the sediments combined with downward diffusion of $SO_4^{2-}$. The extent of $SO_4^{2-}$ depletion observed at Site 1006 can be explained on the basis of the availability of organic matter. It is also possible that the organic matter found at Site 1006 is less difficult to degrade than the organic material deposited at Sites 1003–1005. Differences in the composition of organic matter were previously invoked to explain differences in rates of degradation at Sites 819–822 off Northeast Australia (Davies, McKenzie, Palmer-Julson, et al., 1991).

It is also interesting that the alkalinity increase within the zone of active microbial degradation at Site 1006 is approximately one order of magnitude lower than at Sites 1003–1005. The apparent deficiency in alkalinity may be attributed to the precipitation of pyrite, which removes both $HS^-$ and hence, titration alkalinity. This mechanism is consistent with the near absence of $H_2S$ at Site 1006 compared with the high concentrations observed at the other sites (see "Organic Geochemistry" section, "Site 1003," "Site 1004," and "Site 1005" chapters). It is also consistent with the presence of disseminated pyrite throughout the sediment below Core 166-1006A-5H. Other means of consuming alkalinity include the precipitation of calcite and dolomite as well as clay mineral diagenesis. None of these can be ruled out at Site 1006.

### Carbonate Diagenesis

The near absence of fully lithified sediments until nearly 600 mbsf at Site 1006 (see "Lithostratigraphy" section, this chapter) suggests that rates of carbonate remineralization are somewhat lower than at Sites 1003–1005. This difference in diagenetic potential may be caused by lower abundances of metastable carbonates, organic matter, and possibly decreased fluid flow at Site 1006 relative to the proximal sites.

Changes in the slopes of selected elemental ratios and concentration gradients (e.g., $Sr^{2+}/Ca^{2+}$, $Mg^{2+}/Ca^{2+}$, $Mg^{2+}/Cl^-$, and $Ca^{2+}/Cl^-$; see Fig. 21) at Site 1006 generally coincide with major changes in the carbonate composition of the sediments, and indicate several diagenetic processes including the dissolution of aragonite and precipitation of diagenetic LMC and dolomite. These processes are reflected in decreasing $Mg^{2+}/Ca^{2+}$ and increasing $Sr^{2+}/Ca^{2+}$ with depth (Fig. 21). Because dolomite is not particularly abundant deeper downcore, it is not likely that dolomitization is an important sink for $Mg^{2+}$ deep within Site 1006. The lack of a significant change in $Mg^{2+}/Ca^{2+}$ below 300 mbsf supports this hypothesis. Aragonite dissolution is shown by an increase in dissolved $Ca^{2+}$ and in $Sr^{2+}$ (relatively unchanged $Sr^{2+}/Ca^{2+}$) near 500 mbsf, as well as a small local alkalinity maximum.

In the absence of $SO_4^{2-}$ and of advective transport, strong concentration gradients and extremely high concentrations of $Sr^{2+}$ are maintained. The decrease in dissolved $Sr^{2+}$ at the base of the core may be diffusional. It is also possible that upward diffusion of $SO_4^{2-}$ could control the $Sr^{2+}$ concentration through the formation of celestite ($SrSO_4$) (Swart and Guzikowski, 1988), as observed in a similar depth range at Site 1003 (see "Inorganic Geochemistry" section, "Site 1003" chapter, this volume).

### Mineralogy

The carbonate mineralogy at Site 1006 is dominated by low-magnesium calcite (LMC) and aragonite throughout the entire sedimentary column (Table 10 on CD-ROM; Fig. 22). LMC is, on average, the most abundant mineral. Other carbonates include high-magnesium calcite (HMC) and dolomite. HMC was observed only in the upper 40 mbsf generally, at concentrations of less than 25 wt% (the exception was one sample containing 36 wt% HMC at 6.4 mbsf). Dolomite first appears in trace amounts at 17 mbsf. Its abundance downhole was usually less than 10 wt%, although several samples contained up to 21 wt%. In general, dolomite was most abundant between 300 and 420 mbsf. The acid-insoluble fraction of the sediments, as determined from total carbonate analysis (see "Organic Geochemistry" section, this chapter), increased downcore and ranged from slightly less than 10 wt% in the upper 40 mbsf to nearly 25 wt% near the bottom of Hole 1006A. Quartz was observed throughout the sediments of Site 1006, with abundances generally between 0.5 and 1 wt%, although a few samples collected above 150 mbsf exhibited abundances between 3 and 4 wt% quartz.

Aragonite displays high-frequency cyclicity throughout the upper Pliocene and Pleistocene sediments (upper 150 mbsf), with concentrations varying from less than 10 wt% to greater than 66 wt%. These cycles correlate well with cycles in color reflectance and the occurrence of clay layers in the upper 50 mbsf (see "Lithostratigraphy" section, this chapter). The general trend is one of decreasing aragonite concentration downcore, however, from approximately 40 to 10 wt% at 300 mbsf, the transition between lithologic Subunits IIA and IIB (see "Lithostratigraphy" section, this chapter). Below this depth, the abundance of aragonite is characterized by a lower frequency cyclicity, with concentrations ranging from 15 to 35 wt% between 450 and 550 mbsf. Below 540 mbsf, several other broad aragonite peaks occur, although they have slightly lower concentrations.

## PHYSICAL PROPERTIES

Physical properties at Hole 1006A were measured on whole cores utilizing the MST (NGR, GRAPE density, PWL, and magnetic susceptibility) and on discrete samples from split cores. The depth intervals and other parameters for the MST measurements are explained in the "Explanatory Notes" chapter (this volume). The PWL was activated for APC cores only. Three discrete *P*-wave velocity measurements and one index property sample were taken in every section of unconsolidated cores down to Core 166-1006A-39X. On semilithified cores, the sampling interval for the velocity measurement was increased to five per section and an index property sample was taken every other section. Thermal conductivity was measured on unconsolidated whole-round cores with a frequency of one per section down to Core 166-1006A-38X and every other section down to Core 43X. Cores from Holes 1006B, 1006C, and 1006D were measured on the MST only.

This report focuses on the downhole variation in petrophysical properties and their correlation with lithostratigraphy. Variations in magnetic susceptibility are described within the "Paleomagnetism" section (this chapter).

### Index Properties, GRAPE Density, and *P*-Wave Velocity

Tables 11 through 16 on CD-ROM summarize the index properties, discrete DSV velocity, GRAPE density, MST velocity measurements, magnetic susceptibility, and NGR for Site 1006.

In general, the physical properties of Site 1006 exhibit relatively smooth downcore profiles compared with the previous sites. The porosity decreases gradually from near 70% at the seafloor to 45% at approximately 640 mbsf. The bulk density and the sonic velocity show similar profiles and vary from approximately 1.7 to 1.9 g/cm$^3$ and from 1.6 to 1.9 km/s, respectively.

The cores recovered from Site 1006 can be divided into four petrophysical units on the basis of changes in the trend of the *P*-wave velocity downcore and coincident changes in other properties (Fig. 23). Petrophysical Unit I (0–165 mbsf) is characterized by a semilin-

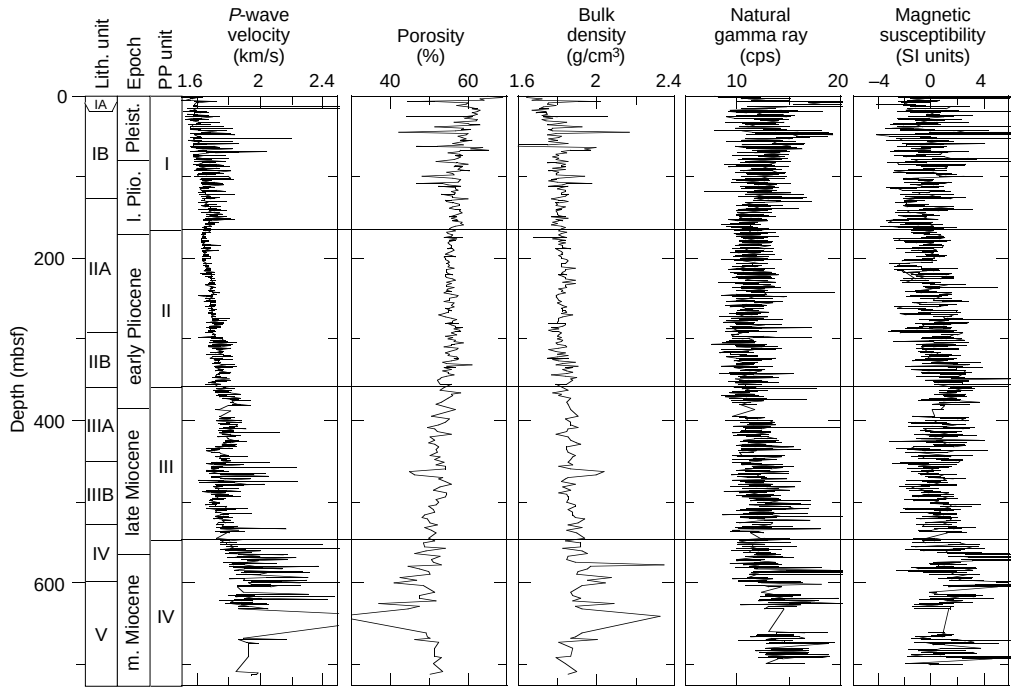


Figure 23. Combined plot of the *P*-wave velocity from the DSV, porosity, bulk density from discrete measurements of the NGR, and magnetic susceptibility from the MST at Hole 1006A. Lithologic and petrophysical units are indicated along with age.

ear downcore increase in the baseline value of the *P*-wave velocity from near 1.5 to 1.65 km/s. This smooth trend is interrupted by a number of positive spikes with amplitudes of 1.8–2.2 km/s, with a few deviating points. The bulk density increases from 1.7 to 1.8 g/cm$^3$ within the top 40 m of this unit and remains relatively constant downcore.

The spikes in the *P*-wave velocity appear to coincide with the clay layers occurring alternately with oozes in lithologic Unit I. Figure 24 compares the profiles of *P*-wave velocity (DSV and PWL), GRAPE density, acoustic impedance (product of velocity and density), natural gamma ray, and magnetic susceptibility in the upper 50 mbsf. The large, positive spikes of *P*-wave velocity match with those of density and magnetic susceptibility; however, the natural gamma ray does not show the same pattern.

The boundary between petrophysical Units I and II is marked by an abrupt, but small, decrease in *P*-wave velocity and bulk density and a coincident increase in porosity at 165 mbsf (Fig. 23). No major lithologic change occurs at this boundary, but it is near the biostratigraphic boundary between the lower and upper Pliocene. Within petrophysical Unit II (165 to 360 mbsf), *P*-wave velocity increases monotonously from 1.6 to 1.8 km/s, with few points deviating from this trend. The bulk-density profile also is relatively smooth, but the downcore increasing trend is less obvious than that of the *P*-wave velocity. Density values are typically between 1.8 and 1.85 g/cm$^3$.

In petrophysical Unit III (360–550 mbsf), the average *P*-wave velocity and bulk density remain constant, although they both show a number of measurements deviating positively from the main trend. Natural gamma ray shows a subtle increasing trend.

At 550 mbsf (top of petrophysical Unit IV), both *P*-wave velocity and bulk density resume a downcore-increasing trend. This depth roughly corresponds to the boundary between lithologic Units III and IV. Within petrophysical Unit IV, the *P*-wave velocity increases with a rate greater than those in any of the units above. The baseline of the *P*-wave velocity increases linearly from 1.7 km/s at 545 mbsf to 1.9 km/s at 600 mbsf and then more sharply to near 2.5 km/s at 640 mbsf. The major peaks in *P*-wave velocity that occur at this depth are matched by peaks in the density and porosity profiles. These peaks correspond to a zone of highly lithified limestone.

In general, the physical properties of Site 1006 exhibit a relatively smooth trend influenced mainly by sediment compaction. This trend probably reflects the location of this site on a sediment drift in the middle of the Straits of Florida, where sedimentation is uniform.

The downcore variation of the discrete *P*-wave velocities differs significantly from that obtained by downhole logging (Fig. 25). The logged velocity increases sharply at 220 mbsf from 1.7 to 1.8 km/s, whereas the discrete values show no such step change. The offset between the two data sets increases with depth. At 600 mbsf, the discrepancy is greater than 0.4 km/s. This may result from two factors: (1) decompaction of the recovered cores, and (2) destruction of the original fabric by the drilling process.

## Shear Strength

Shear strength was measured on cores from Hole 1006A from 0 to 275 mbsf (Table 17 on CD-ROM; Fig. 26). Below this depth, the sediment is semilithified and no longer suitable for shear-vane measurements.

Shear strength at Site 1006 increases gradually with depth from 5 to 30 kPa with sporadic high values over several tens of kilopascals (Fig. 26). This gradual increase is consistent with a compaction trend. The $S_u/P_o'$ ratio decreases with depth in an exponential manner, from 0.4 to less than 0.1 in the first 25 m, and then gradually down to near-zero values at 150 mbsf.

## Thermal Conductivity

A total of 221 thermal conductivity measurements was made on the cores from 0 to 400 mbsf from Hole 1006A (Table 18 on CD-ROM; Fig. 27). Thermal conductivity at this site increases downcore in an exponential manner from near 1.00 W/(m·K) at the seafloor to

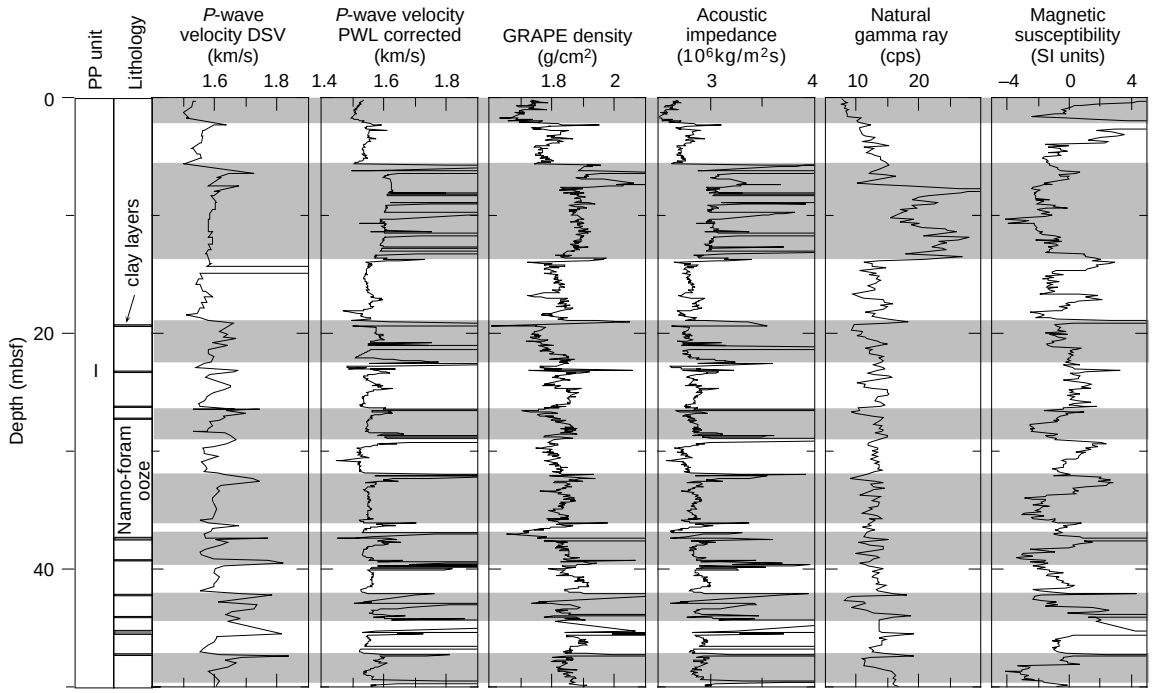


Figure 24. Summary of *P*-wave velocity from the DSV and from the PWL, GRAPE density, acoustic impedance, natural gamma ray, and magnetic susceptibility for the interval 0–50 mbsf. Clay layers in the lithology are also indicated. The alternating changes in physical properties are indicated by the shaded bands.

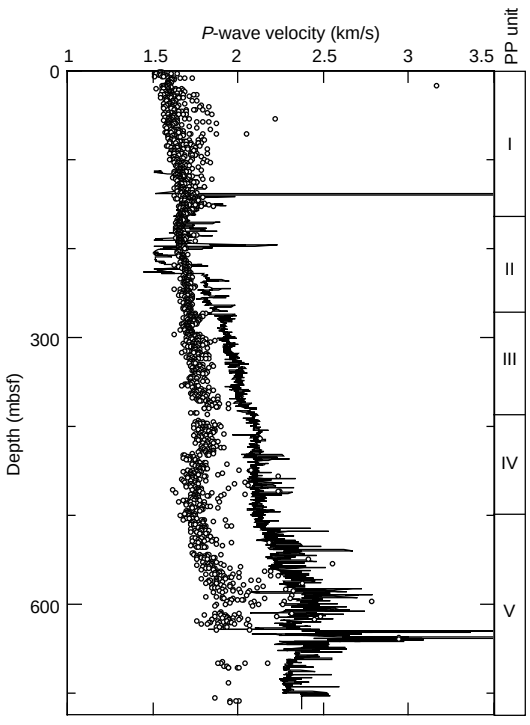


Figure 25. Combined plot of discrete *P*-wave velocity measurements from the DSV (points) and the downhole sonic velocity log in Hole 1006A.

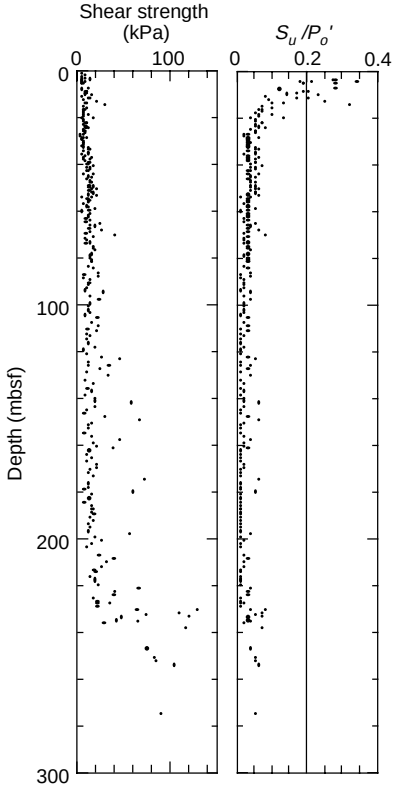


Figure 26. Shear strength and $S_u/P_o'$ calculated from shear strength and overburden stress for cores from Hole 1006A.

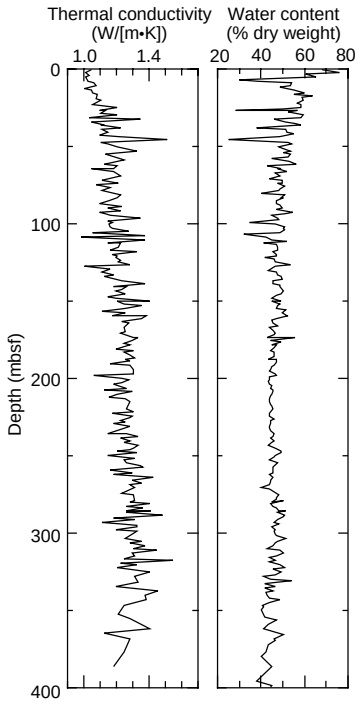


Figure 27. Thermal conductivity and water content for Hole 1006A.

1.3 W/(m·K) at 400 mbsf, exhibiting the compaction trend more clearly than the sites upslope. There is an inverse correlation between the downcore trend in thermal conductivity and the water content of this site (Fig. 27). Some positive peaks of thermal conductivity coincide with negative spikes of water content. This correlation implies uniformity of the grain thermal conductivity of sediments at this site.

## DOWNHOLE LOGGING

### Logging Operations

After drilling operations ended at Hole 1006A, the borehole was prepared for logging (see "Operations" section, this chapter). The lower limit of the bottom-hole assembly (BHA) was placed at 103 mbsf. We deployed four logging tool strings, in the following order: (1) induction-sonic-temperature; (2) integrated porosity-lithology tool (IPLT); (3) Formation MicroScanner (FMS); and (4) well seismic tool (WST; see "Downhole Logging" section, "Explanatory Notes" chapter, this volume). All four tool strings reached the total depth drilled (Fig. 28).

The WST recorded stacks of 5–7 air gun shots at 14 stations spaced about 50 m apart. The resulting interval velocities and time-depth curve are discussed in the "Seismic Stratigraphy" section (this chapter).

### Data Quality

Overall good hole conditions provided high-quality logging data at Site 1006. The general purpose inclinometry tool (GPIT) indicated that the hole was deviated by about 2°–3° at 100 mbsf, gradually increasing to a maximum of 8.5° near the base, with a nearly constant azimuth of N40°E. Hole diameter, measured by the hostile-environment Litho-Density sonde (HLDS), shows an overall uphole increase in diameter from about 11 in (28 cm) at the base to 16 in (41 cm) at 230 mbsf. Between 160 and 230 mbsf, the hole is enlarged beyond the maximum aperture of the HLDS caliper of 16.5 in (42 cm). The

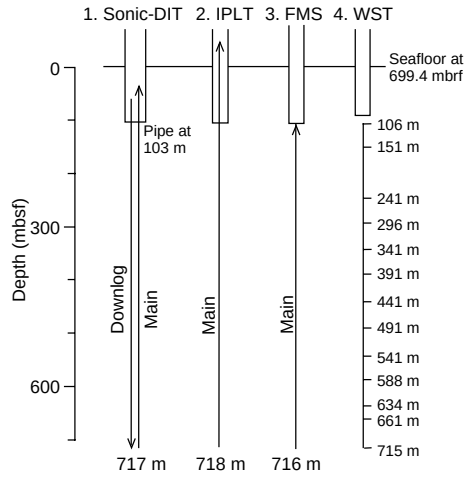


Figure 28. Summary of the logging runs at Hole 1006A. The temperature logging tool was included on the first run. The logging speeds were sonic-DIT at 300 m/hr, IPLT at 350 m/hr, and FMS at 550 m/hr. WST measured sonic traveltimes at 14 stations. See "Explanatory Notes" chapter (this volume) for description of the tool strings.

FMS calipers indicate a high degree of ovalization of the borehole on the order of 9 vs. 11–15 in (23 vs. 28–38 cm).

Comparison of the logging data with index and physical properties measured on cores shows good agreement except for the *P*-wave velocity, which is lower in the core measurements (see "Physical Properties" section, this chapter). The enlarged section of the borehole toward the top severely degraded the quality of most data, in particular porosity (abnormally high), bulk density, gamma ray, sonic velocity (overall low), and FMS. The marked separation between the deep and shallow resistivity curves indicates a highly porous and permeable zone that is most likely invaded by borehole fluids.

FMS images analyzed on board are of good quality, displaying fine-scale bedding down to a few centimeters' thickness over most of the logged section. The HLDS caliper followed the widest axis of the borehole, and the trace left by the caliper arm and density-tool pad can be easily detected on the FMS images over the softest formation intervals.

### Preliminary Observations

Geophysical and geochemical (U, K, Th) data acquired during the logging of Hole 1006A in the interval from 103 to 715 mbsf provide detailed information on the sedimentary properties and the structure of the strata that cannot be obtained from the recovered material. Because sediment recovery was excellent, exclusive of a few intervals, log-to-core correlation is possible, permitting the extraction of valuable information regarding variation in the sedimentation patterns in the Straits of Florida since the late middle Miocene. The changes recorded in the logs can be traced back to the Great Bahama Bank along the seismic sequence boundaries, providing a tie between sedimentation patterns in the basin and on the platform margin.

Figure 29 contains a summary of the principal logging data acquired in Hole 1006A. In general, there is a downhole compaction trend of increasing density, resistivity, and sonic velocity and of decreasing porosity. These geophysical logs, however, contain two intervals that show increased values elevated above the overall trend: a minor excursion occurs between approximately 350 and 450 mbsf and a major excursion is between approximately 500 and 650 mbsf. The lower of these two intervals is marked by higher natural gamma-ray readings. Closer examination of the components composing the radioactive signal reveals that there is a greater than twofold increase

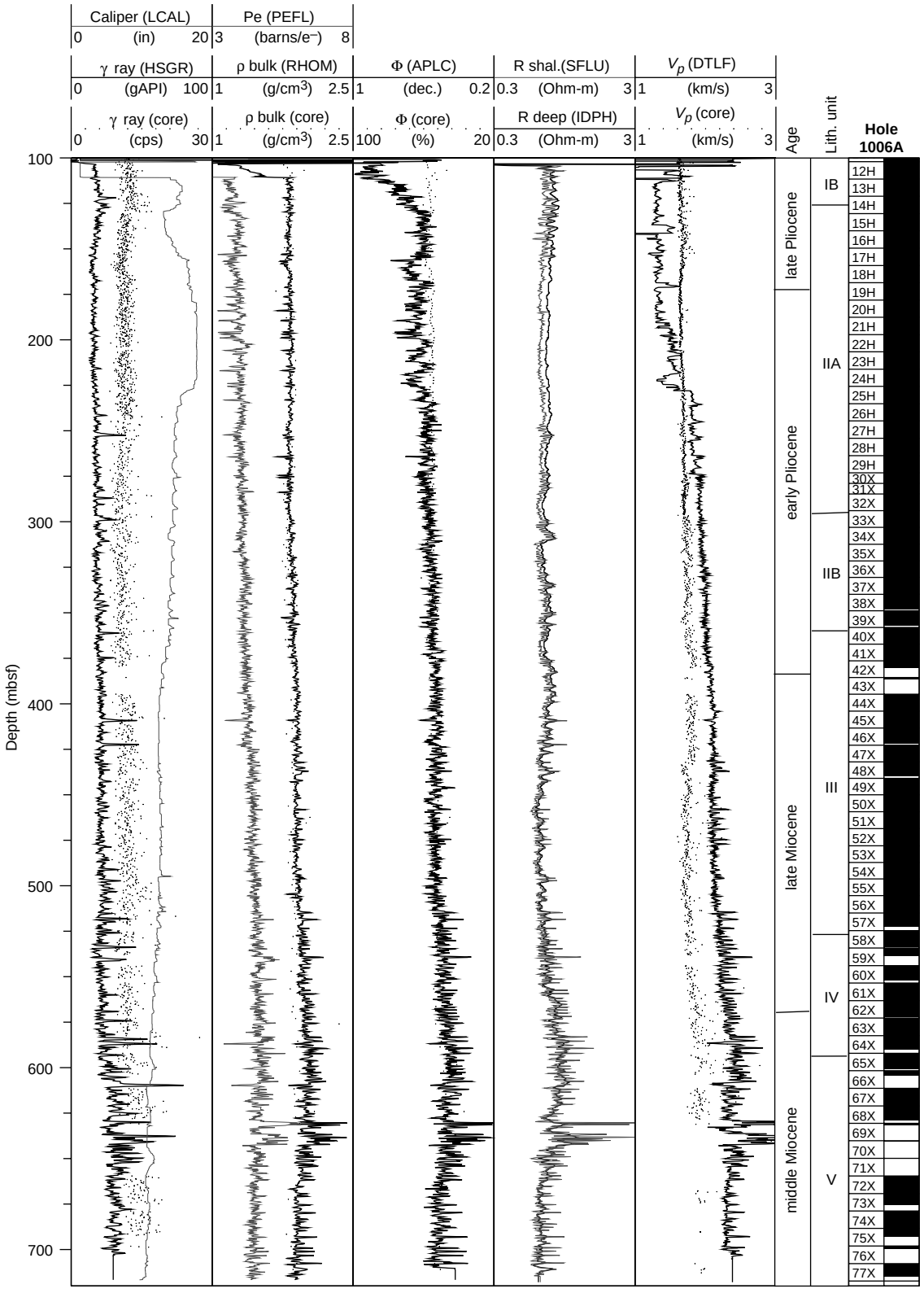


Figure 29. Summary of key geophysical logs acquired with the IPLT and induction-sonic logging strings. From left to right, columns are gamma ray and caliper, bulk density (ρ bulk) and photoelectric index (Pe), porosity (Φ), shallow and deep resistivity (R), sonic velocity ($V_p$), age, lithologic units, and core recovery. The points represent core measurements from the MST (natural gamma ray) and index properties (bulk density, porosity, and velocity) from the DSV instrument.

in the percent of K in this interval, as well as an increase in the Th concentration (Fig. 30). This same trend is observed within the upper excursion, but to a smaller extent. The geochemical logs indicate that the sediments of these two intervals probably contain more detrital minerals, such as K-feldspars, micas, or clay minerals, as well as possibly glauconite (Serra, 1986). The geophysical logs also indicate that these intervals are more indurated than the sediments above and below.

In general, the logs of the cored sedimentary sequence at Site 1006 are characterized throughout by small-scale cyclicity expressed in FMS microresistivity images as alternations between thin, resistive, low natural gamma-ray layers and conductive, higher gamma-ray intervals (Fig. 31). This cyclicity is also well defined by porosity, density, and velocity. The amplitude and spatial frequency of the cycles show long-term variations, with the highest amplitude cycles in the interval at 500–650 mbsf. Firmgrounds recognized in the core are well represented in the intervals with increased natural gamma-ray counts, resistivity, and sonic velocity (Figs. 31A, 32).

FMS imaging of Hole 1006A shows clearly the two intervals of higher resistivity recognized in the geophysical logs, which have been denoted as FMS Zone I (335–445 mbsf) and FMS Zone II (515–665 mbsf) (Fig. 32). These zones are characterized by a higher spatial frequency of thin resistive beds. The upper FMS zone spans the Miocene/Pliocene boundary, whereas the lower zone coincides with the middle/upper Miocene boundary. A plot of the percent aragonite vs. depth together with selected log data shows that the FMS zones correlate well with intervals of low percent aragonite (Fig. 32). These zones also correspond to intervals of low color reflectance (see "Lithostratigraphy" section, this chapter).

We propose that the zones of high microresistivity represent periods of increased contour current activity at Site 1006. This explanation is consistent with the fact that the two zones are marked by properties in the geophysical logs that are above the normal compaction trend, as mentioned previously. These properties of high velocity, density, and resistivity and low porosity could indicate the presence of coarser grain sizes as a result of increased winnowing or more induration resulting from accelerated diagenesis. Both of these explanations are consistent with increased bottom-current speeds at these times. The depletion of aragonite in these intervals could therefore result from the removal of fine-grained carbonate grains by the stronger bottom currents, decreased input related to lower production on the bank during sea-level lowstands, or a combination of the two.

As evident in the microresistivity pattern of the FMS images, both the overall resistivity and the character of the alternations in the two zones appear different (Fig. 31). The more resistive layers of FMS Zone II are more closely spaced, with a cyclicity of about 2 m, whereas the layers in FMS Zone I are less resistive and have a less cyclic nature. At a middle Miocene sedimentation rate of about 5 cm/k.y. (see "Biostratigraphy" section, this chapter), the 2-m cycles would be about 40 k.y. long and therefore could indicate obliquity cycles.

The Lamont temperature logging tool (TLT) was attached at the bottom of the first logging run, and the resulting measurements are presented in Figure 33. The temperature profile is similar to that recorded in Hole 1005A and appears to reflect the drilling and borehole mud disturbance to the thermal equilibrium of the formation.

## IN SITU TEMPERATURE MEASUREMENTS

### Introduction

At Site 1006, 17 in situ temperature measurements were made successfully using two sets of Adara tools and one unit of downhole water sampler, temperature, and pressure probes (WSTP). The "In situ Temperature Measurements" section of the "Explanatory Notes" and "Site 1003" chapters, this volume, explain the methods used to determine the sediment equilibrium temperatures and the errors provided in Table 19. The temperature at the seafloor (10.1°C) has been determined from the mudline stops.

### Geothermal Profile

Figure 34 shows the geothermal profile obtained from the in situ measurements. The temperatures measured at the seafloor through 60 mbsf show no increase with depth. The temperature profile from 60 to 100 mbsf is concave downward. The measurements below 100 mbsf fall on a clear linear trend with a geothermal gradient of 35.2°C/km.

A similar, zero thermal gradient interval near the seafloor was observed at Site 1005, where the thickness of this zone (~50 m) roughly matched that of the zone of no salinity gradient in pore water. Thus, it is suspected that this zero thermal gradient was caused by influx of cold bottom water to the shallow sediments at Site 1005. At Site 1006, however, this chemically inferred "flush zone" is considerably thinner (about 20 m; see "Inorganic Geochemistry" section, this chapter) than the zero thermal gradient zone. Thus, the origin of the zero thermal gradient zone may be different from the zero salinity gradient zone, at least at this site.

The linear extrapolation of the in situ temperatures measured below 100 mbsf to the seafloor gives a bottom-water temperature of ~8.9°C (dashed line in Fig. 34). This is more than 0.7°C lower than the coldest bottom-water temperature measured at the mudline during the 14 Adara deployments (Table 19). One hypothesis is that a recent warming of bottom water has taken place.

In general, the geothermal profile at Site 1006 resembles those reported from some boreholes in Canada (Wang et al., 1992). They show zero or negative thermal gradient from the surface to about 50 m depth, a concave downward profile in the next several tens of meters, and a linear temperature increase below about 100 m depth. These boreholes have been affected little by groundwater movement in the past, and thus, their geothermal profiles are considered to be solely conductive in origin. Many researchers believe that the geothermal profiles reflect changes in surface temperatures that have occurred in the recent past.

The surface temperature history inferred from aforementioned Canadian boreholes is that a warming trend started about 100 years ago. This trend was preceded by a cooling trend in the previous century (Wang et al., 1992). Such a scenario could explain the near-zero thermal gradient of the upper 50 mbsf and the concave downward temperature profile in the underlying 50 m at Site 1006.

There has been no observation reported to show that seafloor temperature is affected by such long-term climatic changes at this depth, but there have been reports suggesting that intermediate depth water (700–1500 mbsl) of the subtropical North Atlantic may have warmed by 0.2°C over the past 30 years (Roemmich and Wunsch, 1984; Parrilla et al., 1994). Such warming may best explain the geothermal profile of Site 1006. An explanation on why Site 1006 seems to show more influence of the surface climate than other Leg 166 sites located in shallower water is still required. In addition, hydrographic and physical oceanographic observations in the past for this region must be examined carefully to interpret such variations.

### Heat Flow

Heat flow at Site 1006 has been determined as the gradient of the temperatures (below 90 mbsf) plotted against the cumulative thermal resistance because the thermal conductivity increases systematically with depth (Fig. 27, "Physical Properties" section, this chapter). The heat flow value here (44.4 $mW/m^2$) is greater than at Sites 1003 and 1004 by about 10% and at Site 1005 by about 20%.

## SEISMIC STRATIGRAPHY

Site 1006 penetrated to 717.3 mbsf through 11 seismic sequence boundaries (SSBs A–L) into the middle Miocene Sequence *m*. Site 1006 is located 25 km westward of the modern platform margin in the basin axis on top of a succession of drift deposits. All SSBs are con-

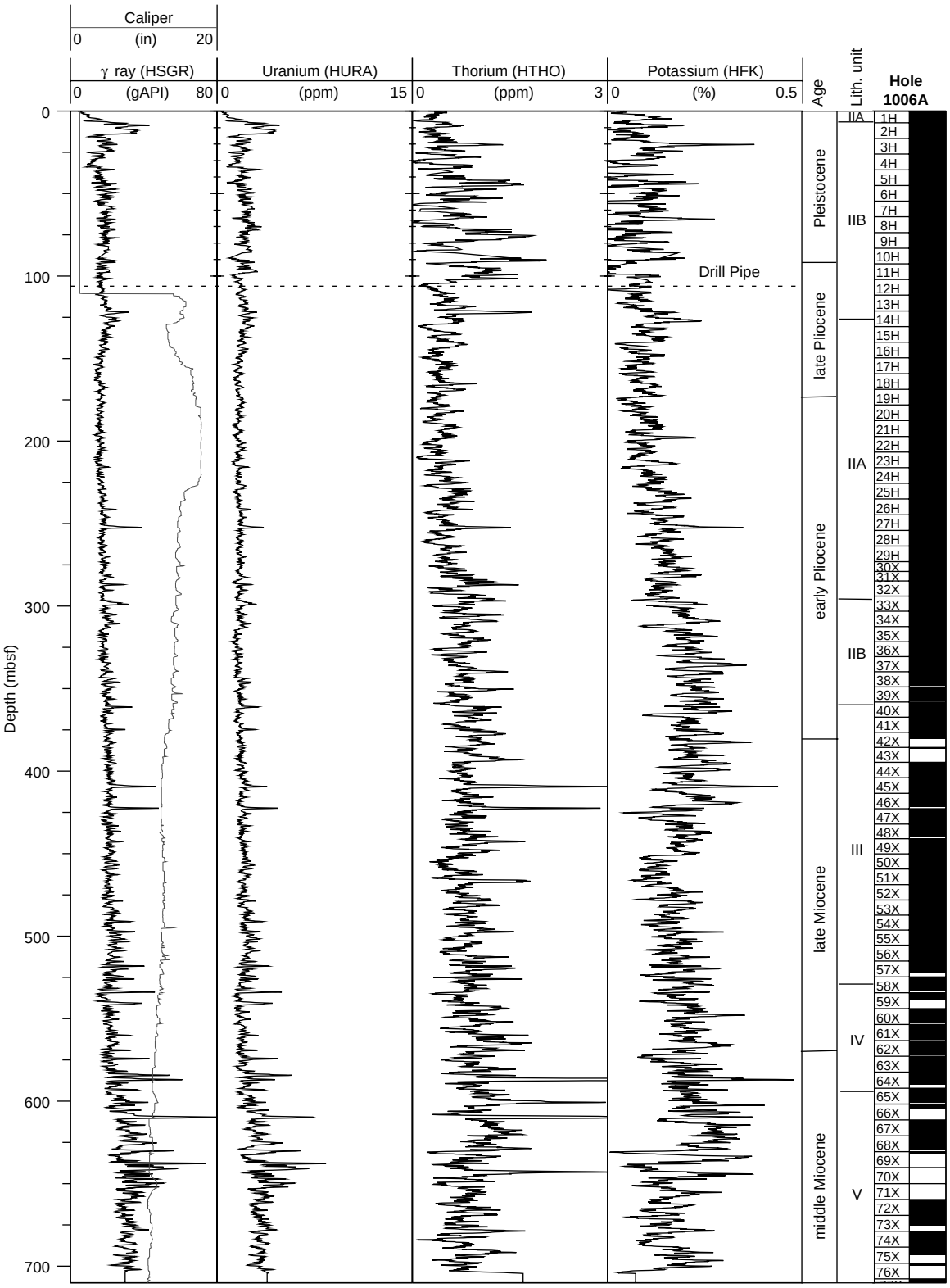


Figure 30. Spectral gamma-ray results using the HNGS tool at Site 1006. The curves between 0 and 103 mbsf were corrected for the attenuation of the gamma-ray spectra caused by measurement in the drill pipe following empirical correction constants obtained by comparing logging runs in Holes 1005A and 1005C (correction factor = 4.0 within the BHA, 1.8 within 5 1/2-in drill pipe, and 1.7 within 5-in drill pipe).

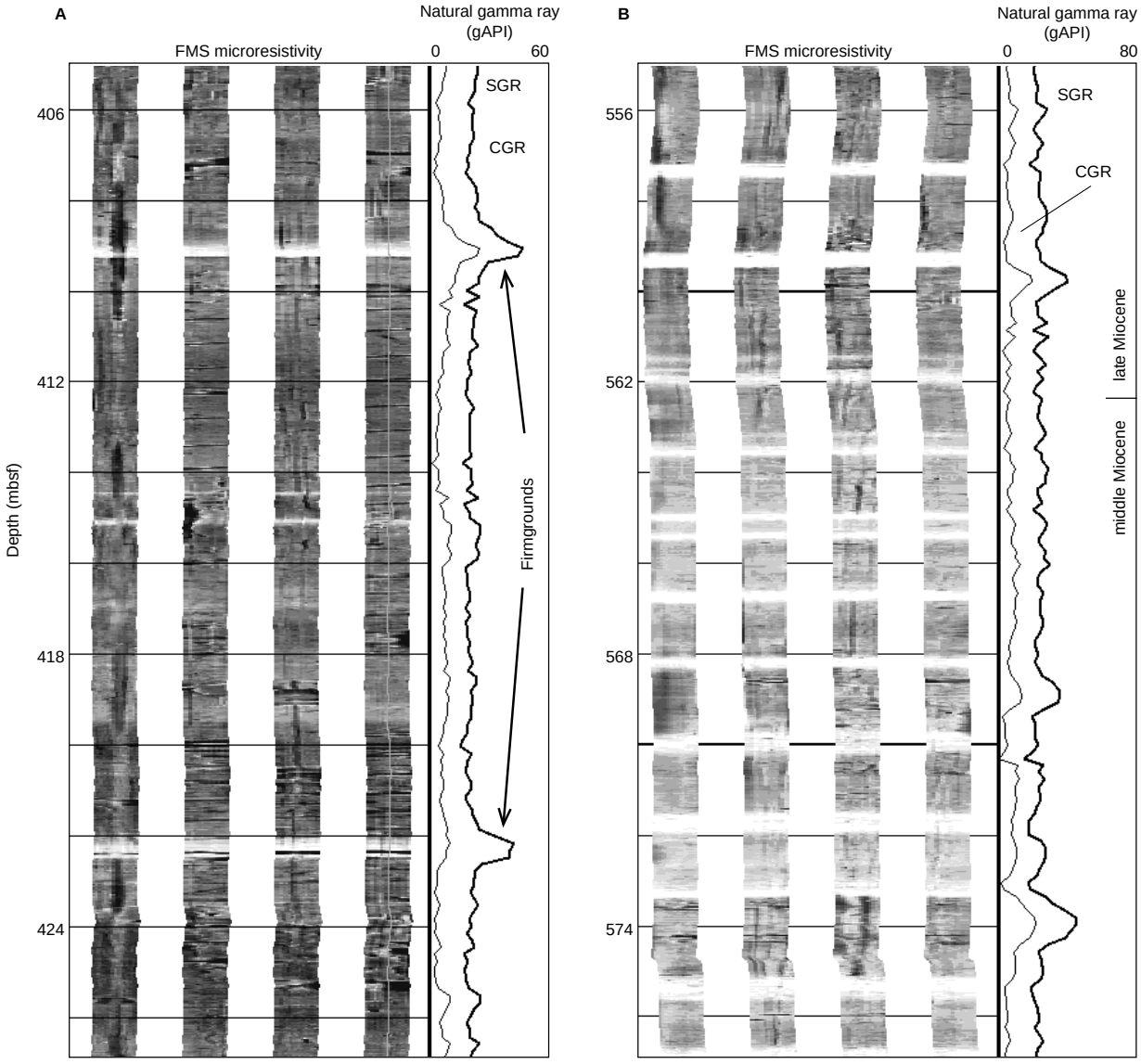


Figure 31. FMS images (static normalization) of two selected intervals in Hole 1006A together with the total gamma-ray intensity (SGR) and the total minus the uranium signal (CGR). The FMS images illustrate the change in character of the resistive bands in (**A**) FMS Zone I and (**B**) FMS Zone II. See text for discussion.

formable at the drilling location (Figs. 35, 36). The drift deposits thin eastward. As a result, many of the reflections of the drift deposits downlap to the east onto the sequence boundaries or onto intra-sequence reflections, whereas platform-derived units form downlaps to the west, documenting the interfingering of the two depositional systems. These two sedimentation processes coexisted primarily between the middle Miocene and the Pliocene (Sequences *k*–*c*; see Frontispiece).

The seismic facies throughout Site 1006 are characterized by highly coherent reflections, which display a very high resolution of approximately 5–10 m. Compared to the proximal sites, the velocity and density downhole pattern at Site 1006 displays relatively little variation and a much smaller range, resulting in small impedance contrasts. Despite those small variations, the seismic image documents the ability of well-layered sediments with high lateral consistence to produce a well-defined seismic reflection pattern.

## Time-Depth Conversion

In the distal location of Site 1006, the overall lithologies and physical properties differ significantly from the other Leg 166 sites. Consequently, the check-shot information from vertical seismic profiles (VSP) from the margin sites could not be extrapolated to Site 1006, and a check-shot survey was necessary to provide the correct time-depth curve for this site. The well seismic tool (WST), lowered to 714 mbsf, provided a complete coverage of downhole traveltimes for Site 1006 (Table 20). The traveltimes of the signal from the airgun to a total of 16 stations were corrected for lateral offset, water depth, gun depth, and two-way distance, enabling a conversion table for two-way traveltime measured in the seismic reflection data to meters below seafloor.

Figure 37 displays the traveltimes and interval velocities at this site compared to the sonic log (combined near and far trace) and the

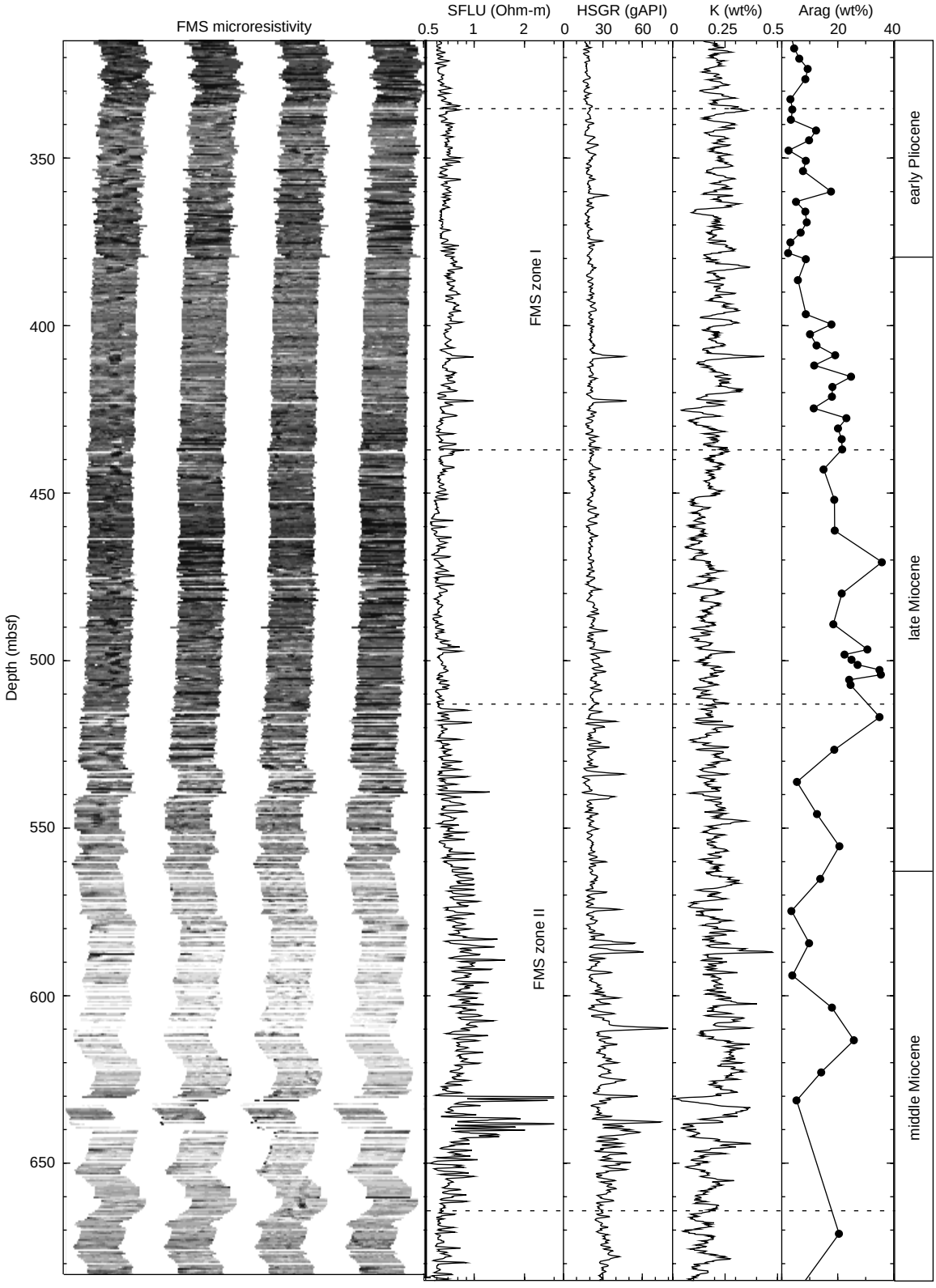


Figure 32. FMS image (static normalization) of Hole 1006A between 300 and 700 mbsf shown with the corresponding resistivity and gamma-ray logs acquired with the IPLT string and percent aragonite estimated from XRD. Two intervals of higher resistivity (FMS Zone I and II) are designated. See text for discussion.

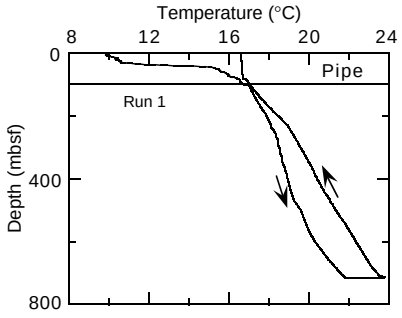


Figure 33. Temperature log in Hole 1006A.

**Table 19. In situ bottom-hole sediment temperatures measured at Site 1006.**

| Core | Depth (mbsf) | Temperature (°C) | Error (°C) | Mudline (°C) | Tool |
|---|---|---|---|---|---|
| 166-1006A- | | | | | |
| 4H | 35.6 | 10.16 | 0.10 | 9.93 | Adara18 |
| 5H | 45.1 | 9.58 | 0.14 | 10.22 | Adara11 |
| 6H | 54.6 | 9.82 | 0.10 | 9.96 | Adara18 |
| 7H | 64.1 | 10.68 | 0.20 | 10.09 | Adara11 |
| 8H | 73.6 | 11.10 | 0.10 | 10.37 | Adara18 |
| 9H | 83.1 | 11.55 | 0.06 | 9.74 | Adara11 |
| 10H | 92.6 | 12.13 | 0.04 | 9.85 | Adara18 |
| 11H | 102.1 | 12.34 | 0.04 | 10.19 | Adara11 |
| 14H | 130.6 | 13.57 | 0.30 | 9.71 | Adara18 |
| 17H | 159.1 | 14.42 | 0.40 | 9.62 | Adara11 |
| 20H | 187.6 | 15.69 | 0.03 | 9.62 | Adara18 |
| 23H | 216.0 | 16.43 | 0.08 | 10.80 | Adara11 |
| 26H | 244.6 | 17.37 | 0.06 | 10.58 | Adara18 |
| 29H | 273.1 | 18.44 | 0.03 | 10.74 | Adara11 |
| 33X | 293.9 | 19.27 | 0.01 | | WSTP201 |
| 36X | 321.5 | 20.19 | 0.02 | | WSTP201 |
| 39X | 348.9 | 21.12 | 0.01 | | WSTP201 |

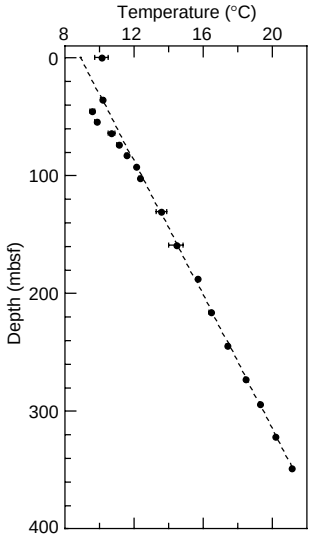


Figure 34. Geothermal profile at Site 1006. Solid circles represent the reliable temperature measurements. Dashed line shows the geothermal gradient obtained from the measurements below 95 mbsf.

VSP data of Site 1005. Unlike Site 1005, where the integrated sonic log resulted in a large offset toward shorter traveltimes (Fig. 37), this site is characterized by a good agreement between the times of the integrated sonic log and the VSP check-shot traveltimes. Thus, the interval velocities from the VSP mimic the sonic log. In the uppermost interval above 200 mbsf, the sonic log gives velocities that are too low. This difference causes the small offset between the two time-depth curves below 200 mbsf, which remains constant downhole, indicating a good match between the two methods. Compared to the VSP at Site 1005, the time-depth curve at Site 1006 is shifted to higher traveltimes (difference of about 7% at 500 mbsf), reflecting the overall slower velocities of the basinal sediments (Fig. 37).

## Holocene-Pleistocene Sequences

According to biostratigraphic ages and sedimentation rates, the age horizons corresponding to SSB A and B lie at 0.5 and 12 mbsf, respectively, and could not be traced on the seismic section because ghost reflections cover the shallow subsurface zone (Table 21). However, strong positive excursions of natural gamma ray, velocity, and density are found in the cores within an interval between 6 and 14 mbsf, which might be the physical record of SSB B (Fig. 24). Lithologically, this SSB coincides with the top of lithologic Subunit IB, where a hardground and a chalky layer with abundant blackened grains and lithoclasts occur within a succession of nannofossil ooze (see "Lithostratigraphy" section, this chapter).

Sequence *c* has its lower boundary at 100 msbsf (TWT) or 90 mbsf at the Pliocene/Pleistocene boundary. This horizon correlates to a level at the base of a thick sedimentary package with abundant clay layers within lithologic Unit I, but not to any prominent physical property signature.

## Pliocene Sequences

Sequence *d* ranges from the base of the Pleistocene (90 mbsf) down to 160 msbsf (TWT) or 145 mbsf. This level lies close to the top of lithologic Unit II at 126 mbsf, which consists mainly of nannofossil ooze and chalk. SSB D might correlate to a strong peak in the sonic log, recorded at 140 mbsf (Fig. 35), but equivalent rocks were not recovered in the cores. SSB E was placed at 190 msbsf (TWT) or 170 mbsf and coincides with a transition from sediments with higher variability in physical properties above to very homogenous lower Pliocene deposits below. A similar pattern was already encountered across this SSB at the previous Sites 1003 and 1005. As a result of the low variability, seismic reflection amplitudes within Sequence *e* are significantly lower than in the more variable lithologies above and below. The Miocene/Pliocene boundary (SSB F) is located at 410 msbsf (TWT) or 380 mbsf, which is marked by a downhole gradient change in the sonic log, a result of gently increasing velocities in Sequence *e* and almost constant velocities below SSB F (Fig. 35).

## Miocene Sequences

Compared to Sites 1003 and 1005, Sequence *f* (Messinian Age) at Site 1006 is much thicker and overlies Sequence *g* at 530 msbsf (TWT) or 505 mbsf without a noticeable biostratigraphic hiatus. Seismic Sequence *f* thins to the east toward the platform, which is seen on the seismic data in an eastward downlap of reflections to the base and a subtle downcutting erosion by SSB E at the top just west of Site 1007 (see Frontispiece and back-pocket foldout). Sequence *g* is approximately equivalent to lithologic Unit III, which is dominated by nannofossil chalk with several firmgrounds near the top of the unit. Two more sequences (*h, i*) were drilled in the upper Miocene; together they form lithologic Unit IV that is dominated by nannofossil chalk with a series of firmgrounds at the base. Sequences *h* and *i* have their lower boundaries at 550 msbsf (TWT) or 530 mbsf and 585 msbsf (TWT) or 570 mbsf, respectively, and both coincide with a spike in the sonic log.

The remainder of Site 1006 contains the middle Miocene section, which consists of Sequences *k, l,* and the top part of *m.* These sequences correspond approximately with lithologic Unit V, which is characterized by a distinct change in physical properties, despite consisting of similar nannofossil chalk as the units above. The gamma-ray values as well as velocities increase across SSB I (Figs. 29, 35)

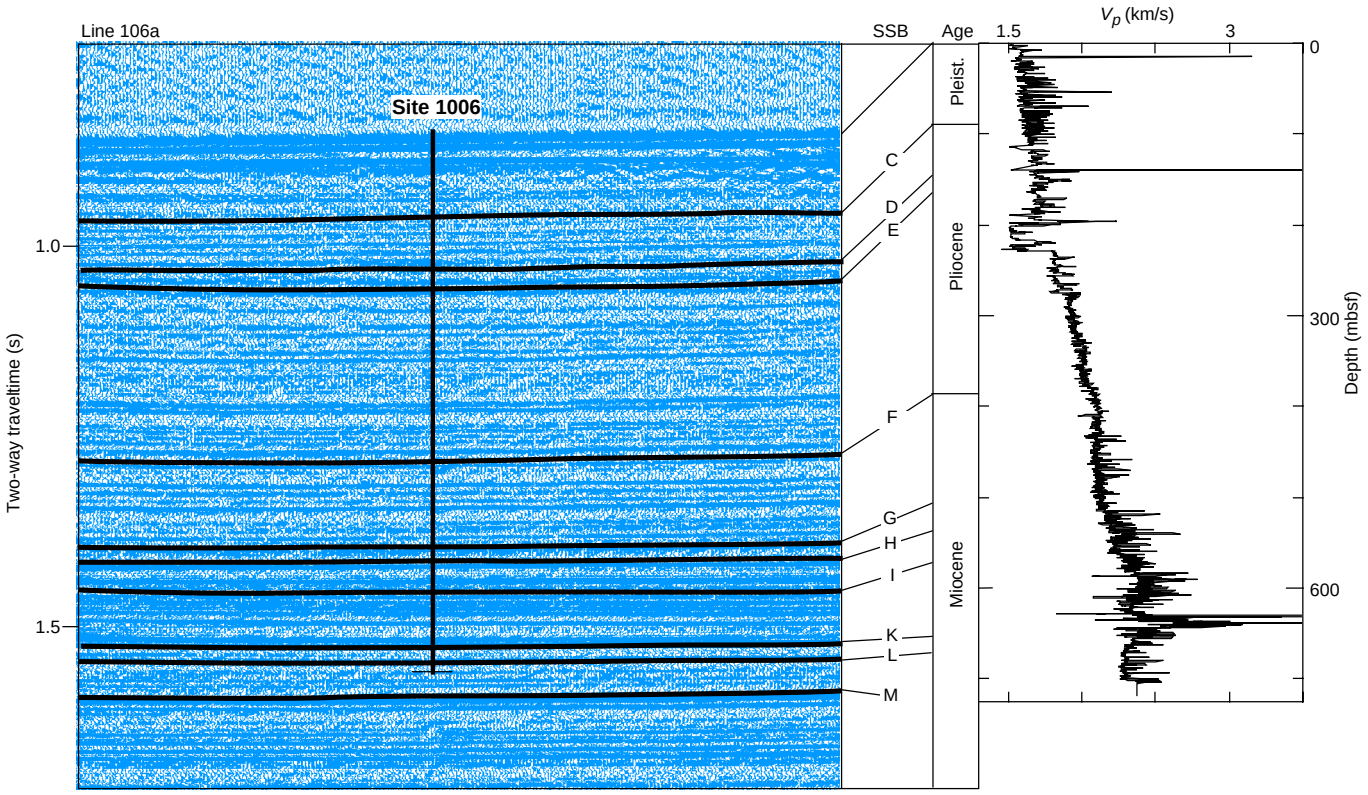


Figure 35. Part of seismic Line 106a with location of Site 1006. The major sequence boundaries have been traced and converted to depth. Origin of seismic reflections can be identified in the displayed sonic log.

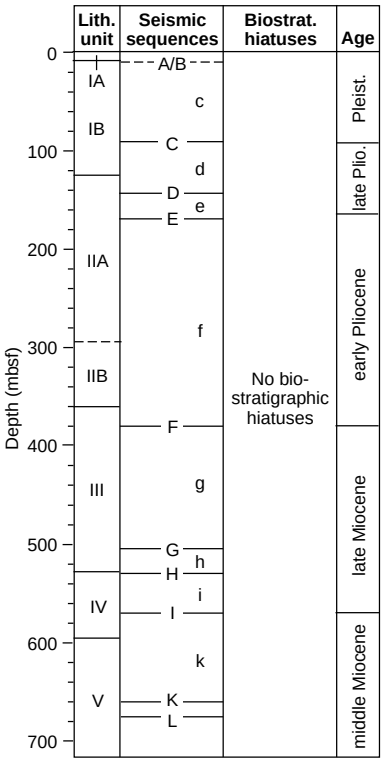


Figure 36. Correlation between lithostratigraphic units, seismic sequences, biostratigraphic hiatuses, and ages.

**Table 20. Check-shot stations of VSP survey in Hole 1006A.**

| Check-shot station | Depth (mbsf) | TWT below seafloor (msbsf) | TWT below sea level (msbsl) |
|---|---|---|---|
| Seafloor | 0 | 0 | 877.5 |
| 166-1006A- | | | |
| 1 | 105.6 | 116.08 | 993.58 |
| 2 | 130.6 | 141.96 | 1019.5 |
| 3 | 150.6 | 166.61 | 1044.1 |
| 4 | 240.6 | 262.03 | 1139.5 |
| 5 | 295.6 | 323.34 | 1200.8 |
| 6 | 340.6 | 369.22 | 1246.7 |
| 7 | 390.6 | 418.11 | 1295.6 |
| 8 | 440.6 | 464.39 | 1341.9 |
| 9 | 490.6 | 512.66 | 1390.2 |
| 10 | 540.6 | 558.72 | 1436.2 |
| 11 | 587.6 | 600.38 | 1477.9 |
| 12 | 633.8 | 639.03 | 1516.5 |
| 13 | 660.6 | 660.66 | 1538.2 |
| 14 | 714.6 | 708.51 | 1586 |

and remain much more variable below the boundary, which is in concert with this downhole trend. The amplitude of the seismic reflections within Sequence *k* increases. Highest velocities are reached in the interval between 630 and 650 mbsf, which lies close to SSBs K and L at 660 and 675 mbsf, respectively.

## SUMMARY AND CONCLUSIONS

Site 1006, situated approximately 25 km from the western margin of GBB, cored a 717.3-m-thick sequence of drift deposits, of Holocene to middle Miocene age. The coring at Site 1006 achieved most of the objectives outlined previously (see “Background and Objectives” section, this chapter). These objectives were to (1) retrieve a

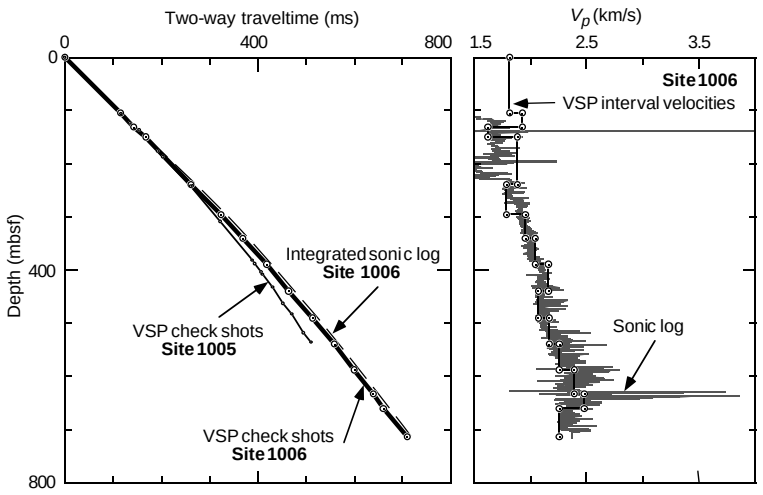


Figure 37. Left side: Time-depth curves for Site 1006. VSP check shots are displayed in thick line and stations are marked by open circles. The measured VSP values are compared with the integrated sonic log of Site 1006 (combined near and far trace) and the VSP curve of Site 1005. Right side: the interval velocities derived from traveltimes between the 14 VSP stations are displayed overlying the sonic log velocities (for discussion see text).

**Table 21. Time-depth conversion and tentative age assignments of seismic sequence boundaries.**

| Seismic sequence boundary | TWT below seafloor (msbsf) | Depth (mbsf) | Nannofossil zone | Foraminifer zone | Age | Age* (Ma) |
|---|---|---|---|---|---|---|
| A | Not resolvable | | | N22 | Holocene/Pleistocene | |
| B | Not resolvable | | NN20 | N22 | Pleistocene | |
| C | 100 | 90 | NN19/18 | N22 | Pleistocene/Pliocene | 1.8 |
| D | 160 | 145 | NN 16 | N20/21 | late Pliocene | 3.1 |
| E | 190 | 170 | NN16/15 | N19 | early/late Pliocene | 3.6 |
| F | 410 | 380 | NN11 | N17-18 | Messinian | 5.4 |
| G | 530 | 505 | NN10 | N16 | late Miocene | 8.7 |
| H | 550 | 530 | NN10/9? | N16 | late Miocene | 9.4 |
| I | 585 | 570 | NN8 | N16 | middle Miocene | 10.7 |
| K | 660 | 660 | NN7 | N12 | | 12.4 |
| L | 675 | 675 | NN7 | N12/11 | | 12.7 |
| M | Below TD | | | | | |

Note: * = ages are preliminary and based on shipboard biostratigraphy (see “Biostratigraphy” section, “Explanatory Notes” chapter, this volume).

complete Neogene section for the purposes of dating, (2) examine changes in the interplay between continentally and platform-derived sediments and the consequent record of sea level and currents, and (3) assess geothermal and geochemical gradients in a basinal setting for comparison to the more proximal sites.

The biostratigraphic control throughout Site 1006 is excellent, and almost all planktonic foraminiferal and nannofossil zones from the Pleistocene to upper middle Miocene are found. At this site, the abundant pelagic biogenic components are less diluted by platform-derived material, and microfossil preservation is less affected by diagenesis than in the upper slope sites (Sites 1003, 1004, and 1007). The sedimentary sequence contains abundant well-preserved foraminifers that will be dated using O- and Sr-isotope stratigraphy and tied to the shallow sites, which will complement and refine the ages of the sequence boundaries and sea-level changes. In addition, the oxygen isotopes will provide their own independent record of the sea-level changes that can be compared to the sequence stratigraphic record. Sequence boundaries have been dated and traced to the proximal sites where the ages agree well with those determined at Sites 1003 and 1005. The position of the boundaries has been verified using a combination of VSP and integrated sonic logs.

Chemical profiles in the interstitial pore waters reveal a shallow zone flushed by seawater extending to 20 mbsf. Below this depth, profiles are mainly diffusionally controlled with the exception of certain elements that are locally influenced by diagenetic reactions.

## Sedimentary Environment and Sequence Stratigraphy

The sedimentary section at Site 1006, consisted of mixed pelagic and bank-derived carbonates with varying amounts of clay material penetrating through 11 SSBs (A–L) into the middle Miocene Sequence *m*. Seismic sequence boundaries fell in the expected positions based on correlations determined at Site 1003. Velocities measured on board ship on discrete samples, however, predicted significantly lower interval velocities, a phenomenon resulting from the soft nature of the rocks and the fact that shipboard velocities are not measured under in situ pressure.

All sequence boundaries are conformable at Site 1006 and show a thinning toward the east and interfingering with downlapping slope deposits. The sediments have been divided into five lithostratigraphic units on the basis of compositional and textural changes. Unit I (0–125.95 mbsf, Hole 1006A; 0–127.9 mbsf, Hole 1006B) was deposited during the Pleistocene–late Pliocene. It consists of largely unlithified bioturbated nannofossil ooze (sand- to silt-sized foraminifers) with a small component of aragonite needles in Subunit IA. Particle abundance and grain size increase downhole to the base of the subunit. In Subunit IB, this ooze is interbedded with gray and olive clays reflecting erosion from a continental source, probably Cuba and Hispaniola. Within this unit, SSBs A, B, and C are present, although the upper two, postulated to lie at 0.5 and 12 mbsf, respectively, could not be traced on the seismic section as a result of ghost reflections

near the sediment-water interface. Sequence *c* has its lower boundary at 90 mbsf coincident with the Pliocene/Pleistocene boundary (1.8 Ma). The base of Sequence *d* occurs at 145 mbsf near the top of Unit II (125.95–360 mbsf, Hole 1006A; 127.9–176.5 mbsf, Hole 1006B) and coincides with a strong peak in the sonic signal (3.1 Ma). This unit consists of nannofossil ooze and chalk in which some grains have been infilled by pyrite. Minor to moderate bioturbation is pervasive, and in some portions there is an alternation between nannofossil ooze and a more aragonite-rich ooze containing some peloids. Subunit IIB is defined by the occurrence of chalk, but is generally uniform as a result of the high rates of sedimentation. The base of Unit II coincides approximately with SSB F and the late Miocene/early Pliocene boundary at 3.6 Ma. Unit III (360–528.7 mbsf) is composed primarily of light gray and light greenish gray chalk with a series of fining-upward intervals. Firmgrounds, characterized by sharp burrowed contacts, are frequent in the upper part. Although Unit III is composed of two sequences, *g* and *h*, the majority of the unit consists of Sequence *g*. Sequence *h* consists of a short 25-m section at the base of Unit III. The excellent nannofossil and foraminifer stratigraphy at this site enabled Sequence *f* to be dated as Messinian. At Site 1003, this sequence did not carry any age-diagnostic fossils. Here SSB F is dated as 5.5 Ma and SSB G as 8.7 Ma in age. Unit IV (528.7– 594.25 mbsf) is late Miocene to latest middle Miocene in age and is composed of light gray and greenish gray nannofossil chalk. The uppermost portion contains a series of thick intervals with sharp basal contacts. Within each interval, nannofossil chalk with bioclasts grade upward into nannofossil chalk and clay. Unit IV mainly consists of Sequence *i*, with SSB I occurring at the boundary between the middle and upper Miocene (10.7 Ma). This boundary is characterized on the downhole logs by an increase in the gamma-ray signal and velocities. The lower part of Unit IV is punctuated by a series of firmgrounds, corresponding to Sequence *k*. This sequence extends into Unit V (594.25–717.3 mbsf), which is composed of alternating intervals of olive nannofossil chalk and light gray nannofossil chalk with foraminifers. Throughout the entire unit, no primary sedimentary structures are visible. The degree of lithification increases downhole, resulting in a lower portion that consists of alternating intervals of chalk and limestone. The greenish gray to olive intervals are characterized by well-defined, flattened burrows that occur in association with *Chondrites*-types. The light gray intervals contain larger, well-defined burrows. SSB K coincides with a zone of higher velocity, which is dated as 12.4 Ma. Sequences *l* and *m* also occur within Unit V and, despite being composed of similar types of sediments, are characterized by distinct changes in physical properties. SSB L is dated as 12.7 Ma. SSB M was not reached.

The facies succession at Site 1006 is interpreted as being governed by an interplay of current activity and sea-level fluctuations. It is suggested that the bottom of high-frequency cycles, which contain clay intervals, reflect the erosion of siliciclastics. These are covered by nannofossil ooze with platform-derived bioclasts indicating neritic production. These changes are reflected in the bulk mineralogy, with high aragonite recording high sea level. Aragonite, abundant in the Pleistocene-aged sediments, also appears to be highly correlated with the color reflectance at 700 nm.

The logging data indicate that there is a downhole compaction trend of increasing density, resistivity, and sonic velocity, whereas porosity decreases. The logs of the cored sedimentary sequence are also characterized throughout by small-scale cyclicity observed in FMS microresistivity images as alternations between thin, resistive, low natural gamma-ray layers and conductive, higher gamma-ray intervals (Fig. 31). This cyclicity is also well-defined by porosity, density, and velocity.

Imaging of the sediments using FMS has shown two clear intervals of high resistivity (335–445 mbsf and 515–665 mbsf). The upper zone spans the Miocene/Pliocene boundary, whereas the lower zone is coincident with the middle/late Miocene boundary. The zones are proposed to represent periods of high-contour current activity. Firmgrounds are recognized by increased gamma ray, resistivity, and sonic velocity. A pattern of larger scale cyclicity reflects changes in the abundance and spatial frequency of the cycles. These patterns may be related to depositional changes associated with current intensity and can be tentatively correlated with sequence boundaries. As a result of the high percentage core recovery, these logs offer an excellent opportunity for core log correlation and spatial analysis of high-frequency sedimentary cycles.

## Chronostratigraphy and Sedimentation Rates

Sediments recovered from Site 1006 yield common to abundant, upper Pleistocene through middle Miocene, calcareous microfossils. The abundant pelagic biogenic components are less diluted by platform-derived material, and the site has an expanded lower Pliocene section that is ideal for paleoceanographic studies. Preservation of microfossils is generally good throughout, which allows a reliable, high-resolution biostratigraphy for Site 1006. Benthic foraminifers indicate an upper middle bathyal paleodepth. An excellent record of magnetic susceptibility exists showing fluctuations between negative and positive values reflecting the input of clay material. A magnetic reversal was found between 4.5 and 6.0 mbsf, which has been tentatively correlated with the Blake Event (0.13 Ma).

Sedimentation rate varies considerably at Site 1006. The rates can be divided into four distinct periods. The rate for the Pliocene–Pleistocene section is 5 cm/k.y., considerably lower than Sites 1003–1005 over the same interval. The rate for the lower Pliocene and uppermost Miocene is 12 cm/k.y., similar to the proximal sites. The upper Miocene has a low sedimentation rate (3 cm/k.y.) that is within the range of normal pelagic sedimentation. The middle Miocene has slightly higher rates, perhaps accounted for by contourite deposition and the deposition of fine-grained, platform-derived material.

## Fluid Chemistry

Chemical profiles reveal a shallow, flushed zone extending to 20 mbsf. This zone is up to 20 m shallower than observed at Site 1005. In contrast to the slope sites, where there were no changes in the nonconservative elements, minor changes are observed in $Ca^{2+}$, $Sr^{2+}$, and alkalinity. These small changes suggest a less active flow than in the proximal sites. Beneath this depth, the sediment profiles are dominated by diffusion from an underlying $Cl^-$ rich brine with local reactions involving $Ca^{2+}$, $Mg^{2+}$, $Sr^{2+}$, $K^+$, $Li^+$, $F^-$, and $H_2SiO_4$, thereby providing deviations from the normally diffusive profiles. At the base of Hole 1006A, the $Cl^-$ concentration reaches a value of 717 mM. The $Sr^{2+}$ concentration rises steadily over this interval, as a result of the dissolution of aragonite, and the precipitation of calcite and dolomite. At 452.95 mbsf, the $Sr^{2+}$ concentration reaches 7 mM, the highest values recorded in ODP or DSDP history. The $Sr^{2+}$ can attain this high concentration primarily because sulfate has been completely utilized in the oxidation of organic material. Concentrations of $H_2S$ are low at this site as a result of the abundance of iron that allows the formation of pyrite. The removal of $H_2S$ from the system prevents it from lowering the pH of the pore waters and causing further dissolution reactions to take place. Rates of closed system diagenesis would therefore be expected to be lower at Site 1006 than at the proximal sites for the following reasons: (1) lower input of metastable minerals as a consequence of the distance of Site 1006 from the platform, (2) lower permeability and less circulation of fluids through the sediments, (3) lower concentrations of organic material, and (4) removal of $H_2S$ by reaction with pyrite.

In summary, Site 1006 has met and exceeded all of its initial expectations. Based on shipboard biostratigraphy, the sequence boundaries have been dated and traced to the proximal sites where the ages agree well with those determined at Sites 1003 and 1005. The posi-

tion of the boundaries has been verified using a combination of VSP and integrated sonic logs. The excellent continuous sedimentary sequence contains abundant well-preserved foraminifers that will be able to be dated using O- and Sr-isotope stratigraphy. Establishing the sea-level changes from the oxygen isotopes of foraminifers will provide the unique opportunity to compare this proxy with the sequence stratigraphic expression of sea-level changes along the same transect. With this correlation, another primary goal of Leg 166 will be achieved as the isotopic and sedimentary record can be compared. The expanded Pliocene and upper Miocene sequence, combined with the excellent preservation, will allow this site to become a classic site for upper Neogene paleoceanography in the low-latitude Atlantic.

## REFERENCES


Berggren, W.A., Kent, D.V., Swisher, C.C., III, and Aubry, M.-P., 1995. A revised Cenozoic geochronology and chronostratigraphy. *In* Berggren, W.A., Kent, D.V., Aubry, M.-P., and Hardenbol, J. (Eds.), *Geochronology, Time Scales and Global Stratigraphic Correlation*. Spec. Publ.—Soc. Econ. Paleontol. Mineral., 54:129–212.

Davies, P.J., McKenzie, J.A., Palmer-Julson, A., et al., 1991. *Proc. ODP, Init. Repts.*, 133 (Pts. 1, 2): College Station, TX (Ocean Drilling Program).

De Carlo, E.H., 1992. Geochemistry of pore water and sediments recovered from the Exmouth Plateau. *In* von Rad, U., Haq, B.U., et al., *Proc. ODP, Sci. Results*, 122: College Station, TX (Ocean Drilling Program), 295–308.

Gieskes, J.M., 1983. The chemistry of interstitial waters of deep-sea sediments: interpretation of deep-sea drilling data. *In* Riley, J.P., and Chester, R. (Eds.), *Chemical Oceanography* (Vol. 8): London (Academic), 221–269.

Gross, M.G., 1982. *Oceanography: a View of the Oceans* (3rd ed.): London (Prentice Hall).

Hagelberg, T., Shackleton, N., Pisias, N., and Shipboard Scientific Party, 1992. Development of composite depth sections for Sites 844 through 854. *In* Mayer, L., Pisias, N., Janecek, T., et al., *Proc. ODP, Init. Repts.*, 138 (Pt. 1): College Station, TX (Ocean Drilling Program), 79–85.

Handford, C.R., and Loucks, R.G., 1993. Carbonate depositional sequences and systems tracts: responses of carbonate platforms to relative sea-level changes. *In* Loucks, R.G., and Sarg, J.F. (Eds.), *Carbonate Sequence Stratigraphy.* AAPG Mem., 57:3–41.

Kendall, C.G.St.C., and Schlager, W., 1981. Carbonates and relative changes in sea level. *In* Cita, M.B., and Ryan, W.B.F. (Eds.), *Carbonate Platforms of the Passive-type Continental Margins, Present and Past.* Mar. Geol., 44:181–212.

Krauskopf, K.B., 1979. *Introduction to Geochemistry* (2nd ed.): New York (McGraw-Hill).

Morse, J.W., and Mackenzie, F.T., 1990. *Geochemistry of Sedimentary Carbonates.* Dev. in Sedimentology, 48: Amsterdam (Elsevier).

Parrilla, G., Lavin, A., Bryden, H., Garcia, M., and Millard, R., 1994. Rising temperatures in the subtropical North Atlantic Ocean over the past 35 years. *Nature*, 369:48–51.

Reijmer, J.J.G., Schlager, W., Bosscher, H., Beets, C.J., and McNeill, D.F., 1992. Pliocene/Pleistocene platform facies transition recorded in calciturbidites (Exuma Sound, Bahamas). *Sediment. Geol.*, 78:171–179.

Roemmich, D., and Wunsch, C., 1984. Apparent changes in climatic state of the deep North Atlantic Ocean. *Nature*, 307:447–450.

Serra, O., 1986. *Fundamentals of Well-Log Interpretation* (Vol. 2): *The Interpretation of Logging Data.* Dev. Pet. Sci., 15B.

Swart, P.K., and Guzikowski, M., 1988. Interstitial-water chemistry and diagenesis of periplatform sediments from the Bahamas, ODP Leg 101. *In* Austin, J.A., Jr., Schlager, W., Palmer, A.A., et al., *Proc. ODP, Sci. Results*, 101: College Station, TX (Ocean Drilling Program), 363–380.

Wang, K., Lewis, T.J., and Jessop, A.M., 1992. Climatic changes in central and eastern Canada inferred from deep borehole temperature data. *Palaeoceanogr., Palaeoclimatol., Palaeoecol.*, 98:128–141.


**Ms 166IR-109**

**NOTE: Core description forms ("barrel sheets") and core photographs can be found in Section 3, beginning on page 377. Forms containing smear slides can be found in Section 4, beginning on page 831. Thin sections can be found in Section 5, beginning on page 849. See the Table of Contents for material contained on CD-ROM.**

# SHORE-BASED LOG PROCESSING

## Hole 1006A

**Bottom felt:** 669.4 mbrf
**Total penetration:** 717.3 mbsf
**Total core recovered:** 646.93 m (90.2%)

### Logging Runs

**Logging string 1:** DIT/SDT/GPIT/NGT
**Logging string 2:** APS/HLDS/HNGS
**Logging string 3:** FMS/GPIT/NGT
**Logging string 4:** WST

Wireline heave compensator was used to counter ship heave.

### Bottom-Hole Assembly

The following bottom-hole assembly depths are as they appear on the logs after differential depth shift (see "Depth shift" section) and depth shift to the seafloor. As such, there might be a discrepancy with the original depths given by the drillers on board. Possible reasons for depth discrepancies are ship heave, use of wireline heave compensator, and drill string and/or wireline stretch.

DIT/SDT/GPIT/NGT: Bottom-hole assembly at ~104 mbsf.
APS/HLDS/HNGS: Bottom-hole assembly at ~103 mbsf.
FMS/GPIT/NGT: Bottom-hole assembly at ~104 mbsf.

### Processing

**Depth shift:** Original logs have been interactively depth shifted with reference to HNGS from APS/HLDS/HNGS run and to the seafloor (−668.3 m). This amount differs 1.1 m from the "bottom felt" depth given by the drillers and is based on correlation between logs and lithologic markers seen on core.

**Gamma-ray environmental corrections:** Corrections for borehole size and type of drilling fluid were performed on the NGT data from the FMS/GPIT/NGT and DIT/SDT/GPIT/NGT tool strings. HNGS data from the APS/HLDS/HNGS tool string were corrected in real-time during the recording.

**Acoustic data processing:** The array sonic tool was operated in standard depth-derived, borehole compensated, long spacing (8−10 and 10−12 ft) mode. The sonic logs have been processed to eliminate some of the noise and cycle skipping experienced during the recording.

### Quality Control

Data recorded through bottom-hole assembly, such as the HNGS and NGT data above 104 mbsf, should be used qualitatively only because of the attenuation on the incoming signal. Invalid data were recorded at 99−103 mbsf with the NGT form the DIT/SDT/GPIT/NGT tool string.

Hole diameter was recorded by the caliper on the HLDS tool (LCAL) and the caliper on the FMS string ($C_1$ and $C_2$).

Details of standard shore-based processing procedures are found in the "Explanatory Notes" chapter, this volume. For further information about the logs, please contact:

Cristina Broglia
Phone: 914-365-8343
Fax: 914-365-3182
E-mail: chris@ldeo.columbia.edu

Zhiping Tu
Phone: 914-365-8336
Fax: 914-365-3182
E-mail: ztu@ldeo.columbia.edu

Hole 1006A: Natural Gamma Ray-Resistivity-Sonic Logging Data

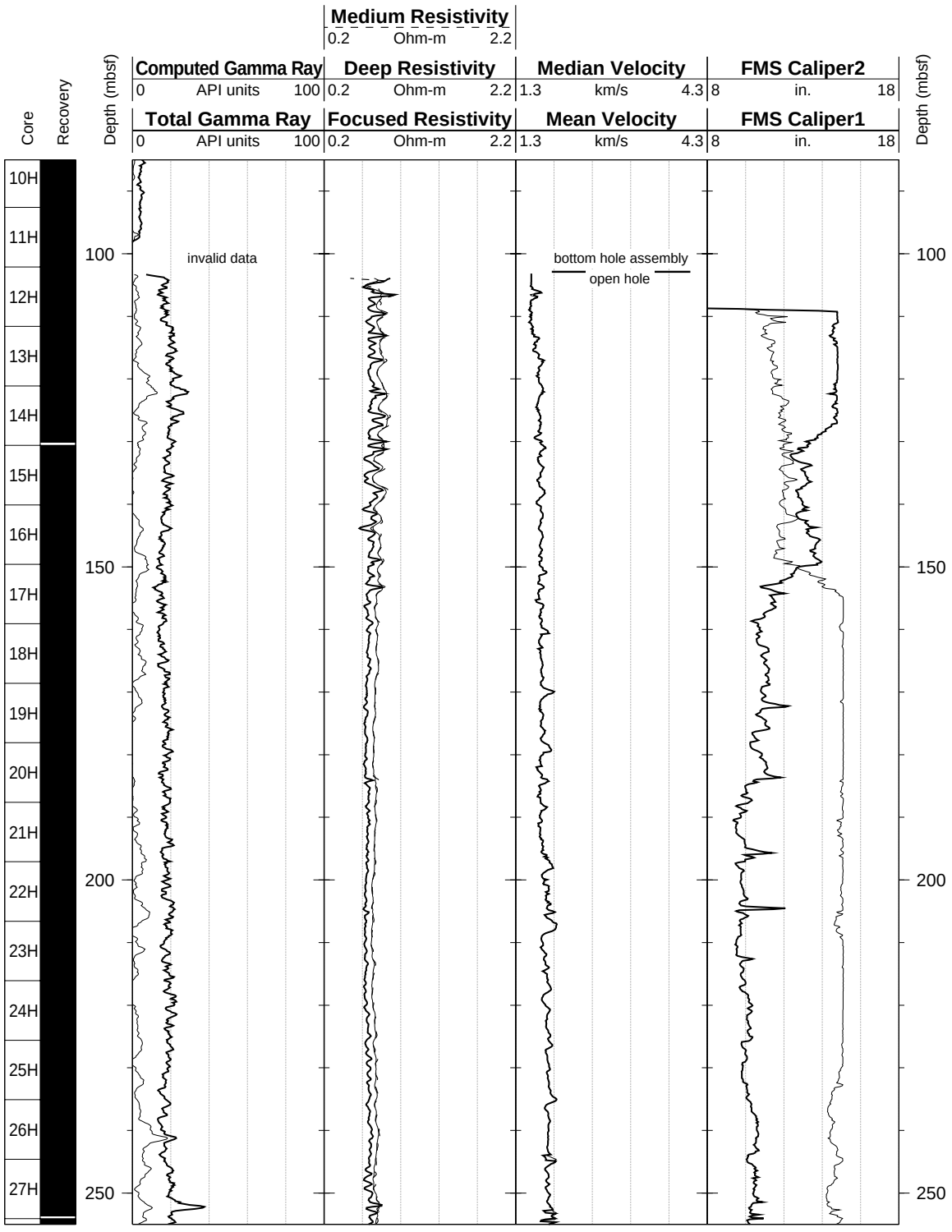

Hole 1006A: Natural Gamma Ray-Resistivity-Sonic Logging Data (cont.)

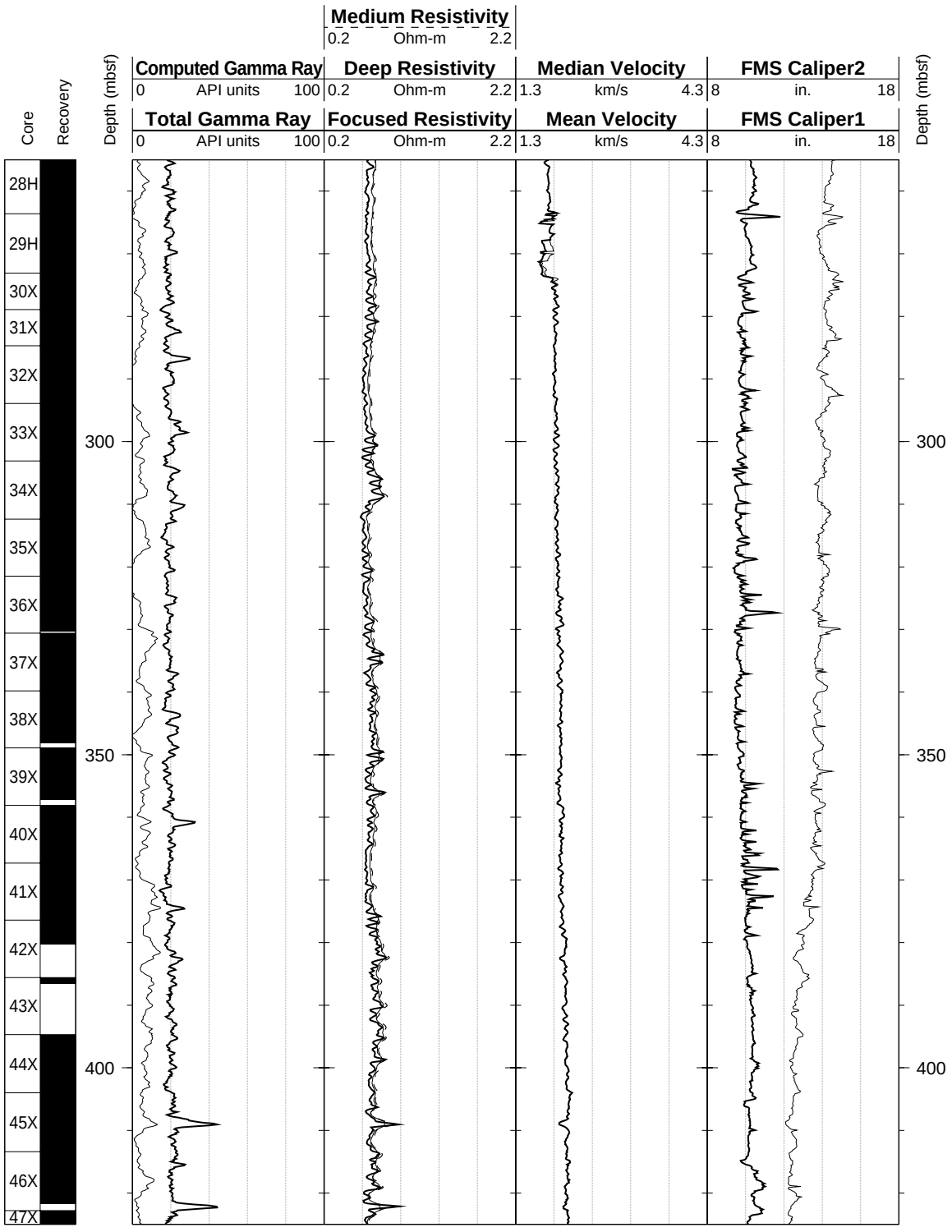

Hole 1006A: Natural Gamma Ray-Resistivity-Sonic Logging Data (cont.)

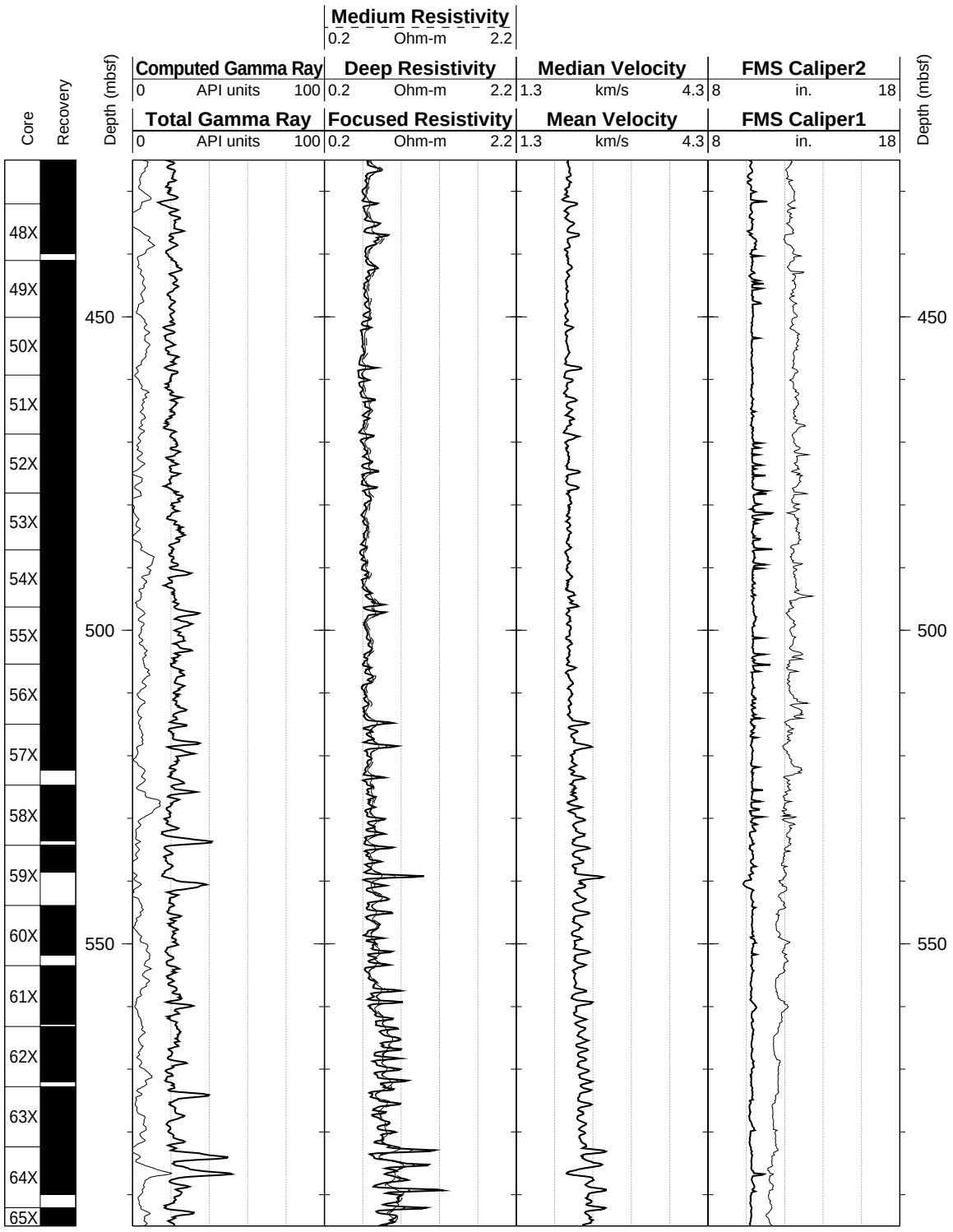

Hole 1006A: Natural Gamma Ray-Resistivity-Sonic Logging Data (cont.)

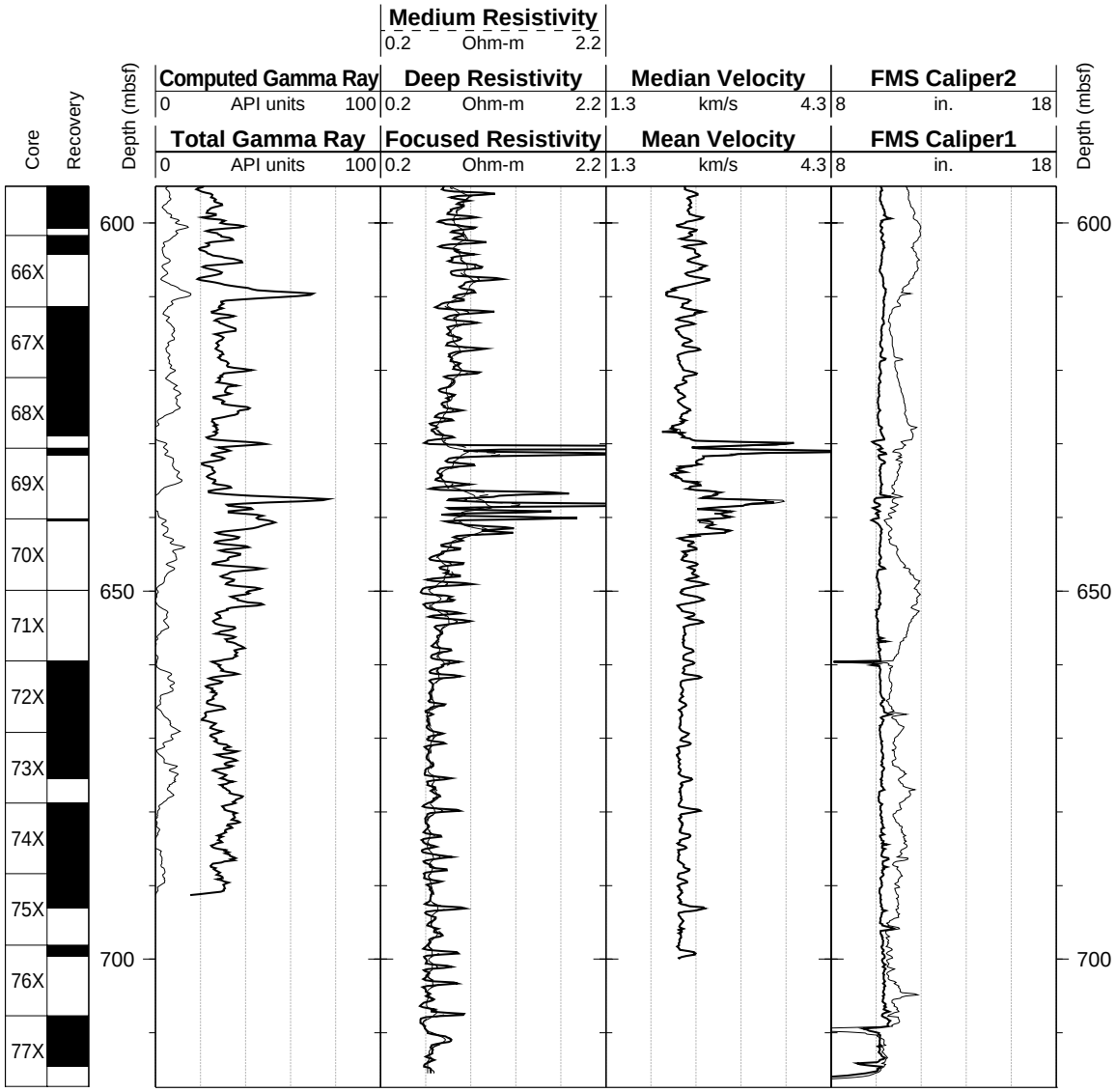

Hole 1006A: Natural Gamma Ray Logging Data

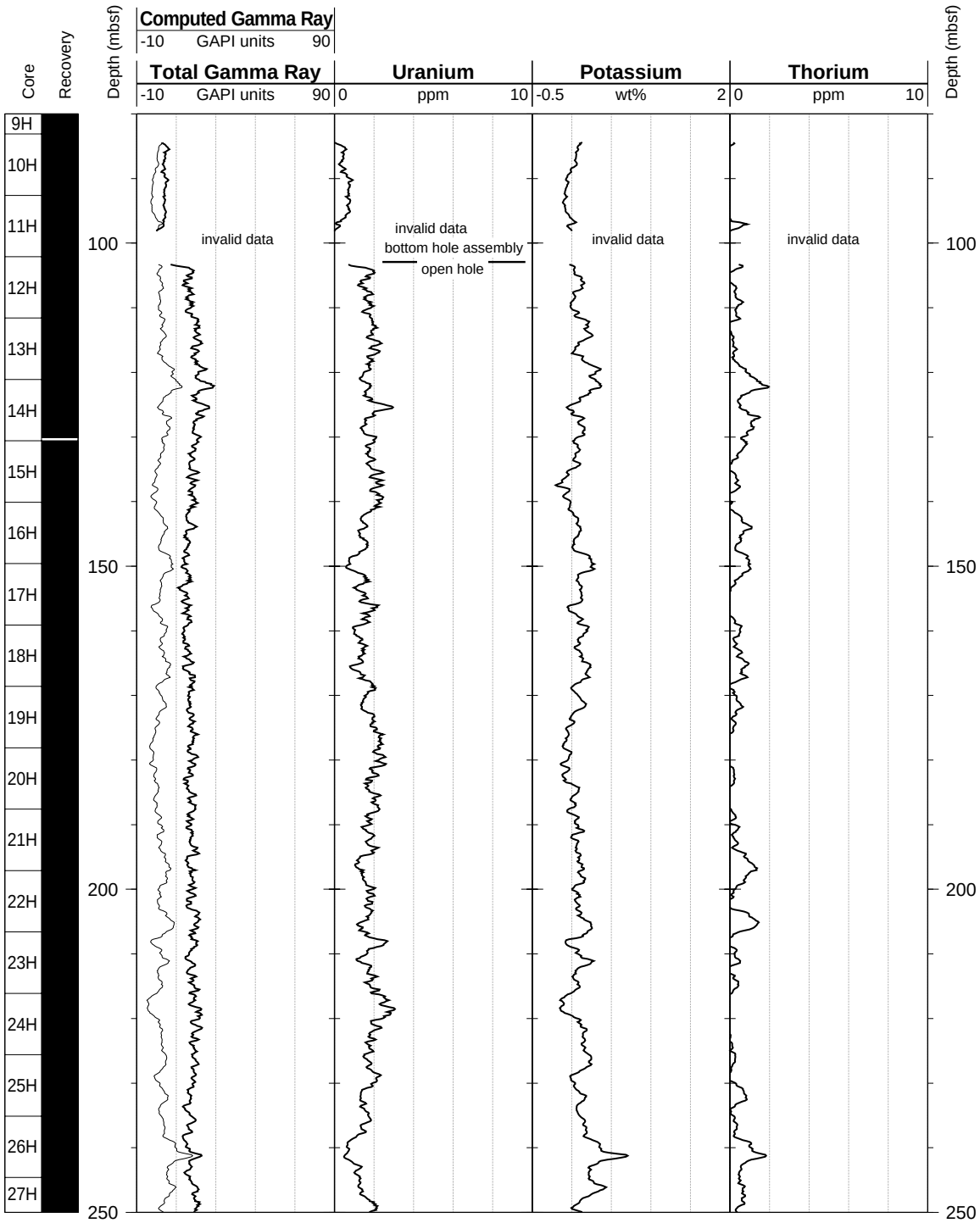

Hole 1006A: Natural Gamma Ray Logging Data (cont.)

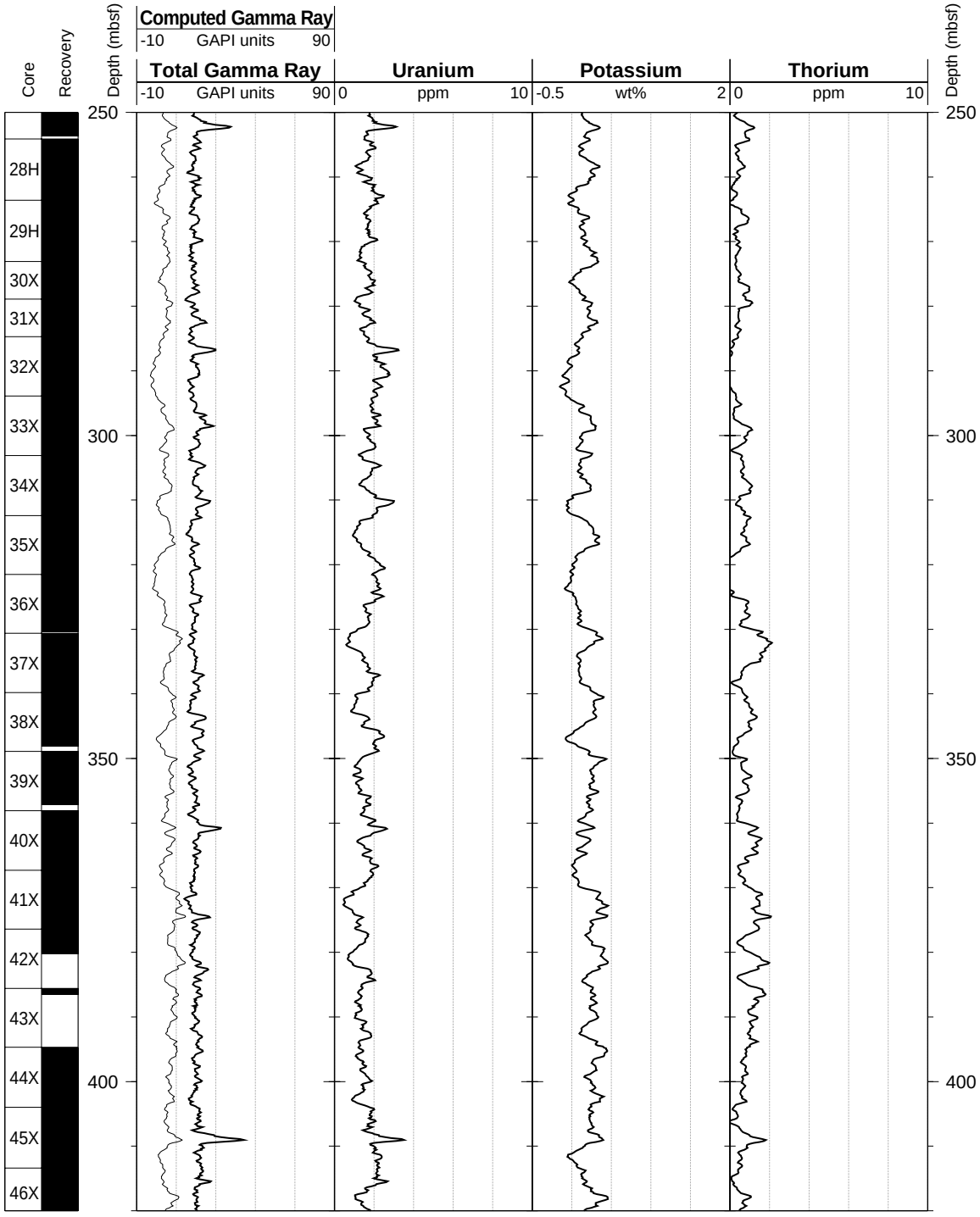

Hole 1006A: Natural Gamma Ray Logging Data (cont.)

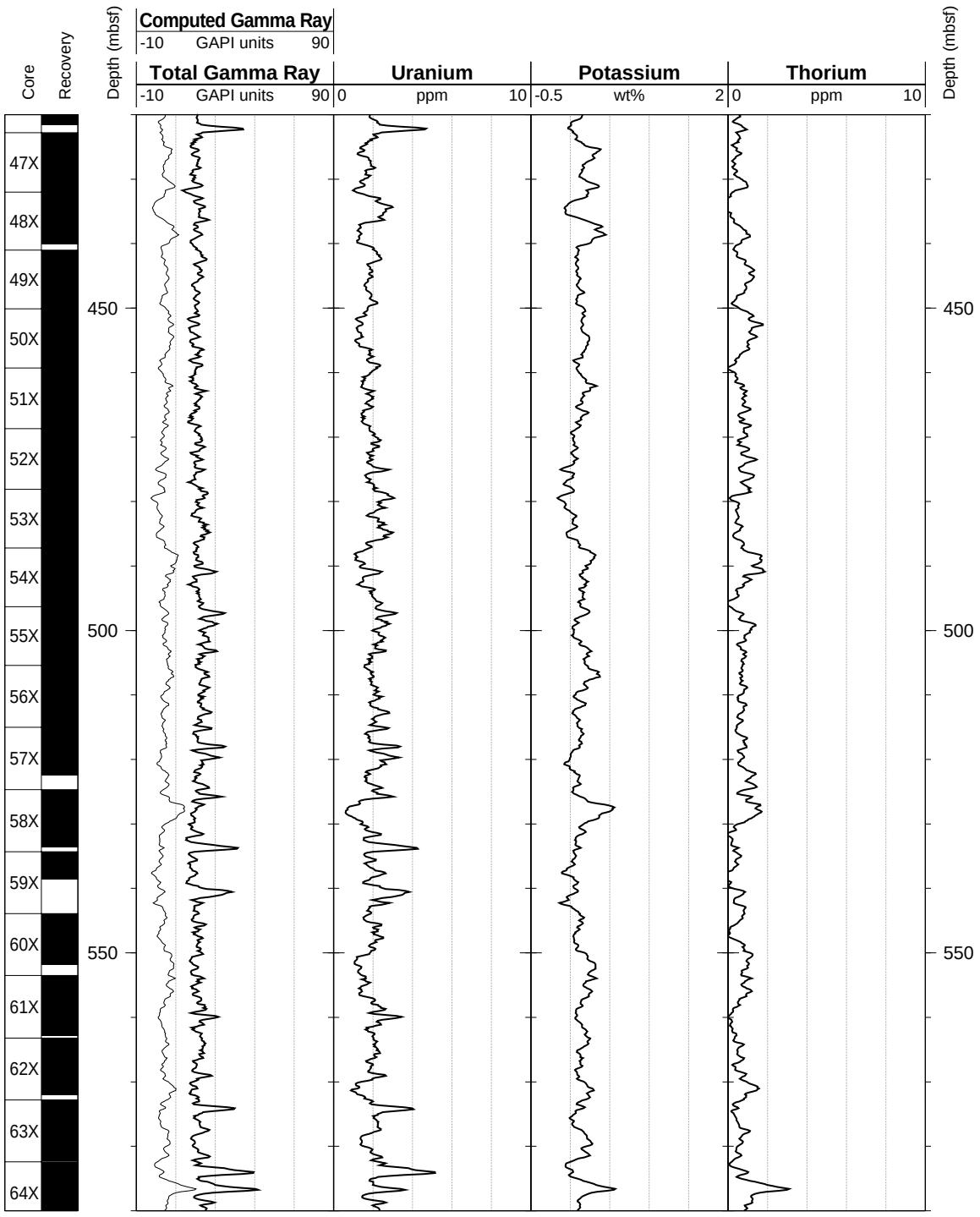

Hole 1006A: Natural Gamma Ray Logging Data (cont.)

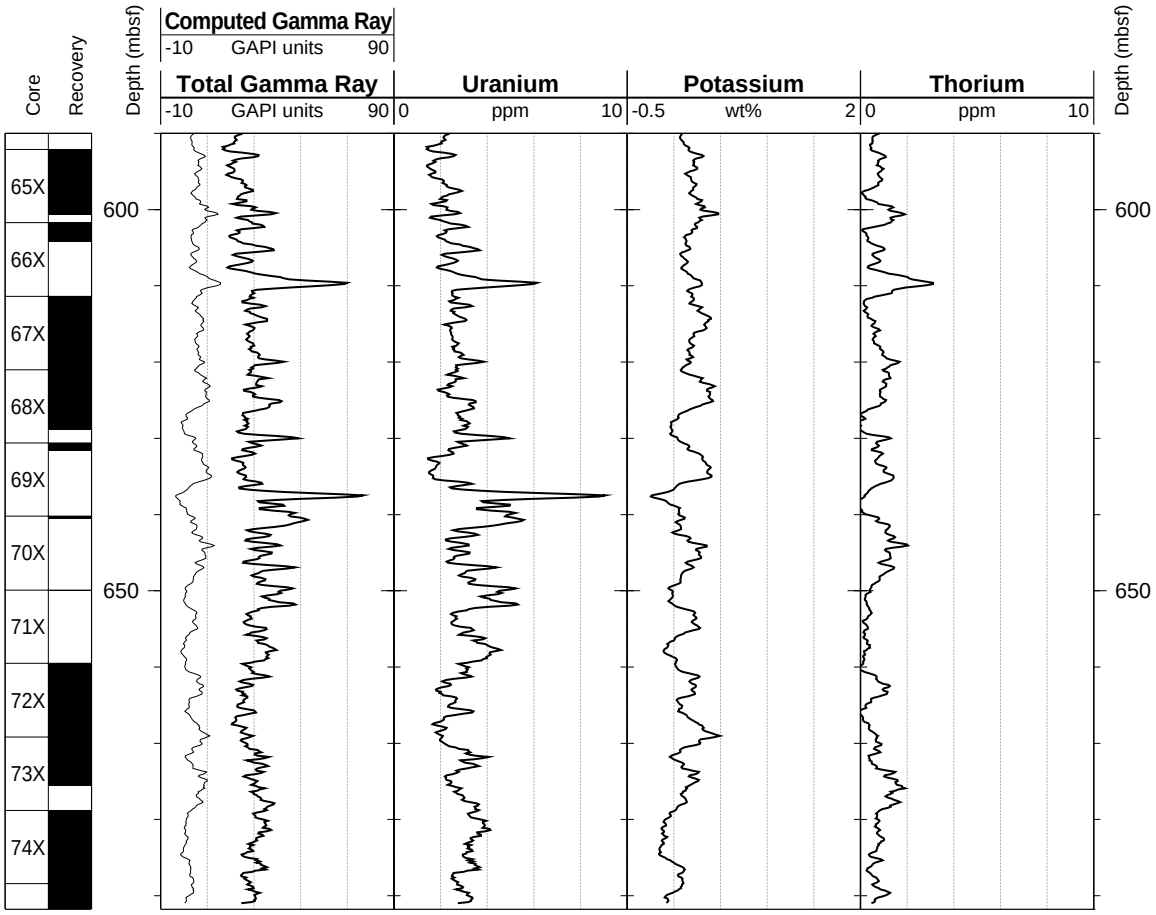

Hole 1006A: Natural Gamma Ray-Density-Porosity Logging Data

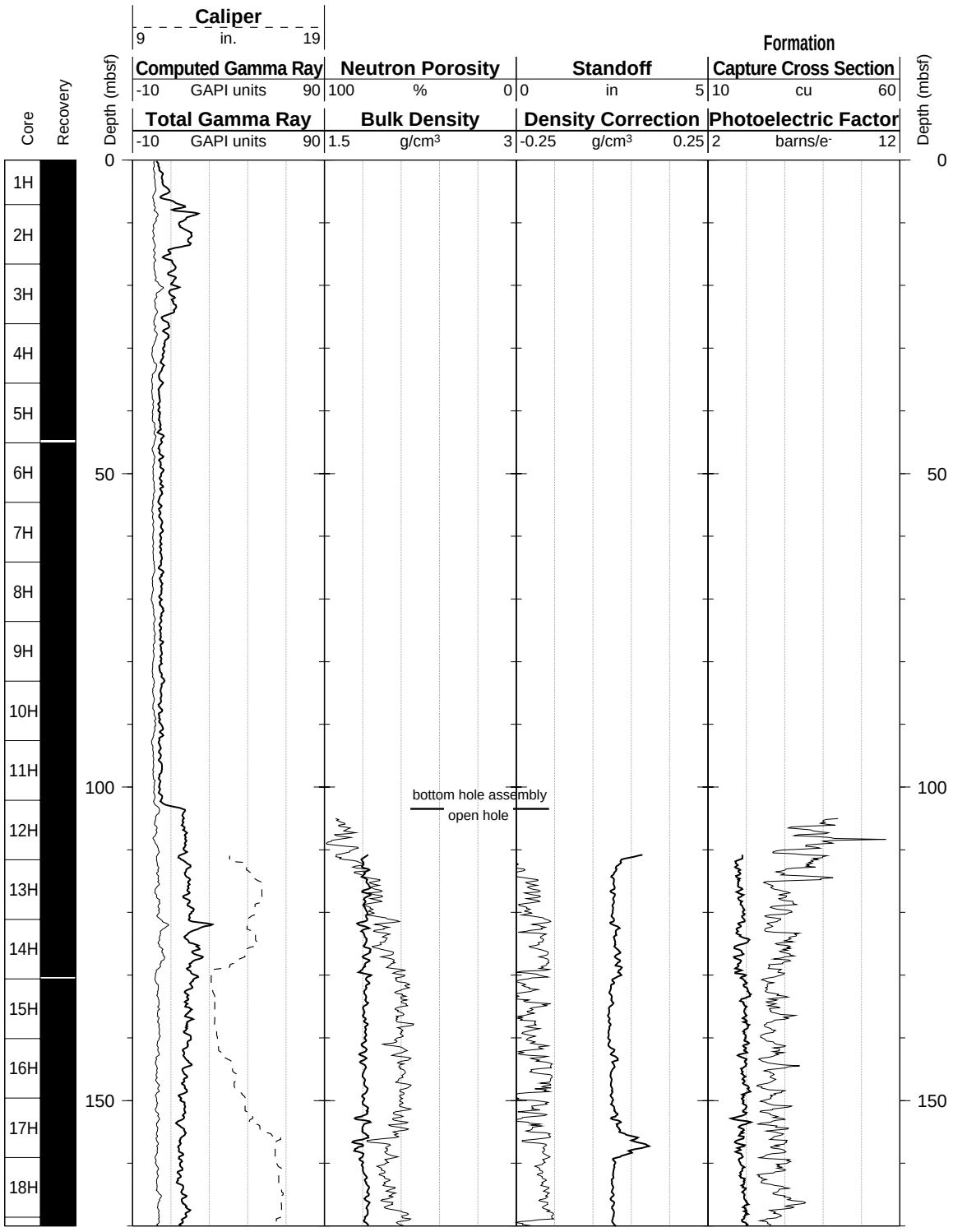

Hole 1006A: Natural Gamma Ray-Density-Porosity Logging Data (cont.)

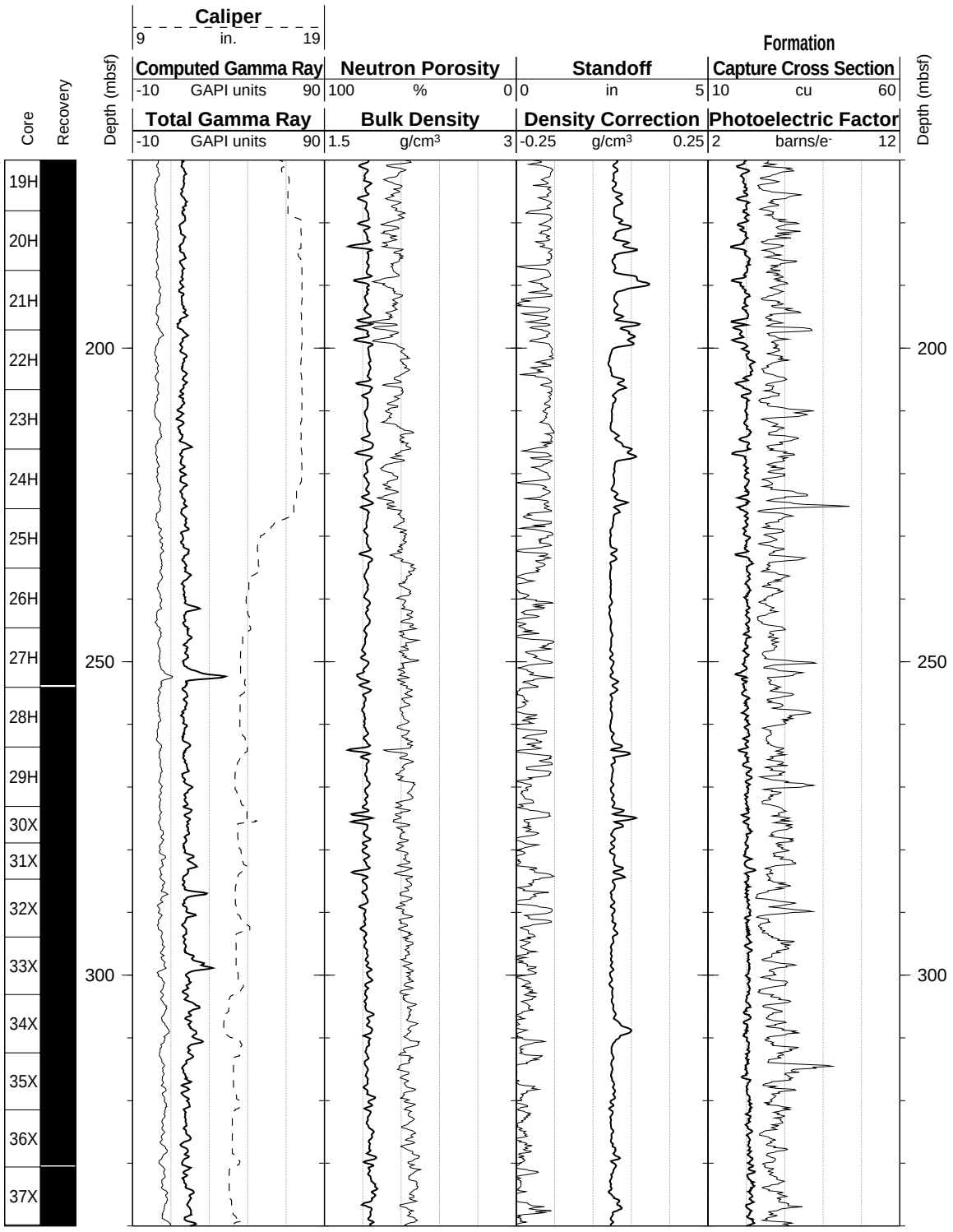

Hole 1006A: Natural Gamma Ray-Density-Porosity Logging Data (cont.)

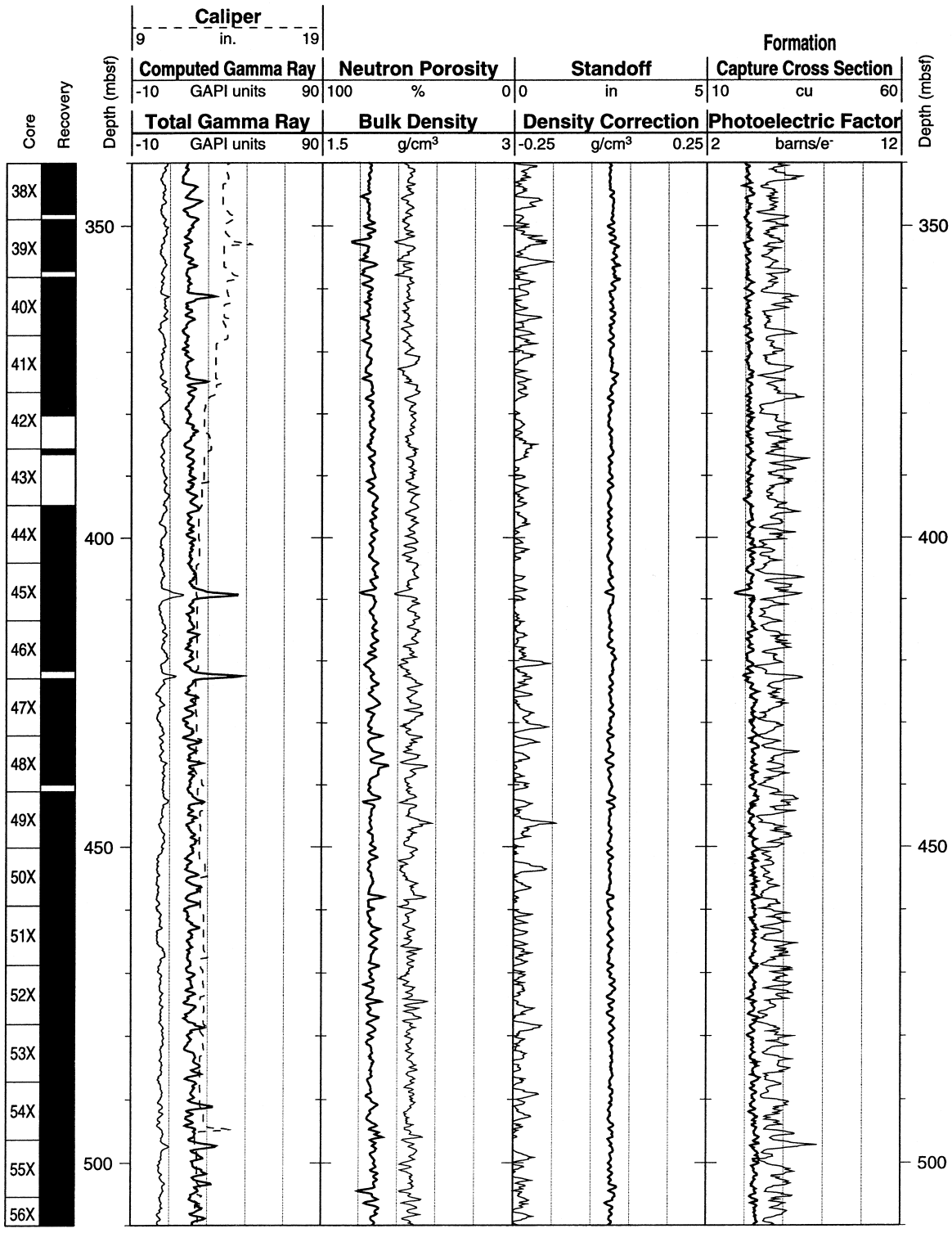

Hole 1006A: Natural Gamma Ray-Density-Porosity Logging Data (cont.)

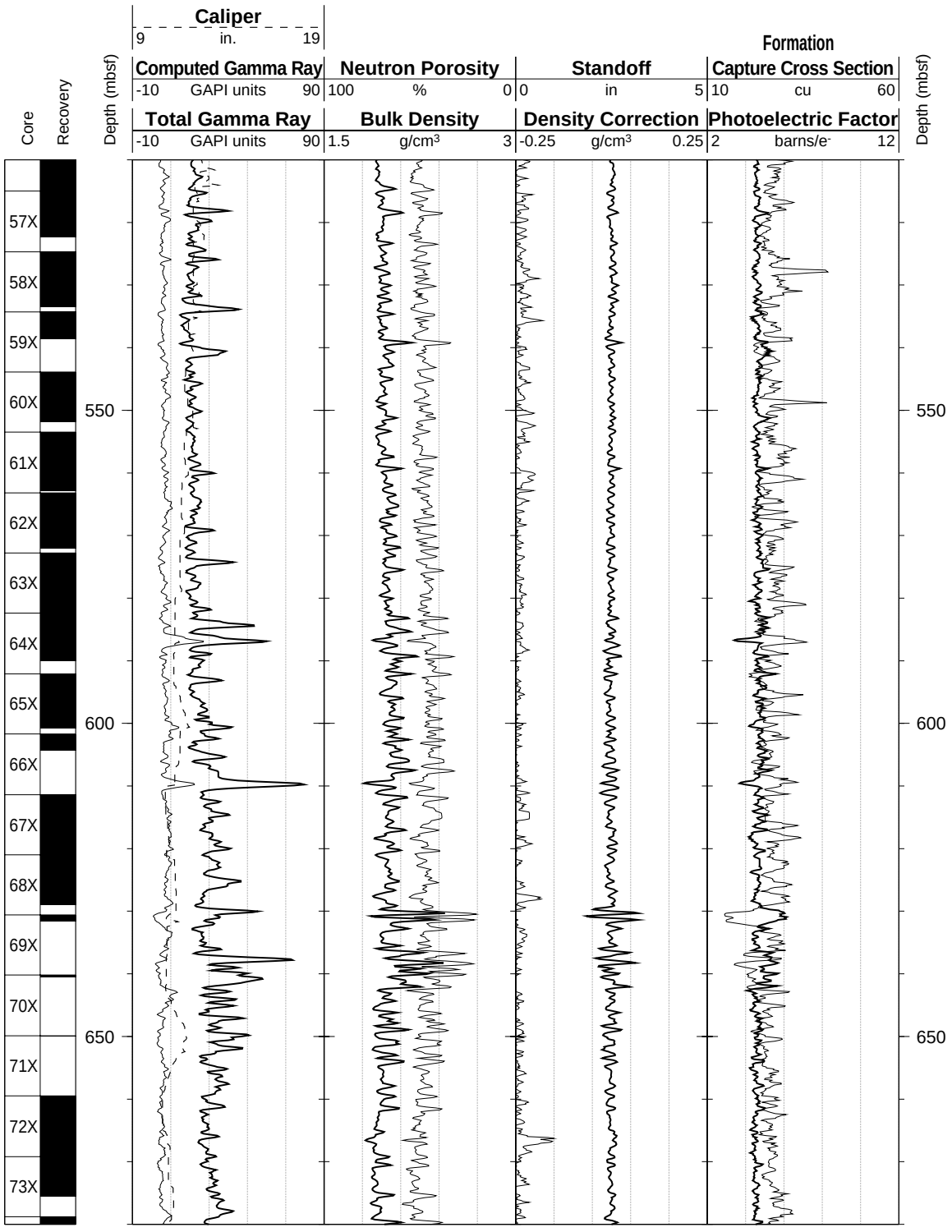

Hole 1006A: Natural Gamma Ray-Density-Porosity Logging Data (cont.)

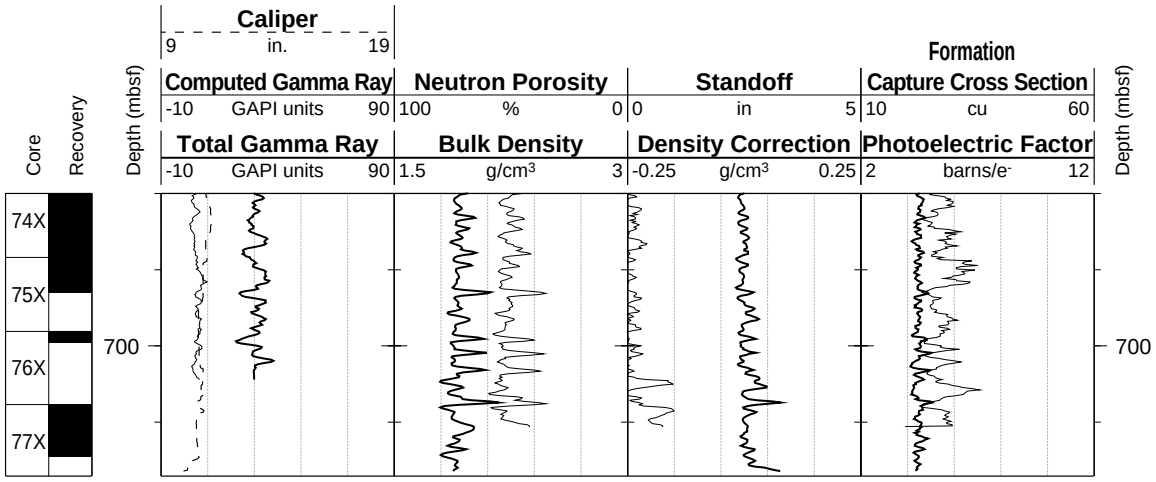

Hole 1006A: Natural Gamma Ray Logging Data

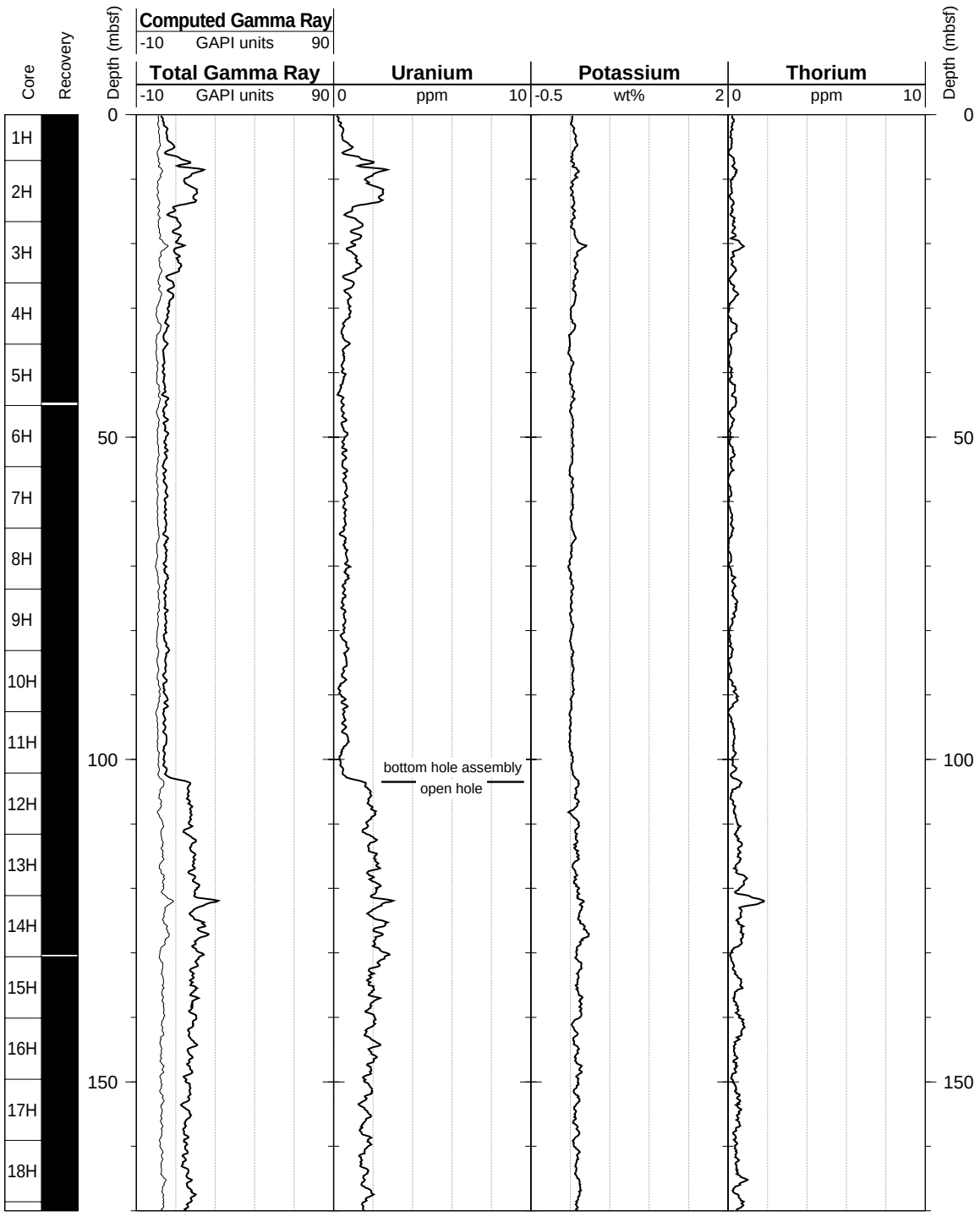

Hole 1006A: Natural Gamma Ray Logging Data (cont.)

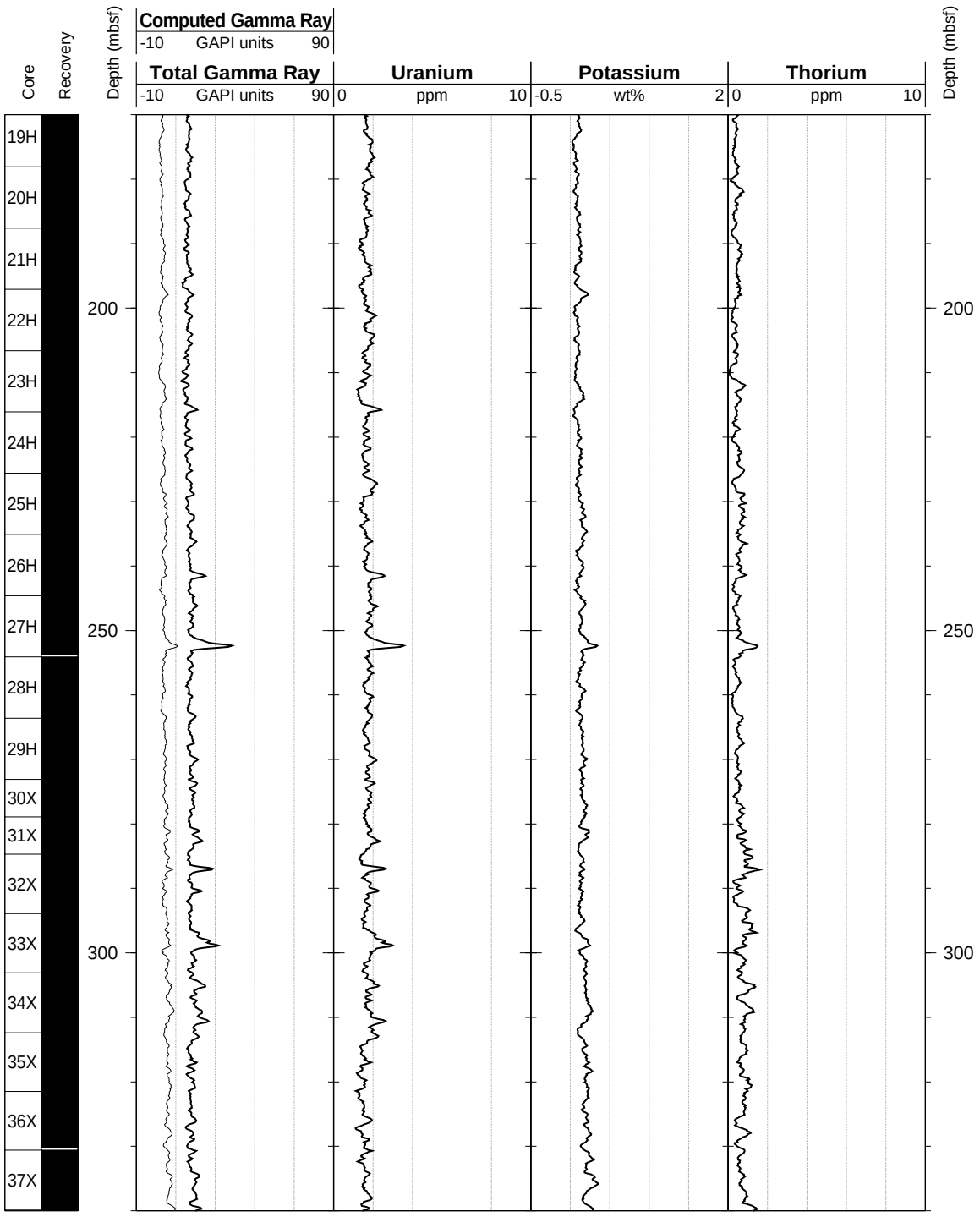

Hole 1006A: Natural Gamma Ray Logging Data (cont.)

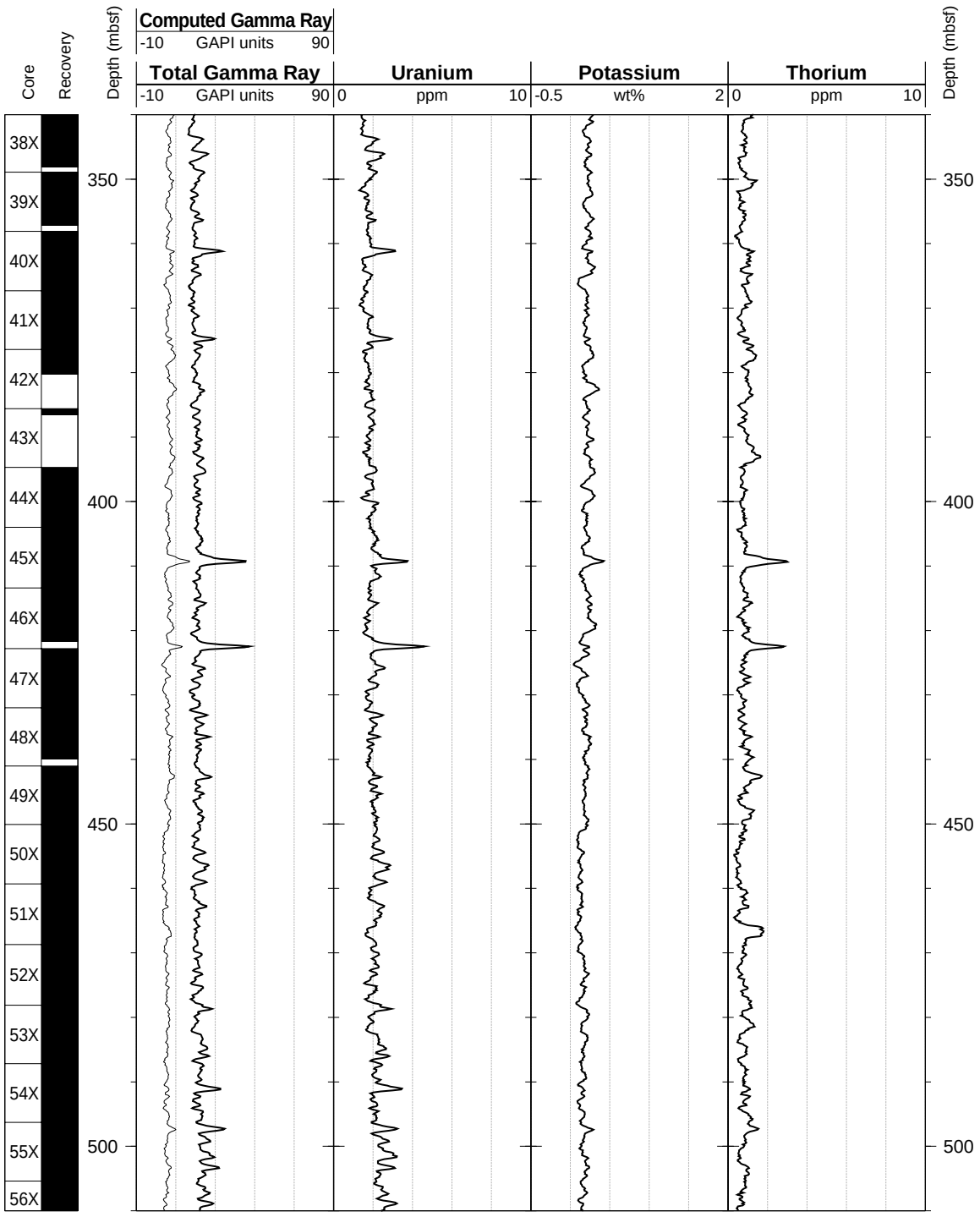

Hole 1006A: Natural Gamma Ray Logging Data (cont.)

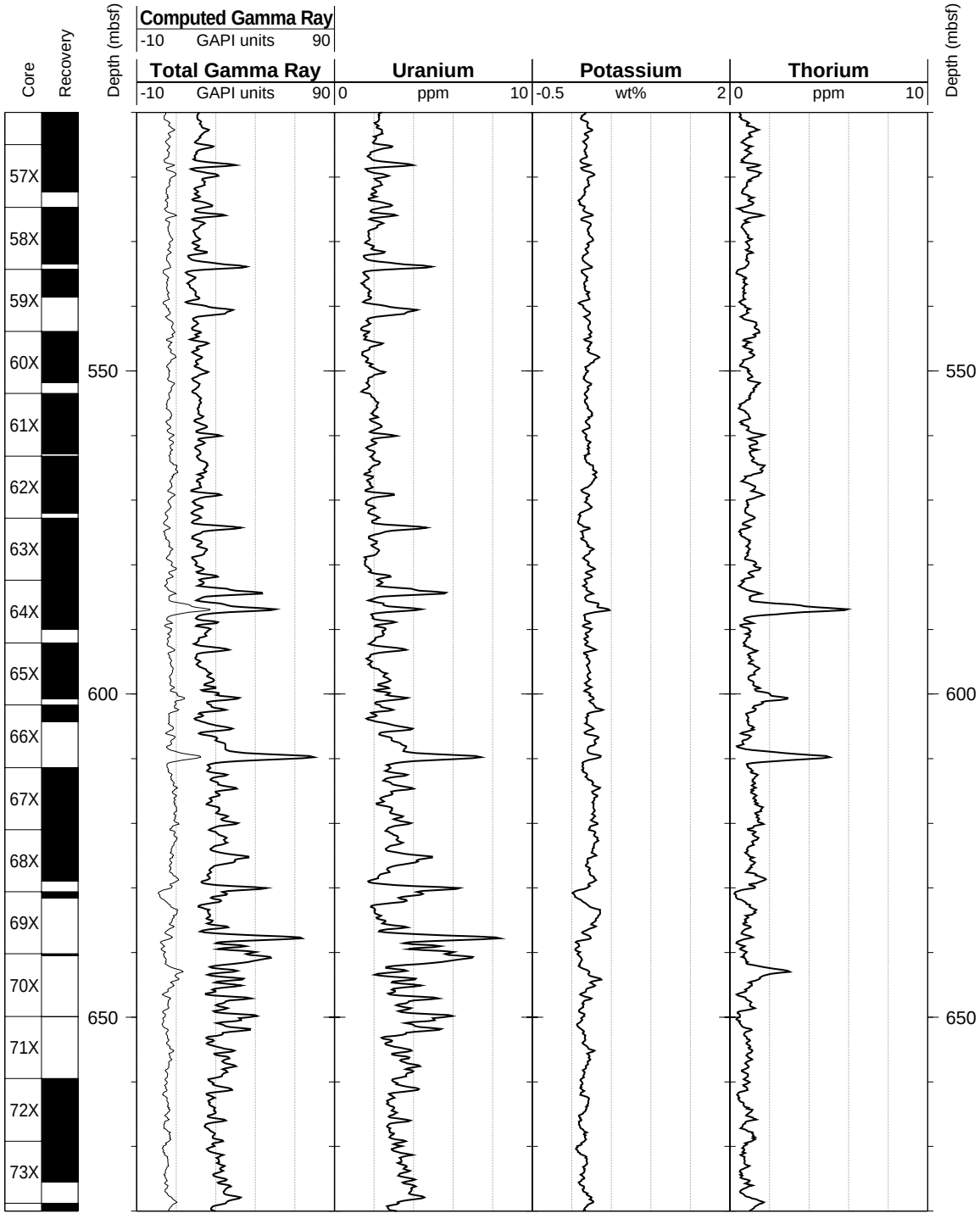

Hole 1006A: Natural Gamma Ray Logging Data (cont.)

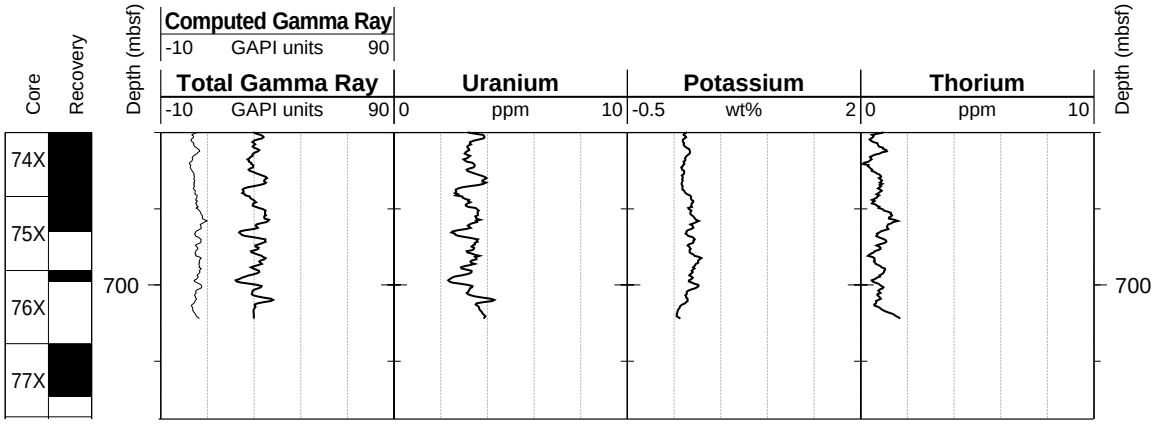




Previous Chapter Table of Contents Next Chapter